

# Orbital Polarization in Relativistic Density Functional Theory

D I S S E R T A T I O N

zur Erlangung des akademischen Grades

**Doctor rerum naturalium**

(Dr. rer. nat.)

vorgelegt

der Fakultät Mathematik und Naturwissenschaften  
der Technischen Universität Dresden

von

**Mahdi Sargolzaei**

geboren am 23 July 1976 in Mashhad (Iran)

Referenten: **Herr Prof. Dr. Helmut Eschrig**  
**Herr Prof. Dr. Peter Fulde**  
**Herr Prof. Dr. Warren E. Pickett**

TECHNISCHE UNIVERSITÄT DRESDEN  
2006



# Contents

|          |  |           |
|----------|--|-----------|
| <b>1</b> | <b>Introduction</b>  | <b>1</b>  |
| <b>2</b> | <b>Relativistic density functional theory</b>                                  | <b>7</b>  |
| 2.1      | Ground state energy functional . . . . .                                       | 7         |
| 2.2      | The Hohenberg-Kohn variational principle . . . . .                             | 9         |
| 2.3      | Current density functional theory . . . . .                                    | 11        |
| 2.4      | Hartree-Fock interaction . . . . .   | 13        |
| 2.5      | Correlation interaction . . . . .  | 15        |
| 2.6      | Kohn-Sham-Dirac equation . . . . .   | 16        |
| 2.7      | The local density approximation . . . . .                                      | 19        |
| 2.8      | RDFT and orbital magnetism . . . . .   | 20        |
| <b>3</b> | <b>Orbital polarization corrections</b>  | <b>23</b> |
| 3.1      | Definition of spin and orbital moments in DFT . . . . .                        | 24        |
| 3.2      | Semi-empirical orbital polarization correction . . . . .                       | 25        |
| 3.3      | Orbital polarization energies in KSD theory . . . . .                          | 27        |
| 3.3.1    | The orbital density $\mathbf{L}(\mathbf{r})$ . . . . .                         | 29        |
| 3.3.2    | Orbital magnetism in an intra-shell with Hartree-Fock<br>interaction . . . . . | 29        |
| 3.4      | Complete KSD equation . . . . .  | 31        |
| 3.4.1    | Numerical results . . . . .  | 33        |
| 3.5      | Conclusion . . . . .   | 35        |
| <b>4</b> | <b>The Kohn-Sham-Dirac equation in solids</b>                                  | <b>37</b> |
| 4.1      | Orbital moment and occupation number in FPLO . . . . .                         | 40        |
| 4.1.1    | Projection arguments . . . . .   | 41        |
| 4.2      | The OPB functional . . . . .   | 43        |
| 4.3      | The OPE functional . . . . .   | 44        |
| 4.4      | Orbital magnetism in bcc Fe, hcp Co and fcc Ni . . . . .                       | 45        |
| 4.4.1    | Computational details . . . . .  | 45        |
| 4.4.2    | Results and discussion . . . . .   | 45        |
| 4.5      | Conclusion . . . . .   | 48        |

|          |   |           |
|----------|---|-----------|
| <b>5</b> | <b>Orbital magnetism in full-Heusler alloys (<math>\text{Co}_2\text{YZ}</math>)</b> | <b>49</b> |
| 5.1      | Crystal structure and computational details . . . . .                               | 51        |
| 5.2      | Results and discussion . . . . .  | 52        |
| 5.2.1    | Calculated spin moments . . . . .   | 52        |
| 5.2.2    | Orbital moments . . . . .   | 56        |
| 5.2.3    | Ligand field model for the orbital moments . . . . .                                | 57        |
| 5.2.4    | Volume dependent properties of $\text{Co}_2\text{FeSi}$ . . . . .                   | 60        |
| 5.2.5    | Half-metallicity . . . . .  | 64        |
| 5.3      | Conclusion . . . . .  | 65        |
| <b>6</b> | <b>Co impurities in Au host matrices</b>  | <b>67</b> |
| 6.1      | Computational details . . . . .   | 68        |
| 6.2      | Results and discussion . . . . .  | 70        |
| 6.2.1    | Geometry optimization . . . . .   | 70        |
| 6.2.2    | Electronic structure and magnetic properties . . . . .                              | 70        |
| 6.2.3    | Model calculations . . . . .  | 73        |
| 6.2.4    | Importance of OP corrections . . . . .  | 74        |
| 6.3      | Conclusion . . . . .  | 77        |
| <b>7</b> | <b>Summary</b>  | <b>79</b> |
| <b>A</b> | <b>Appendix: Functional derivatives</b>   | <b>81</b> |
| <b>B</b> | <b>Appendix: Complex and real spherical harmonics</b>                               | <b>83</b> |
|          | <b>Bibliography</b>   | <b>85</b> |

# List of Figures

|     |  |    |
|-----|--|----|
| 3.1 | The expectation values of $\langle C^V \rangle$ , $\langle C^\Sigma \rangle$ and $C_{m_l}^{C,L}$ coefficients for 3d (left panel) and 4f (right panel) ions. . . . .   | 32 |
| 3.2 | Orbital polarization corrections to the total energy of 2+ ions of 3d elements (upper panel) and 3+ ions of 4f elements (lower panel): the contributions to $E^{\text{OPE}}$ (black thick lines) according to (Eq.3.37) are denoted by black thin lines ( $\Delta E_{\text{OP}}^{\text{LSDA}}$ ), blue thin lines with bullets ( $\Delta E^{C,L}$ ) and red thin lines with open circles ( $\Delta E_{\text{OP}}^{\text{HF}}$ ). The $E^{\text{OPB}}$ values are shown with violet dashed lines. . | 34 |
| 4.1 | Total spin density of states for bcc Fe, hcp Co, and fcc Ni, evaluated with full relativistic FPLO scheme. Indices $\uparrow$ and $\downarrow$ denote for majority and minority density of states, respectively.   | 46 |
| 5.1 | Crystal structure of full-Heusler alloy, $\text{Co}_2\text{FeSi}$ . . . . .  | 51 |
| 5.2 | Total densities of states of all considered compounds close to the Fermi level, obtained by fully relativistic LSDA calculations. Majority (minority) spin channels with dashed red (solid blue) lines are shown in the upper (lower) parts of the individual panels.  | 55 |
| 5.3 | Co 3d partial DOS for $\text{Co}_2\text{MnAl}$ (upper panel) and $\text{Co}_2\text{MnSi}$ (lower panel). The three-fold degenerate $t_{2g}$ (two-fold degenerate $e_g$ ) states are shown with dashed red (solid blue) lines in majority ( $\uparrow$ ) and minority ( $\downarrow$ ) spin sub-shell. . . . .  | 58 |
| 5.4 | Density of states of $\text{Co}_2\text{FeSi}$ close to the Fermi level, evaluated for two different lattice parameters. Theoretical lattice parameter: full black lines; 1.02-fold experimental lattice parameter: dashed red lines. Majority (minority) spin DOS are given in the upper (lower) part of the figure. . . . .   | 61 |
| 5.5 | Band structure of $\text{Co}_2\text{FeSi}$ (upper panel) and $\text{Co}_2\text{MnSi}$ (lower panel) close to the Fermi level. The spin character is indicated by the red dashed lines (majority spin) and blue full lines (minority spin). . . . .   | 61 |

|     |   |    |
|-----|---|----|
| 5.6 | Volume dependence of the calculated total magnetic moment of $\text{Co}_2\text{FeSi}$ . LSDA: black line with diamonds; LSDA+OPB: red line with squares; LSDA+OPE: blue line with bullets. The dashed lines show the range of experimental errors in Ref. [102] $[(5.97 \pm 0.05)\mu_B \text{ at } T=5 \text{ K}]$ . . . . .  | 62 |
| 6.1 | Supercell of gold atoms including a Co impurity. Red sphere shows the Co atom at the position of $(\frac{1}{2}, \frac{1}{2}, \frac{1}{2})$ and the green spheres show the first nearest neighbor of gold atoms to Co atom in a cubic symmetry. . . . .  | 69 |
| 6.2 | Geometry optimization I: calculated total energy (TE) in dependence of the nearest neighbor Co-Au distance in the scalar-relativistic (upper panel) and full-relativistic including spin-orbit coupling and OPB correction (lower panel) approaches. . .  | 71 |
| 6.3 | Geometry optimization II: calculated total energy of $\text{Au}_{32}$ (black circle points) and $\text{Au}_{31}\text{Co}$ (red square points) as a function of supercell lattice constant in the scalar-relativistic scheme. The total energy of $\text{Au}_{32}$ is shifted to be compared with the total energy of $\text{Au}_{31}\text{Co}$ . Dashed and solid vertical lines show the optimized lattice constants of $\text{Au}_{32}$ and $\text{Au}_{31}\text{Co}$ , respectively. . . | 71 |
| 6.4 | Calculated densities of states for supercell structure and Co atom. The solid line show the spin resolved DOS for the whole matrix and dashed lines show the Co projected DOS. The vertical line shows the Fermi level. . . . .   | 72 |
| 6.5 | Spin and orbital magnetic moments of Co in dependence of the distance between Co and nearest neighbor Au atoms. The red (blue) filled squares show the spin magnetic moments of Co in presence of OPB (in absence of OPB). The thick vertical line denotes the optimized neighbor distance, the vertical dotted line shows the Au-Au distance in the unrelaxed structure. The red (blue) filled circles show the orbital magnetic moment of Co with (without) OPB correction. . . . .       | 74 |
| 6.6 | The $m_l$ -resolved densities of states for 3d bands of a Co impurity in gold in the LSDA (upper panel) and in the LSDA+OPB (lower panel) approach. . . . .   | 75 |

# List of Tables

|     |   |    |
|-----|---|----|
| 4.1 | Spin ( $M_s$ ) and orbital ( $M_l$ ) moments of bcc Fe, hcp Co and fcc Ni. The indices a and b show the results based on orthogonal and non-orthogonal projections to OP corrections. Experimental values are presented by Stearns [72]. . . . .  | 47 |
| 5.1 | The experimental lattice constants (Villars <i>et al.</i> [106] ) are compared with the calculated LSDA lattice constants. The values are in atomic units. . . . .  | 53 |
| 5.2 | Spin ( $M_s$ ) and orbital ( $M_l$ ) moments for constituents of the Co <sub>2</sub> YZ full-Heusler alloys together with total spin and total orbital moments and their sum, calculated at the LSDA lattice constant. The first line for each compound gives the LSDA results and related model results (see text) in parentheses. Lines with the indices OPB and OPE show results of calculations with orbital polarization corrections suggested by O. Eriksson <i>et al.</i> [20, 21] and by H. Eschrig <i>et al.</i> [23] added to the LSDA-XC energy functional, respectively. The influence of OP corrections on the spin moments is marginal and left out in the Table. . . . | 54 |
| 5.3 | Comparison of available experimental (XMCD) and calculated ratios $M_l/M_s$ . Calculated data obtained by LSDA and LSDA+OPE [23] are given for both LSDA and experimental lattice constants.  | 57 |
| 5.4 | Comparison of available experimental and calculated total magnetic moments per formula unit. Calculated data obtained by LSDA and LSDA+OPE are given for both LSDA and experimental lattice constants. The degree of order within the L2 <sub>1</sub> structure has not always been analyzed. All experimental data were obtained at low temperature. . . . .   | 60 |
| 5.5 | Spin polarization degree for half-ferromagnetic Co <sub>2</sub> YZ full-Heusler alloys. SPD values at LSDA lattice constants without spin-orbit coupling (SO: no) and with spin-orbit coupling (SO: yes) are given in percent. . . . .  | 64 |

---

|     |  |    |
|-----|--|----|
| 6.1 | Calculated spin ( $M_s$ ) and orbital ( $M_l$ ) moments of Co impurities in Au and their ratios ( $M_l/M_s$ ). Values obtained with the LSDA and both version of orbital polarization corrections (OPB, OPE) are shown for relaxed and unrelaxed structures. All values are calculated at the lattice constant of $\text{Au}_{31}\text{Co}$ ( $a = 8.125$ Bohr radii) The values of OPB and OPE indicated in parentheses have been calculated with hybridized OP functionals and values without parentheses have been calculated with orthogonal OP functionals. . . . . | 73 |
| 6.2 | Occupation numbers $n(m_l)$ for minority $m_l$ -3d states of Co impurity in Au. . . . .  | 76 |



# List of Abbreviations

|          |   |
|----------|---|
| CDFT     | Current Density Functional Theory                                   |
| DFT      | Density Functional Theory   |
| FLAPW    | Full-Ptential Linearized Augmented Plane Wave                       |
| FPLO     | Full-Potential Local-Orbital  |
| HF       | Hartree-Fock  |
| KKR      | Korringa-Kohn-Rostocker   |
| KS       | Kohn-Sham   |
| KSD      | Kohn-Sham-Dirac   |
| LMTO     | Linear-Muffin-Tin-Orbital   |
| ASA      | Atomic-Sphere Approximation   |
| L(S)DA   | Local (Spin) Density Approximation                                  |
| OP       | Orbital Polarization  |
| OPB      | Brooks's Orbital Polarization                                       |
| OPE      | Eschrig's Orbital Polarization                                      |
| PCAR     | Point Contact Andreev Reflection                                    |
| QED      | Quantum Electrodynamic  |
| RDFT     | Relativistic Density Functional Theory                              |
| RFPLO    | Relativistic Full-Potential Local-Orbital                           |
| SDFT     | Spin Density Functional Theory                                      |
| SO       | Spin-Orbit  |
| SOPR-MST | Spin- and Orbital Polarized Relativistic Multiple-Scattering Theory |
| SPD      | Spin Polarization Degree  |
| XC       | Exchange-Correlation  |
| XMCD     | X-Ray Magnetic Circular Dichroism                                   |



# Chapter 1

## Introduction

Magnetism of interacting many-particle systems has been an important goal in physics. The task is to derive the magnetic properties of such systems purely from quantum mechanical principles. It is well understood that the magnetization in an atom is described by quantum numbers, spin ( $S$ ), orbital ( $L$ ), and total angular momentum ( $J$ ) of its electrons. A set of guidelines, named Hund's rules after Friedrich Hermann Hund [1] helps us to determine the corresponding quantum numbers for the valence electrons. In free atoms, the valence electrons are assumed to be involved into open shells. Hund's rules can be applied to those electrons and maybe read as follows

- i. Multiplicity rule: The lowest energy in the multiplet of states with different electron configurations has the largest multiplicity (couple the valence electrons (or holes) to give maximum total spin).
- ii. Orbital angular momentum rule: Among the multiplets with the same multiplicity, the lowest-energy state is that with the largest total orbital angular momentum.
- iii. Fine structure rule: In configurations containing shells less than half filled with electrons, the term having the lowest total angular momentum  $J$  lies lowest in energy, whereas in those with shells more than half filled, the term having the largest value of  $J$  lies lowest.

According to Hund's rules, the method of adding up all the spins  $S$  and all the angular momenta  $L$  respectively, is the so-called LS or Russell-Saunders coupling [2]. Hund's rule of maximum multiplicity, a greater total spin state makes the resulting atom more stable, most commonly manifested in a lower energy state, because it forces the unpaired electrons to reside in different spatial orbitals. An accepted reason for the increased stability of high multiplicity states is that the different occupied spatial orbitals create larger average distances between the electrons, which reduces the electron-electron repulsion energy. The results of Hund's rules will change when the electrons become

relativistic in heavy atoms where the spin-orbit effect becomes comparable to the electron repulsion. For heavy atoms, we calculate first the angular momentum ( $j$ ) for every electron and then we add up them to get total angular momentum  $J$ . This is the so-called  $j$ - $j$  coupling.

The question “Are Hund’s rules applicable on different systems such as molecules and solids?” is still on the agenda. Finding the ground state of the considered system is frequently a problem. Density functional theory (DFT) methods apparently are the most widely spread self-consistent methods to investigate the ground state properties of condensed matter. This is due to their high computational efficiency and very good accuracy. The importance of DFT was initiated by the famous works of Walter Kohn, Pierre C. Hohenberg, and Lu Jeu Sham [3, 4, 5]. In contrast to the text-books presenting the Hartree-Fock method, which begins conceptually with a many-body wave function and the description of individual electrons interacting with the nuclei and all other electrons in the system, density functional theory works with the ground state density of the entire electron system. Recall that if there are  $N$  electrons in the system (and  $N$  might be macroscopically large  $\sim 10^{23}$ ), the wave function of the electron system is a function of  $3N$  variables (since the electron wave function is usually expanded over some basis functions, the actual number of the variables is governed by the number of basis functions which is typically much larger than  $3N$ ). However, within DFT, the ground state of the system of interacting electrons in an external potential  $V^{ext}(\mathbf{r})$ , is described by the electronic charge density  $n(\mathbf{r})$ . Note that the charge density is a function of three variables only!

In the framework of DFT, the total energy is decomposed into kinetic energy, Coulomb energy, and a term called the exchange-correlation energy. They capture all many-body interactions in the considered system. This decomposition is formally exact, but the actual expressions for the many-body exchange and correlation interactions are still unknown. The local density approximation (LDA) turned out to be computationally convenient and surprisingly accurate. In this approximation the exchange-correlation energy is taken from the known results of the many-electron interactions in an electron system of constant density (homogeneous electron gas).

Taking into account the relativistic kinetic energy leads to direct and indirect relativistic effects on the electronic structure of a solid. The most pronounced direct effect (although not the biggest in magnitude) is the spin-orbit splitting of band states leading to the magneto-crystalline anisotropy energy of itinerant magnetism and to magneto-optical effects [6, 7].

A well-known indirect relativistic effect is the change of screening of valence electrons from the nuclear charge by inner-shell electrons. It is for instance responsible for the color of gold (due to a relativistic reduction of the distance of the  $d$ -band from the chemical potential which lowers the corresponding absorption edge). Now the next question arises. Can such relativistic effects

somehow be included in ordinary density functional theory formulated in terms of the local electron density and ordinary Kohn-Sham orbitals? The answer to this question, unfortunately, is NO.

Four-current density functional theory (CDFT), the quantum electrodynamic version of the Hohenberg-Kohn theory [3] is a powerful tool to treat relativistic effects. Although it is principally designed for systems in strong magnetic fields, CDFT can also be applied in situations where currents are presented without external magnetic fields. As already pointed out by A.K. Rajagopal and J. Callaway [8], the most natural way to incorporate magnetism into DFT is the generalization to CDFT. These authors treated its most simple approximation, the spin density functional theory (SDFT), which keeps the spin current only and neglects completely correlation effects of orbital currents. Compared to ordinary DFT, this SDFT meets already more subtle problems [9, 10]. The orbital magnetism as a consequence of Hund's second rule is absent in this theory and there is not any more a one-to-one mapping of spin densities onto external fields. In solids, in particular in metals, the importance of Hund's second rule (orbital polarization) and Hund's third rule (spin-orbit coupling) is usually interchanged in comparison to atoms. The reason is that the crystal field and the hybridization of the valence states tend to quench the orbital magnetism. Thus, in applications of the relativistic CDFT to solids, the usual way has been to keep the spin-orbit coupling in the Kohn-Sham-Dirac (KSD) equation (a relativistic generalization of the ordinary Kohn-Sham (KS) equation), to neglect the orbital contribution to the total current density and to approximate the exchange-correlation energy functional with the related spin density expression. This scheme includes a spontaneous exchange and correlation spin polarization. On the other hand, orbital polarization comes into play not only as a correlation effect but also as an effect due to the interplay of spin polarization and spin-orbit coupling. In the presence of both couplings, time reversal symmetry is broken and a non-zero orbital current density may occur. Using this scheme for 3d and 4f magnets yields orbital moments where they are smaller than related experimental values by typically a factor of two [6].

An alternative scheme, based on the non-relativistic treatment of "paramagnetic" current density and spin density as separate quantities, was suggested by G. Vignale *et al.* [11, 12, 13]. Since the spin-orbit interaction is not taken into consideration, this scheme can be suited, for example, for systems in high magnetic fields [14, 15] or for ground state calculations in very light open-shell atoms. It is inappropriate for 3d magnetic metals, where the orbital magnetization is induced just by the spin-orbit coupling and also for 4f or 5f metals, where the orbital polarization and the spin-orbit interaction are comparable in their magnitudes [16, 17]. H. Ebert *et al.* [18] calculated the orbital moments in Fe, Co, Ni in presence of the spin-orbit coupling and found approximately 10% enhancement of the orbital moments compared with the calculated or-

bita moments in absence of the spin-orbit coupling. This enhancement is indeed small in comparison to the remaining discrepancy between theory and experiment for both Fe and Co.

In this Thesis, to overcome such discrepancies, two different orbital polarization (OP) corrections are suggested. Those OP corrections, essentially, can be described by the introduction of an additional operator, originating from an OP contribution to the total energy functional [19, 20, 21, 22, 23]. Alternatively, it was demonstrated by I.V. Solovyev *et al.* [24] how OP corrections can be obtained in the framework of the "LSDA+ $U$ " idea [25]. The suggested approaches appear to be similar to the idea of L. Severin *et al.* [22], with the important additional feature of rotational invariance. Numerical results obtained in the different schemes suggested in Ref. [20] and Ref. [22] are found to largely coincide [26]. There is no direct comparison of the OP correction method with the LSDA+ $U$  method for specific systems available in the literature. In this context, a systematic investigation of the orbital contribution to the magnetism of metals is suggested.

In this Thesis, atomic units, a.u., will be used throughout by putting

$$\hbar = m_e = \epsilon^2 = 1 \text{ a.u.},$$

where  $m_e$  is the electron mass and  $\epsilon = e/\sqrt{4\pi\epsilon_0}$  is the electrostatic electron charge,  $e$  is the electrodynamic electron charge and  $\epsilon_0$  is the vacuum permittivity. This means that energies are given in units of Hartree [1 Hartree = 27.212 eV] and lengths in units of the Bohr radius [ $1 a_{\text{Bohr}} = 0.529177 \times 10^{-10} m$ ]. The speed of light in vacuum is  $c = 137.03599$  a.u. The four-component Dirac spinor quantities are given in the standard representation in which the Dirac matrices  $\gamma_\mu$ , ( $\mu = 0, 1, 2, 3$ ) are (in terms of  $2 \times 2$  blocks) :

$$\gamma^0 = \beta = \begin{pmatrix} \mathbf{1} & 0 \\ 0 & -\mathbf{1} \end{pmatrix}, \gamma^i = \begin{pmatrix} 0 & \sigma_i \\ -\sigma_i & 0 \end{pmatrix}, \gamma^\mu \gamma_\mu = \beta^2 - \gamma^2 = 4,$$

where  $\mathbf{1}$  means a  $2 \times 2$  unit matrix, and  $\sigma_i$ , ( $i = 1, 2, 3$ ) are the well known Pauli matrices defined as,

$$\sigma_1 = \frac{1}{2} \begin{pmatrix} 0 & 1 \\ 1 & 0 \end{pmatrix}, \quad \sigma_2 = \frac{1}{2} \begin{pmatrix} 0 & -i \\ i & 0 \end{pmatrix}, \quad \sigma_3 = \frac{1}{2} \begin{pmatrix} 1 & 0 \\ 0 & -1 \end{pmatrix}.$$

Furthermore,

$$\boldsymbol{\alpha} = \beta \boldsymbol{\gamma} = \begin{pmatrix} 0 & \boldsymbol{\sigma} \\ \boldsymbol{\sigma} & 0 \end{pmatrix}, \quad \text{and} \quad \boldsymbol{\Sigma} = -\frac{i}{2} \boldsymbol{\alpha} \times \boldsymbol{\alpha} = \begin{pmatrix} \boldsymbol{\sigma} & 0 \\ 0 & \boldsymbol{\sigma} \end{pmatrix},$$

are the  $4 \times 4$  velocity and spin matrices, respectively. The vector  $\boldsymbol{\sigma}$  is defined as  $\boldsymbol{\sigma} = (\sigma_1, \sigma_2, \sigma_3)$ . Bold letters denote vectors. A combined variable  $x = (\mathbf{r}, \boldsymbol{\sigma})$ , will be used throughout for both the position and the spin of a particle.

The Thesis is organized as follows: The theoretical background of the relativistic four-current density functional theory as a basis for understanding the orbital magnetism is presented in Chapter 2. In Chapter 3, two different orbital polarization corrections are given. The OP energies for transition metal ions and lanthanide ions are calculated. The implementation of both corrections to periodic systems in the framework of the full-potential local-orbital minimum scheme (FPLO) is introduced in Chapter 4. The calculated orbital moments of bcc Fe, hcp Co, and fcc Ni are presented also in Chapter 4 and compared with experiment. The study of orbital magnetism in eight full-Heusler alloys and orbital magnetism of Co impurities in gold host matrices, both probed by X-ray magnetic circular dichroism (XMCD) experimentally, are the topics of Chapters 5 and 6, respectively. Finally, the Thesis will be summarized in Chapter 7.





# Chapter 2

## Relativistic density functional theory

### 2.1 Ground state energy functional

It is supposed that all the needed information of a physical system at each time  $t$  is given by a quantum state  $|\Psi\rangle$  in an abstract Hilbert space and the time evolution of the system is governed by the time-dependent Schrödinger equation:

$$i\hbar \frac{\partial |\Psi\rangle}{\partial t} = \hat{H}|\Psi\rangle, \quad (2.1)$$

where  $\hat{H}$  is the Hamiltonian operator which contains kinetic energy operator and all relevant interaction operators. The total energy of the system is given by the expectation value of the Hamiltonian operator, which in the Dirac notation, is given by  $E = \langle \Psi | \hat{H} | \Psi \rangle / \langle \Psi | \Psi \rangle$ . The total probability of finding the system somewhere in the position space  $\mathbf{R}^3$  is equal to 1, namely,  $\langle \Psi | \Psi \rangle = 1$ , which allows unbound particles to disappear at infinity. Therefore, the system must be put into a large box as into a torus of finite volume. The total energy of the ground state can be obtained as:

$$E_0 = \langle \Psi | \hat{H} | \Psi \rangle \Leftrightarrow |\Psi\rangle = |\Psi_0\rangle, \quad (2.2)$$

where  $E_0$  and  $|\Psi_0\rangle$  are the corresponding total energy and quantum state for ground state of an arbitrary system, respectively. The problem arises is that for which expression of  $|\Psi_0\rangle$  we can calculate properly the total energy of the ground state. There is not a simple way to achieved such expression. Density functional theory can provide an effective way to reach ground state.

Consider a system of  $N$  identical particles interacting with each other with pair forces and moving in a given external potential. The related Hamiltonian consists of the kinetic energy operator  $\hat{t}$ , the potential operator  $\hat{v}$  of the interaction of the particles with the external field, and the two-particle interaction

operator  $\hat{w}$ :

$$\hat{H} = \hat{t} + \hat{v} + \hat{w}. \quad (2.3)$$

Now, we replace the position space  $\mathbf{R}^3$  by a torus  $\mathbf{T}^3$ , i.e. a box with periodic boundary conditions and with volume  $|\mathbf{T}|^3$  sufficiently large not to significantly change the considered results. This makes the spectrum of the Hamiltonian discrete and ground state existing and normalizable. The ground state energy (the lowest expectation value of the Hamiltonian) as a functional of the external potential  $v$  and the particle number  $N$  is given by definition:

$$E[v, N] = \inf_{\hat{\rho}} \left\{ \text{tr}(\hat{\rho}\hat{H}) \mid \text{tr}(\hat{\rho}\hat{N}) = N \right\}, \quad (2.4)$$

where,  $\{A|B\}$  means set  $A$  under constraints  $B$  and the infimum search is over all ensemble states (N particle density matrices) and the most general density operator for a mixed state is written as:

$$\hat{\rho} = \sum_k |\Psi_k\rangle p_k \langle\Psi_k| \quad ; \quad 0 \leq p_k \leq 1 ; \quad \sum_k p_k = 1, \quad (2.5)$$

where  $|\Psi_k\rangle$  are the normalized pure states with  $N_k$  electrons and  $p_k$  is the probability to find the system in the corresponding pure state. In the following, convexity and gauge properties of the ground state are presented.

a) **Convexity property:** Now, fix external potential  $v$  and pick two particle numbers  $N_1$  and  $N_2$ . There exist sequences  $\hat{\rho}_j^i$ ,  $i = 1, 2$ ;  $j = 1, 2, \dots$  with  $\text{tr}(\hat{N}\hat{\rho}_j^i) = N_i$  and  $\lim_j \text{tr}(\hat{H}\hat{\rho}_j^i) = E[v, N_i]$ . Take the sequence  $\hat{\rho}_j = c\hat{\rho}_j^1 + (1 - c)\hat{\rho}_j^2$ ,  $0 \leq c \leq 1$ . Obviously  $\text{tr}(\hat{N}\hat{\rho}_j) = cN_1 + (1 - c)N_2$ , and  $\lim_j \text{tr}(\hat{H}\hat{\rho}_j) = cE[v, N_1] + (1 - c)E[v, N_2]$ . On the other hand, by definition  $E[v, cN_1 + (1 - c)N_2] \leq \lim_j \text{tr}(\hat{H}\hat{\rho}_j)$ . This proves the convexity of  $E[v, N]$  in  $N$  for fixed  $v$ :

$$E[v, cN_1 + (1 - c)N_2] \leq cE[v, N_1] + (1 - c)E[v, N_2], \quad 0 \leq c \leq 1, \quad (2.6)$$

by definition (Eq.2.4) and the text above,  $N \geq 0$  with  $E[v, 0] = 0$  for all  $v$ . One may, however, formally define  $E[v, N] = +\infty$  for all  $N < 0$  and all  $v$ , which makes  $E[v, N]$  defined for all  $N$ , convex.

On the other hand, since the functional dependence of  $\hat{H}$  on  $v$  is of course affine-linear, namely,

$$\hat{H}[cv_1 + (1 - c)v_2] = c\hat{H}[v_1] + (1 - c)\hat{H}[v_2], \quad 0 \leq c \leq 1, \quad (2.7)$$

and for fixed  $N$  one can obtain,

$$\begin{aligned}
E[cv_1 + (1 - c)v_2, N] &= \\
&= \inf_{\hat{\rho}} \left\{ \text{ctr}(\hat{\rho}\hat{H}_{v_1}) + (1 - c)\text{tr}(\hat{\rho}\hat{H}_{v_2}) \mid \text{tr}(\hat{\rho}\hat{N}) = N \right\} \geq \\
&\geq c \inf_{\hat{\rho}} \left\{ \text{tr}(\hat{\rho}\hat{H}_{v_1}) \mid \text{tr}(\hat{\rho}\hat{N}) = N \right\} + \\
&+ (1 - c) \inf_{\hat{\rho}} \left\{ \text{tr}(\hat{\rho}\hat{H}_{v_2}) \mid \text{tr}(\hat{\rho}\hat{N}) = N \right\} = \\
&= cE[v_1, N] + (1 - c)E[v_2, N], \tag{2.8}
\end{aligned}$$

where it is used the simple fact that the infimum of a sum cannot be lower than the sum of the corresponding independent infima. In summary, the ground state energy  $E[v, N]$  is a convex functional of  $N$  for fixed  $v$  and a concave functional for fixed  $N$ .

b) **Gauge invariance:** If a functional for ground state exists, it is obviously gauge invariant with respect to potential constants, i.e. it is the same for all potentials  $v + \text{const.}$ ,

$$E[v + \text{const.}, N] = E[v, N] + N \cdot \text{const.} \tag{2.9}$$

These simple convexity properties of  $E[v, N]$  together with the above gauge property form the deep logical foundation of density functional theory. It is also important to know that the convexity properties are independent from the form of internal operators, such as  $\hat{t}$  and  $\hat{w}$ . Most concepts considered in this chapter can be found in the monograph by H. Eschrig [27].

## 2.2 The Hohenberg-Kohn variational principle

Starting with the convexity of the ground state energy functional with respect to the particle number  $N$  one defines a Legendre transform of the functional,

$$\begin{aligned}
G[v - \mu] &= \sup_N \{ \mu N - E[v, N] \} \\
&= \sup_N \{ -E[v - \mu, N] \} \\
&= -\inf_N \{ E[v - \mu, N] \}, \tag{2.10}
\end{aligned}$$

where  $\mu$  (chemical potential) is the dual variable of  $N$  and supremum search for maximum values and in the second line the gauge property (Eq.2.9) and in the last line simple fact by definition  $\sup\{-g\} = -\inf\{g\}$ , has been used.

The functional  $G[v]$  is just as  $-E[v, N]$  convex in  $v$  and can be Legendre transformed with respect to  $v$  by introducing the dual variable  $-n$ ,

$$H[n] = \sup_{v \in X^*} \{(v| - n) - G[v]\}, \quad (2.11)$$

where  $X^* \equiv \mathbf{L}^{3/2}(\mathbf{T}^3)$  is the dual space of position space  $X \equiv \mathbf{L}^3(\mathbf{T}^3)$ . The above relation helps us to rewrite the ground state energy functional with dual variables of  $v$  and  $N$ ,

$$\begin{aligned} E[v, N] &= \sup_{\mu} \{N\mu - G[v - \mu]\} \\ &= \sup_{\mu} \left\{ N\mu - \sup_{n \in X} \{(v - \mu| - n) - H[n]\} \right\} \\ &= \sup_{\mu} \left\{ N\mu + \inf_{n \in X} \{(v - \mu|n) + H[n]\} \right\} \\ &= \sup_{\mu} \left\{ \inf_{n \in X} \{\mu(N - (1|n)) + (v|n) + H[n]\} \right\}. \end{aligned} \quad (2.12)$$

The expression in the curved brackets can be regarded as a functional of  $\mu$  and  $N$ . The rule  $\inf \sup \geq \sup \inf$  can be applied since  $\mu$  can be treated as a constant potential function in space,  $(\mu|N) = (1|N)\mu$ , which leads to the inequality,

$$E[v, N] \leq \inf_{n \in X} \left\{ \sup_{\mu} \{\mu(N - (1|n)) + (v|n) + H[n]\} \right\}. \quad (2.13)$$

The above inequality can be sharpened into an equality [27]. Since the expression under the supremum is linear in  $\mu$ , the supremum is either  $+\infty$ , if  $(1|n) \neq N$ , or zero, if  $(1|n) = N$ . One should note that  $\inf[+\infty]$  does not exist. So that, taking the condition  $(1|n) = N$  and coming back to (Eq.2.13), one can arrive at the expression,

$$E[v, N] = \inf_{n \in X} \{(v|n) + H[n] | (1|n) = N\}. \quad (2.14)$$

This last equation express the variational principle by Hohenberg and Kohn [3]. This variational principle together with above text has important advantages:

i- The dual value  $n$  for the external potential is just the density of particles for the ground state in position space  $\mathbf{T}^3$ .

ii- Taking the fact that the  $E[v, N]$  is a convex functional, then its Legendre transformation  $H[n]$  is also convex, lower semi-continuous and has a non-empty sub-differential  $\partial H[n]$  at every  $n$  where  $H[n]$  is finite.

## 2.3 Current density functional theory

The correct frame to describe interacting relativistic electrons is the quantum electrodynamics (QED) where the matter field is the four-component operator-valued electron-positron field  $\hat{\psi}(u^\sigma)$  acting in the Fock space and depending on space-time variable  $u^\sigma = (ct, \mathbf{r})$ ; ( $u_\sigma = (ct, -\mathbf{r})$ ). In a static external field, the operator Hamiltonian for an interacting relativistic system in a large periodic spatial volume  $V$  with respect to that reference frame, can be presented as:

$$\hat{H}_A = \int d^3r (\hat{H} - e\hat{j}^\mu A_\mu), \quad (2.15)$$

where  $e$  is the electrodynamic charge quantum and  $\hat{H}$  is the Hamiltonian density operator which contains the kinetic and internal interaction density operators in the considered system. The  $A_\mu$  denotes the static external field in the relativistic regime. The four-current density operator  $\hat{j}^\mu$  is given by,

$$\hat{j}^\mu = c : \hat{\psi} \gamma^\mu \hat{\psi} :^1, \hat{\psi} = \hat{\psi}^\dagger \gamma^0. \quad (2.16)$$

In QED the total charge of the system in the quantum state  $|\Psi\rangle$  is given by:

$$Q = -\frac{e}{c} \int d^3r \langle \Psi | \hat{j}^0 | \Psi \rangle. \quad (2.17)$$

We fix the total charge in the system and consider the ground state of the quantum field as that state minimizing,

$$E[A, Q] = \min \left\{ \langle \Psi | \hat{H}_A | \Psi \rangle \mid -\frac{e}{c} \int d^3r \langle \Psi | \hat{j}^0 | \Psi \rangle = Q \right\}. \quad (2.18)$$

The first demonstration of the existence theorems for a density functional theory of many electron systems characterized in terms of quantum electrodynamics by A.K. Rajagopal and J. Callaway [28] emerged in connection with the discussion of spin-polarized non-relativistic systems. The relativistic case was analyzed in a later contribution by A.K. Rajagopal [29] and further by A.H. MacDonald, and S.H. Vosko [30] and H. Eschrig *et al.* [31]. For the purpose of discussing the relativistic extensions of the Hohenberg-Kohn theorem we may specify the Hamiltonian without addressing the questions of renormalization and the quantization of the electromagnetic field.

The non-relativistic limit of  $E[A, Q]$  from (Eq.2.18) is  $E[v, N]$ , where  $v = -eA^0$  and  $N = -Q/e$ . One therefore may proceed in analogy with the previous section 2.2. As the first step, it is important to prove convexity properties for the relativistic ground state energy. Note that if a ground state  $\Psi$  exists then provided  $\hat{H}_A$  is bounded from below.

---

<sup>1</sup>The colons ( $: X :$ ) stand for normal order of the Fock space operators.

First of all,  $E[A, Q]$  for fixed  $A$  is a convex functional of the total charge  $Q$ . To see this, one fixes  $A$  (for which  $\hat{H}_A$  is bounded from below) and takes two different charges  $Q_i$ ,  $i = 1, 2$  to be integer multiples of the charge quantum  $e$ . If  $|\Psi_{AQ_i}\rangle$  are the corresponding ground states according to (Eq.2.18) and  $0 < \alpha < 1$ , then  $|\Psi_\alpha\rangle = \sqrt{\alpha}|\Psi_{AQ_1}\rangle + \sqrt{1-\alpha}|\Psi_{AQ_2}\rangle$ . Note that  $|\Psi_{AQ_i}\rangle$  are orthogonal to each other (because of an integer difference of charge quanta) and are common eigenstates of  $\hat{H}_A$  and  $\hat{Q}$ . The state  $|\Psi_\alpha\rangle$  shows the property  $\langle\Psi_\alpha|\hat{Q}|\Psi_\alpha\rangle = \alpha Q_1 + (1-\alpha)Q_2$ . Therefore we can obtain,  $E[A, \alpha Q_1 + (1-\alpha)Q_2] \leq \langle\Psi_\alpha|\hat{H}_A|\Psi_\alpha\rangle = \alpha\langle\Psi_{AQ_1}|\hat{H}_A|\Psi_{AQ_1}\rangle + (1-\alpha)\langle\Psi_{AQ_2}|\hat{H}_A|\Psi_{AQ_2}\rangle = \alpha E[A, Q_1] + (1-\alpha)E[A, Q_2]$ . It means for fixed  $A$ , the functional  $E[A, Q]$  is always a convex functional of  $Q$  as, for fixed  $v$ , the non-relativistic  $E[v, N]$  was always a convex functional of  $N$ .

Next, since  $\hat{H}_A$  has an affine-linear dependence on the external four-potential  $A^\mu$ ,  $E[A, Q]$  for fixed  $Q$  is a concave functional of  $A^\mu$ . After fixing  $Q$  one can take  $A_1, A_2$  for which the  $\hat{H}_{A_i}$  are bounded from below and  $0 < \alpha < 1$ . Then  $\hat{H}_{\alpha A_1 + (1-\alpha)A_2}$  is also bounded from below, namely

$$\begin{aligned} E[\alpha A_1 + (1-\alpha)A_2, Q] &= \\ &= \inf \left\{ \alpha \langle\Psi|\hat{H}_{A_1}|\Psi\rangle + (1-\alpha)\langle\Psi|\hat{H}_{A_2}|\Psi\rangle \mid \langle\Psi|Q|\Psi\rangle = Q \right\} \geq \\ &\geq (\alpha) \inf \left\{ \langle\Psi'|\hat{H}_{A_1}|\Psi'\rangle \mid \langle\Psi'|Q|\Psi'\rangle = Q \right\} + \\ &+ (1-\alpha) \inf \left\{ \langle\Psi''|\hat{H}_{A_2}|\Psi''\rangle \mid \langle\Psi''|Q|\Psi''\rangle = Q \right\} = \\ &= \alpha E[A_1, Q] + (1-\alpha)E[A_2, Q]. \end{aligned} \quad (2.19)$$

The third simple but important fact is the gauge invariance of the ground state  $\Psi_{AQ}$  with respect to addition of a scalar constant to the potential,

$$A^0 \rightarrow A^0 + w : \quad E[A, Q] \rightarrow E[A, Q] + cQw. \quad (2.20)$$

The four current density  $J^\mu$  is a dual variable of the external four vector potential  $A_\mu$  (note that  $J^\mu$  is a function and  $\hat{j}^\mu$  is an operator). Using mentioned convexity property and the gauge invariance, one can obtain the relativistic version of the Hohenberg-Kohn variational principle, what is called also Hohenberg-Kohn-Rajagopal variational principle,

$$E[A, Q] = \inf \left\{ H[J^\mu] - e \int d^3r J^\mu A_\mu \mid \frac{e}{c} \int d^3r J^0 = Q \right\}. \quad (2.21)$$

We can present the four current density  $J^\mu$  in terms of the new variational quantities, bispinor orbitals  $\psi_k(\mathbf{r})$  and orbital occupation numbers  $n_k$ . The four-current density reads as  $J^\mu = c \sum_k n_k \bar{\psi}_k \gamma^\mu \psi_k$ , where  $\langle\psi_k|\psi_{k'}\rangle = \delta_{kk'}$  and  $Q = -e \sum_k n_k$  is the total electron charge, if all  $\psi_k$  are in the electron sector.

The current density functional  $H[J^\mu]$  of the Hohenberg-Kohn-Rajagopal variational principle may be split into:

$$H[J^\mu] = \mathcal{K}[J^\mu] + \mathcal{L}[J^\mu], \quad (2.22)$$

with

$$\mathcal{K}[J^\mu] = \min_{\psi_k, n_k} \left\{ k[\psi_k, n_k] \mid c \sum_k n_k \bar{\psi}_k \gamma^\mu \psi_k = J^\mu \right\}, \quad (2.23)$$

and

$$\mathcal{L}[J^\mu] = \int d^3r J^0(\mathbf{r}) \mathcal{P}(J^\mu(\mathbf{r}), \nabla J^\mu(\mathbf{r})). \quad (2.24)$$

If  $k[\psi_k, n_k]$  is explicitly given, then  $\mathcal{L}[J^\mu] = H[J^\mu] - \mathcal{K}[J^\mu]$  is also defined. One should note that the form of (Eq.2.24) is already a model approximation and there is no an exact form for  $\mathcal{L}[J^\mu]$ . However, it is commonly called the local density approximation, if  $\mathcal{P}$  is assumed to depend on the electron density  $J^0$  or the spin density.

Substitution of the two previous expressions into (Eq.2.22) yields the relativistic variational principle for the ground state energy  $E[A, Q]$  in the external four-potential  $A_\mu(\mathbf{r})$ :

$$E[A, Q] = \min_{\psi_k, n_k} \left\{ k[\psi_k, n_k] + \mathcal{L} \left[ c \sum_k n_k \bar{\psi}_k \gamma^\mu \psi_k \right] - \right. \\ \left. - ec \sum_k n_k \langle \psi_k | \gamma^0 \gamma^\mu A_\mu | \psi_k \rangle \parallel \langle \psi_k | \psi'_k \rangle = \delta_{kk'}, -e \sum_k n_k = Q \right\}. \quad (2.25)$$

It has to be clarified that the  $k[\psi_k, n_k]$  and  $\mathcal{L} \left[ c \sum_k n_k \bar{\psi}_k \gamma^\mu \psi_k \right]$  are taken for kinetic and internal energies. In a many-body system the internal interactions are Hartree-Fock (HF) and correlation interactions. The next two sections are devoted to these two interactions.

## 2.4 Hartree-Fock interaction

For a non-relativistic system of  $N$  non-interacting fermions the wave function can be constructed as a Slater determinant of the orthonormalized single-particle spin-orbitals [32]:

$$\Psi_{\text{Slater}} = \frac{1}{\sqrt{N!}} \det \|\phi_{l_i}(x_k)\|. \quad (2.26)$$

Such a Slater determinant is perfectly anti-symmetric. Furthermore, it is easily verified that the Slater determinant obeys the Pauli exclusion principle [33]. For an interacting  $N$ -fermion system a single Slater determinant can of course in general not be a solution of the stationary Schrödinger equation.

However, one can ask for the best Slater determinant approximation to the true N-particle ground state, what minimizes its expectation value with the Hamiltonian  $\hat{H}$ . The corresponding minimum value estimates the true ground state energy.

If one minimizes the total energy of interacting system in a Slater determinant state and enforces orthogonality between the single-particle spin-orbitals, the Hartree-Fock method emerges [32, 34]. In this context we will provide a very brief description of the Hartree-Fock method, to define the physical approximation and the related equations for the orbital polarization corrections.

At self-consistency the Hartree-Fock wave function  $\Psi_{\text{HF}}$  is the Slater determinant of single particle states. The Hartree-Fock energy is determined:

$$E^{\text{HF}} = T^{\text{HF}} + U^{\text{HF}} + W^{\text{HF}}, \quad (2.27)$$

where  $T^{\text{HF}}$  is the expectation value of the operator  $\hat{t}$ , and  $U^{\text{HF}}$  is the expectation value of  $\hat{u}$  using the Hartree-Fock wave function:

$$T^{\text{HF}} = \langle \Psi_{\text{HF}} | \hat{t} | \Psi_{\text{HF}} \rangle, \quad U^{\text{HF}} = \langle \Psi_{\text{HF}} | \hat{u} | \Psi_{\text{HF}} \rangle. \quad (2.28)$$

The Hartree-Fock electron-electron interaction energy  $W^{\text{HF}}$  can be written as:

$$\begin{aligned} W^{\text{HF}} = & \frac{e^2}{2} \sum_{kk'}^{\text{occ}} \int d^3r d^3r' \frac{\phi_k^\dagger(\mathbf{x}) \phi_k(\mathbf{x}) \phi_{k'}^\dagger(\mathbf{x}') \phi_{k'}(\mathbf{x}')}{|\mathbf{r} - \mathbf{r}'|} - \\ & - \frac{e^2}{2} \sum_{kk'}^{\text{occ}} \int d^3r d^3r' \frac{\phi_k^\dagger(\mathbf{x}) \phi_{k'}(\mathbf{x}) \phi_{k'}^\dagger(\mathbf{x}') \phi_k(\mathbf{x}')}{|\mathbf{r} - \mathbf{r}'|}. \end{aligned} \quad (2.29)$$

Here  $k$  and  $k'$  sums run over all occupied single-particle states  $\phi$ , an asterisk denotes complex conjugation and  $\phi_k^\dagger(\mathbf{x}) \phi_k(\mathbf{x}) = \sum_{\sigma} \phi_k^*(\mathbf{r}, \sigma) \phi_k(\mathbf{r}, \sigma)$ .

It can be seen that the first term in (Eq.2.29), which in DFT in sloppy manner is called the Hartree energy, is equivalent to the classical Coulomb interaction between two charge densities. The second term has no classical equivalent and is called HF-exchange energy. In DFT the definition of exchange energy is slightly different, as it is the same summation of integrals but using the Kohn-Sham-Dirac (KSD) single-particle states instead of the Hartree-Fock states. In this context, when referring to exchange energy, it will be the KSD exchange energy. So that, the Hartree and exchange interaction energy functional, using KSD bispinors  $\psi_k$ , is given by:

$$\begin{aligned} W^{\text{HF}} = & \frac{e^2}{2} \sum_{kk'} n_k n_{k'} \int d^3r d^3r' \frac{\bar{\psi}_k(\mathbf{r}) \psi_k(\mathbf{r}) \bar{\psi}_{k'}(\mathbf{r}') \psi_{k'}(\mathbf{r}')}{|\mathbf{r} - \mathbf{r}'|} - \\ & - \frac{e^2}{2} \sum_{kk'} n_k n_{k'} \int d^3r d^3r' \frac{\bar{\psi}_k(\mathbf{r}) \psi_{k'}(\mathbf{r}) \bar{\psi}_{k'}(\mathbf{r}') \psi_k(\mathbf{r}')}{|\mathbf{r} - \mathbf{r}'|}, \end{aligned} \quad (2.30)$$



with  $\bar{\psi}_k = \psi_k^\dagger \gamma^0$ . Furthermore, the Hartree-Fock interaction has to give leading contribution to the current-field interaction term, therefore we can conclude that the HF four-potential can be presented with a scalar potential, namely as  $\hat{A}_\mu^{\text{HF}} = (\hat{V}^{\text{HF}}, 0)$ .

## 2.5 Correlation interaction

In the context of many-particle physics, the word correlation is used in a narrower meaning and is reserved for particle correlation due to interaction and beyond exchange. For interacting systems, both exchange and correlation contribute to the total energy. Therefore, the Hartree-Fock energy is not the correct ground state energy, as one Slater determinant does not provide enough variational freedom to expand the entire Hilbert space of a set of fully interacting fermions. The difference between the exact ground state energy and the Hartree-Fock energy is called as correlation energy in quantum chemistry:

$$E^C = E^{\text{EXACT}} - E^{\text{HF}}. \quad (2.31)$$

There is a good interpretation of why the correlation energy is always negative. The mathematical reason is the variational argument; Further variational freedom must lower the energy compared with the HF energy. A physical interpretation of this is that the Hartree-Fock method relaxes each one-electron orbital in the mean field of the other electrons and the energy is then calculated as an integral over these orbitals. In reality two electrons in overlapping orbitals will with great force push each other away if they get too close. This depletion in the electron density in the vicinity of (increased density further away from) any electron is referred to as the correlation hole. The electrons are thus on the average a little further apart than estimated by the HF method. This lowers their repulsive energy, thus the exact energy should be lower than the HF energy. There is also an enhancement of kinetic energy by correlated motion. The Schrödinger variational principle ensures nevertheless, that the total energy is lowered by correlation.

Whereas all other quantities discussed so far are easy to obtain (in the sense that they are well defined and can be found for a medium sized system in relatively short time on a computer), the correlation energy is a very difficult quantity to calculate. This is because the correlation energy is so directly related to the degrees of freedom in Hilbert space which can not be spanned by the single Slater determinant. The large majority of wave function methods tries to span the Hilbert space by introducing multiple Slater determinants and including the unoccupied Hartree-Fock one-electron orbitals in this expansion. The ultimate goal of this would be to give a correct representation of the full electronic wave function. The wave function of  $N$  electrons in the Born-Oppenheimer approximation in which the nuclei are fixed at their positions,

can be read as a  $3N$  dimensional complex function with  $N$  bispinor indices. The multi-dimensional search of such a wave function is prohibitively expensive from a computational point of view for even very small systems. This is the motivation for looking at density functional theory.

Since the correlation energy shall contribute to the current-field interaction term, in the variation of the four-current density the correlation four-potential  $A_\mu^C = (V^C, \mathbf{A}^C)$  emerges as a functional derivative to the correlation energy functional.

## 2.6 Kohn-Sham-Dirac equation

Taking the Hartree-Fock (HF) expression for  $k$  in (Eq.2.25) yields:

$$k[\psi_k, n_k] = \sum_k n_k \langle \psi_k | -ic\boldsymbol{\alpha} \cdot \boldsymbol{\nabla} + \beta c^2 | \psi_k \rangle + W^{\text{HF}}, \quad (2.32)$$

and the local spin density approximation  $E^C[J^\mu]$  for  $\mathcal{L}$ . This decision is motivated by the idea that the spin polarization is more directly related to the fermionic symmetry than the orbital polarization. After variation of (Eq.2.25) we arrive at the KSD equation,

$$\left[ -ic\boldsymbol{\alpha} \cdot \boldsymbol{\nabla} + \beta c^2 - ec\beta\gamma^\mu (A_\mu + \delta_\mu^0 \hat{A}^{\text{HF}} + A_\mu^C) \right] \psi_k = \psi_k \varepsilon_k, \quad (2.33)$$

where  $-ec(\hat{A}^{\text{HF}}\psi_k)(\mathbf{r}) = (\hat{V}^{\text{HF}}\psi_k)(\mathbf{r})$  is the HF potential operator, and

$$-eA_\mu^C(\mathbf{r}) = \frac{\delta E^C[J^\mu]}{\delta J^\mu(\mathbf{r})}, \quad (2.34)$$

is the correlation four potential. To get rid of the nasty vector potential, we apply Gordon's decomposition of the three-current density  $\mathbf{J}$  figuring in  $J^\mu = (cn, \mathbf{J})$  and in the stationary situation may be written as:

$$\mathbf{J} = \mathbf{I} + \boldsymbol{\nabla} \times \mathbf{S}, \quad (2.35)$$

with the orbital current density

$$\mathbf{I}(\mathbf{r}) = \sum_k n_k \left( -\text{Re}(\bar{\psi}_k(\mathbf{r}) i \boldsymbol{\nabla} \psi_k(\mathbf{r})) + \mathbf{A}(\mathbf{r}) \bar{\psi}_k(\mathbf{r}) \psi_k(\mathbf{r}) \right), \quad (2.36)$$

and the spin density,

$$\mathbf{S} = \frac{1}{2} \sum_k n_k \bar{\psi}_k \boldsymbol{\Sigma} \psi_k, \quad \boldsymbol{\Sigma} = \begin{pmatrix} \boldsymbol{\sigma} & 0 \\ 0 & \boldsymbol{\sigma} \end{pmatrix}. \quad (2.37)$$

The total stationary current density  $\mathbf{J}$  must have zero divergence due to charge conservation. Since the divergence of the spin current density vanishes

by its very structure as a curl, the orbital current density must also be divergence free:  $\nabla \cdot \mathbf{I} = 0$ . Once more we take the advantage of including our system in a finite torus  $\mathbf{T}^3$ , with periodic boundary conditions: the charge flux through its surface is zero, such that  $\mathbf{I}$  vanishes there. As a consequence it may be expressed as a curl of some vector field  $\mathbf{L}$ , to be visualized as an “angular momentum density”:

$$\mathbf{I} = (1/2) \nabla \times \mathbf{L}. \quad (2.38)$$

Recall that an orbital angular momentum density cannot really figure in quantum mechanics because, due to Heisenberg uncertainty principle, position and momentum cannot be simultaneously measured at the same time. Accordingly, above equation defines  $\mathbf{L}$  only up to an arbitrary additive gradient term. The total current density may then be expressed as:

$$-e\mathbf{J} = \frac{1}{\mu_0} \nabla \times \mathbf{m} = -\frac{e}{2} \nabla \times (\mathbf{L} + 2\mathbf{S}), \quad (2.39)$$

where  $\mathbf{m}$  has the dimension of a magnetization density, related in a non-renormalized way to the angular momenta by the Bohr magneton ( $\mu_B = \mu_0 e/2$ ). Note that except for the non-relativistic case, the decomposition of the current given above is formal, which is also indicated by the appearance of ideal gyro-magnetic factors. Moreover, what was said above on the ‘angular momentum density’ refers likewise to the orbital part of the magnetization density.

The four-current density is now given by  $J^\mu = (nc, -\nabla \times \mathbf{m}/e)$ , and hence the functional  $E^C[J]$  may be rewrite as a functional  $E^C[n, \mathbf{m}]$ , which it yields the mechanical correlation potential acting on an electron:

$$V^C = cA_0^C = \frac{\delta E^C[J^\mu]}{\delta J^0(\mathbf{r})}, \quad (2.40)$$

and the magnetic correlation field:<sup>2</sup>

$$\begin{aligned} \mu_0 \mathbf{H}^C &= \nabla \times \mathbf{A}^C(\mathbf{r}) = \int d^3 r' \delta(\mathbf{r}' - \mathbf{r}) \nabla' \times \mathbf{A}^C(\mathbf{r}') = \\ &= - \int d^3 r' [\nabla' \delta(\mathbf{r}' - \mathbf{r})] \times \mathbf{A}^C(\mathbf{r}') = \\ &= \int d^3 r' e \mu_0 \frac{\delta \mathbf{J}(\mathbf{r}')}{\delta \mathbf{m}(\mathbf{r})} \frac{\delta E^C}{\delta \mathbf{J}(\mathbf{r}')} \frac{1}{e} = \mu_0 \frac{\delta E^C}{\delta \mathbf{m}(\mathbf{r})}. \end{aligned} \quad (2.41)$$

So that finally we can obtain:

$$-eA_\mu^C(\mathbf{r}) = \frac{\delta E^C[J^\mu]}{\delta J^\mu(\mathbf{r})} \implies \mathbf{H}^C(\mathbf{r}) = \frac{\delta E^C}{\delta \mathbf{m}(\mathbf{r})}, \quad (2.42)$$

---

<sup>2</sup>Writing (Eq.2.39) formally as  $-e\mu_0 \mathbf{J}(\mathbf{r}') = \int d^3 r \delta(\mathbf{r}' - \mathbf{r}) \nabla \times \mathbf{m}(\mathbf{r})$ , it finds  $-e\mu_0 \delta \mathbf{J}(\mathbf{r}')/\delta \mathbf{m}(\mathbf{r}) = \delta(\mathbf{r}' - \mathbf{r}) \nabla \times = -[\nabla \delta(\mathbf{r}' - \mathbf{r})] \times = [\nabla' \delta(\mathbf{r}' - \mathbf{r})] \times$ .

where  $\mathbf{H}^C(\mathbf{r})$  is a local field and it is simply a function of the position  $\mathbf{r}$ . However, it depends also functionally on  $\mathbf{m}$ , possibly in a most non-local way. This yields the alternative KSD equation:

$$\begin{aligned} & \left[ -ic\boldsymbol{\alpha} \cdot \nabla + \beta c^2 + V(\mathbf{r}) + \hat{V}^{\text{HF}} + V^C(\mathbf{r}) \right] \psi_k(\mathbf{r}) - \\ & - \frac{\beta}{n_k} \int d^3r' \left( \mathbf{H}(\mathbf{r}') + \mathbf{H}^C(\mathbf{r}') \right) \cdot \frac{\delta \mathbf{m}(\mathbf{r}')}{\delta \bar{\psi}_k(\mathbf{r})} = \psi_k(\mathbf{r}) \varepsilon_k, \end{aligned} \quad (2.43)$$

where  $V(\mathbf{r})$  and  $\mathbf{H}(\mathbf{r})$  are possible external potential and external field, respectively, and

$$\frac{\delta \mathbf{m}(\mathbf{r}')}{\delta \bar{\psi}_k(\mathbf{r})} = -\mu_B \left( \frac{\delta \mathbf{L}(\mathbf{r}')}{\delta \bar{\psi}_k(\mathbf{r})} + n_k \delta(\mathbf{r}' - \mathbf{r}) \boldsymbol{\Sigma} \psi_k(\mathbf{r}) \right). \quad (2.44)$$

Here, we have to cope with the HF operator and with the non-local term  $\delta \mathbf{L}(\mathbf{r}')/\delta \bar{\psi}_k(\mathbf{r})$ . The HF operator can in most cases be replaced by the approved LSDA approximation,  $\hat{V}^{\text{HF}} \approx V^{\text{H}}(\mathbf{r}) + V_{ss'}^{\text{X}}(\mathbf{r})$ , where  $V^{\text{H}}$  is the Coulomb potential of the electron charge density (which includes the self-interaction of orbitals) and  $V^{\text{X}}$  is the LSDA exchange potential spin matrix:

$$V_{ss'}^{\text{X}}(\mathbf{r}) = V^{\text{X}}(\mathbf{r}) + \mu_B \mathbf{H}^{\text{X}}(\mathbf{r}) \cdot \beta \boldsymbol{\Sigma}. \quad (2.45)$$

With the above approximations, the scalar  $V^{\text{X}}$  may be again combined with  $V^C$  into the LSDA expression for  $V^{\text{XC}}$  and the action of  $\mathbf{H}^{\text{X}}$  may be combined with the action of  $\mathbf{H}^C$  on the spin part of  $\mathbf{m}$  into the LSDA expression  $\mu_B \mathbf{H}^{\text{XC}}(\mathbf{r}) \cdot \beta \boldsymbol{\Sigma} \psi_k(\mathbf{r})$ .

This is known to work well except for the cases of strong local correlation, and except for the semiconductor gap problem in which corrections to the scalar exchange potential  $V^{\text{X}}$  must be introduced. In the rest of the  $\mathbf{H}^C$  expression, the magnetization density  $\mathbf{m}$  has to be replaced with  $-\mu_B \mathbf{L}$ , the remaining term which is not contained in the LSDA expression. Corrections to  $V^{\text{XC}}$  and  $\mathbf{H}^{\text{XC}}$  are included into the full KSD equation:

$$\begin{aligned} & \left[ -ic\boldsymbol{\alpha} \cdot \nabla + \beta c^2 + V(\mathbf{r}) + V^{\text{H}}(\mathbf{r}) + V^{\text{XC}}(\mathbf{r}) + \mu_B \beta \boldsymbol{\Sigma} \cdot (\mathbf{H} + \mathbf{H}^{\text{XC}}) \right] \psi_k(\mathbf{r}) - \\ & - \mu_B \frac{\beta}{n_k} \int d^3r' \left( \mathbf{H}(\mathbf{r}') + \mathbf{H}^C(\mathbf{r}') \right) \cdot \frac{\delta \mathbf{L}(\mathbf{r}')}{\delta \bar{\psi}_k(\mathbf{r})} = \psi_k(\mathbf{r}) \varepsilon_k. \end{aligned} \quad (2.46)$$

According to (Eq.2.38), the angular momentum density  $\mathbf{L}(\mathbf{r})$  is a gauge freedom vector field. The crucial problem remaining is to find a suitable expression for  $\frac{\delta \mathbf{L}(\mathbf{r}')}{\delta \bar{\psi}_k(\mathbf{r})}$ , which it has to described properly the orbital magnetism of the considered system. In the next chapter, a quasi-local functional expression for  $\mathbf{L}[\psi_k]$  will be provided.

## 2.7 The local density approximation

The relativistic density functional theory presented above is exact in principle, however the density functionals  $E^{\text{XC}}[n(\mathbf{r})]$  and  $V^{\text{XC}}[n(\mathbf{r})]$ , in which all complications of the many-particle problem are hidden, are not exactly known and must be approximated. The widespread use of density functional based calculation of physical and chemical properties arises from the fact that approximations for  $E^{\text{XC}}$  and  $V^{\text{XC}}$  have been found which are both simple and accurate enough for practical applications.

A rather simple and remarkably good approximation for inhomogeneous system is the so-called local density approximation (LDA), where it replaces the exact functional  $E^{\text{XC}}$  by

$$E^{\text{XC}}[n] \approx E_{\text{LDA}}^{\text{XC}}[n] = \int n(\mathbf{r}) \varepsilon_{\text{LDA}}^{\text{XC}}(n(\mathbf{r})) d\mathbf{r}, \quad (2.47)$$

where  $\varepsilon_{\text{LDA}}^{\text{XC}}(n)$  is a function of density. This function is used in above equation locally at each point  $\mathbf{r}$  with the value  $n = n(\mathbf{r})$  of the density at this point. The LDA states for regions of a material where the charge density is slowly varying, the exchange-correlation energy at that point can be approximated by that expansion, what is derived for a locally uniform electron gas with the same charge density. The function  $\varepsilon_{\text{LDA}}^{\text{XC}}(n(\mathbf{r}))$  can be spilt into two terms, exchange ( $\varepsilon^{\text{X}}$ ) and correlation ( $\varepsilon^{\text{C}}$ ). The exchange part is given by

$$\varepsilon^{\text{X}}(n) = -\frac{3}{4} \left( \frac{3}{\pi} \right)^{1/3} n^{1/3}, \quad (2.48)$$

and can be obtained by the Hartree-Fock method, which neglects correlation, but includes exchange. The exchange potential in KSD equations follows from the previous equation:

$$V^{\text{X}}(n) = -\left( \frac{3}{\pi} \right)^{1/3} n^{1/3}. \quad (2.49)$$

The polarization dependence of  $\varepsilon_{\text{LDA}}^{\text{XC}}$  is more difficult to calculate. Following a suggestion of U. von Barth and L. Hedin [35], the spin polarization dependence of the exchange and correlation energy of the homogeneous electron liquid is generally interpolated between the paramagnetic ( $\xi = 0$ ) and the saturated ferromagnetic ( $\xi = 1$ ) cases and can be approximated by:

$$\varepsilon^{\text{XC}}(n, \xi) \approx \varepsilon^{\text{XC}}(n, 0) + [\varepsilon^{\text{XC}}(n, 1) - \varepsilon^{\text{XC}}(n, 0)] f(\xi), \quad (2.50)$$

where  $\xi$  is the relative spin polarization degree and is given by:

$$\xi = \frac{n(\uparrow) - n(\downarrow)}{n} = \frac{2S_z}{n}, \quad (2.51)$$

where  $n(\uparrow)$  and  $n(\downarrow)$  denote the up and down spin densities and  $S_z$  is the spin magnetization density, which in collinear approximation is assumed to aligned

in  $z$ -direction. The  $f(\xi)$  is the von Barth-Hedin interpolation function and it is given by:

$$f(\xi) = \frac{(1 + \xi)^{\frac{4}{3}} - (1 - \xi)^{\frac{4}{3}} - 2}{2^{\frac{4}{3}} - 2}, -1 \leq \xi \leq 1. \quad (2.52)$$

Most accurate results for the correlation part have been obtained by quantum Monte Carlo method [36] and reliable parameterizations for these results are available in [37, 38, 39].

Although the local density approximation is extremely simple, it is surprisingly accurate and forms the core of most modern DFT codes. It even works reasonably well in systems where the charge density is rapidly varying. However it tends to under-predict atomic ground state energies, ionization energies, and it gives too short bond lengths.

## 2.8 RDFT and orbital magnetism

In this section we provide arguments that how RDFT can be related to the orbital magnetism. Novel phenomena caused by strong coupling among spin, orbital, and lattice degrees of freedom are the central issue in the physics of solid state in the last few years. One of the modes, when this coupling is mediated by relativistic spin-orbit interaction leads to the orbital magnetism, which is manifested into different fields of study such as, the magneto-crystalline anisotropy, magneto-optical effects, magnetic x-ray circular dichroism (XMCD), etc.

In 1929, P.A.M. Dirac himself thought that relativistic effects would be "of no importance in the consideration of atomic and molecular structure" [40], because the average valence-electron speeds are small. As it is discussed by P. Pyykkö, Dirac's argument was wrong for two reasons [41]: (i) The valence  $s$  and  $p$  electrons do have high speeds close to the nucleus. Due to mass enhancement, their shell radii shrink and speeds are increased. Since relativistic effects are in lowest order proportional to  $v^2/c^2$   $Z^2/c^2$ , Dirac's argument considering the average speed is invalid. (ii) The shrinking of  $s$  and  $p$  shell radii leads to a more effective screening of the nuclear potential. Thus, the  $d$  and  $f$  states, possessing low weight in the inner regions of the atom, are destabilized. One should add (iii), that relativistic spin-orbit coupling is the origin of Hund's third rule. To give a few examples for the importance of relativistic effects on the valence electronic structure [6], we note the following facts:

1- Due to the relativistic  $s$  and  $p$  shrinking, the energy level of  $4f$  states in lanthanide atoms or localized- $4f$  solids are raised by 5 eV, in comparison to the  $6s$  states. In the early actinide atoms this energy shift ( $5f$  vs.  $7s$ ) is in the order of 9 eV.

2- "Non-relativistic" gold would be white, like silver.

3- The single-particle spin-orbit coupling is considerably large in the lanthanide  $4f$  shell (0.5 ... 1 eV) while in the actinide  $5f$  shell (1 ... 2 eV).

Let us consider the question, how orbital magnetism comes into play in the case of localized  $4f$  states. The spin-orbit coupling in the lanthanide  $4f$  shell is stronger than the exchange field originating from the spatial overlap between  $4f$  and  $5d$  charge densities [6]. Thus, the total angular momentum  $J$  of the  $4f$  core shell is a good quantum number and therefore more or less an atomic picture will be arise. In this picture, a large total orbital moment is figured in the atomic shells with more than one electron or hole.

The situation is different for itinerant  $3d$  states. Here, the exchange and the ligand fields (including band dispersion by hybridization) are much stronger than the spin-orbit coupling which acts merely as a perturbation. The spin polarization breaks the time reversal symmetry and orbital moment occurs which is still small ( $\sim 0.1\mu_B$  /atom).

The most complicated case is presented by the itinerant  $5f$  states of light actinide where the spin-orbit coupling and the spin splitting are of the same order of magnitude. Thereby, large spin and orbital moments are observed, which partially compensate each other. The fact that the band dispersion is smaller than in  $3d$  metals, gives reason for a quite subtle interplay between lattice and magnetic structure that results, for example, in a frequent occurrence of non-collinear magnetic ground states [42].

From these arguments, orbital moment ordering is a relativistic effect in any case. Hence, the non-relativistic DFT cannot be expected to serve as a sound basis for the consideration of orbital magnetism and its relativistic generalization is necessary. In the framework of LSDA, the ordinary density functional theory does not provide any term that could lead to the formation of an orbital moment. Current and spin density functional theory [12] would provide a natural starting point for the description of orbital magnetism.





## Chapter 3

# Orbital polarization corrections

Magnetic dipoles or magnetic moments can often result on the atomic scale due to the movements of electrons. In an atom each electron has magnetic moments that originate from two sources. The first is the orbital motion of the electron around the nucleus. In a sense this motion can be considered as a current loop, which results in a magnetic moment along its axis of rotation. The second source of electronic magnetic moment is due to a quantum mechanical property called *spin*.

In an atom the orbital magnetic moments of some electron pairs cancel each others. The same is true for the spin magnetic moments. The total magnetic moment of the atom is thus the sum of all magnetic moments of its individual electrons, accounting for moment cancellation between properly paired electrons. For the case of a completely filled electron shell or subshell, the magnetic moments completely cancel each other. Thus only atoms with partially filled electron shells have magnetic moment. The magnetic properties of materials are in large part determined by the nature and magnitude of the atomic magnetic moments.

In hydrogenic atoms the possible interaction is the Coulomb interaction between the nucleus and the electron and it is the origin of the internal motion for the electron in the hydrogenic atom. One should note that due to the Heisenberg uncertainty principle, the motion of the electron cannot be established by its position and speed, simultaneously. However, in the classical physics, one can assume an electron as a charged particle in a circular orbit is like a current loop, where the current is the charge times the frequency of the orbit:  $I = qf$ . This current loop creates a magnetic moment whose magnitude is the current times the area of the loop:  $M = IA = \pi r^2 qf$ , where  $r$  is the radius of the orbit. The angular momentum of the electron orbit is defined as,  $L = m_e r v = 2\pi m_e r^2 f$ , where  $v$  is the speed of electron. So that the orbital moment of this "classical" electron is given by,

$$M_l = \frac{q}{2m_e} L. \quad (3.1)$$

Recall that the spin and orbital moments of the electrons are quantized, and above equation also has to be quantized. Since the electron has negative charge, we expect the direction of orbital magnetic moment to be opposite to that of  $L$ .

We know that in atomic physics the total moment is a sum of spin and orbital contributions. As it was discussed the orbital moment results, in a classical picture, from the orbital motion of the electron around the nucleus. Compared to the situation in a free atom, where the orbital moment can be even larger than the spin moment, in a solid this motion is of course restricted in presence of other atoms. Hund's second rule predicts in atoms maximum orbital angular momentum  $L$  compatible with maximum spin multiplicity. As it is known, the orbital moments of atoms more or less are quenched when incorporated into a crystal. The main reason is that the delocalization of the electrons due to the overlap of the wavefunctions with the neighboring atoms. The delocalization leads to a reduction of the kinetic energy and is an important contribution to the binding energy of the crystals. The hybridization of the electron orbitals with the neighboring atoms causes a broadening of the atomic energy levels to bands. In most cases the bandwidth is larger than the relatively small energies governed by Hund's second rule. Then, in contrast with an atom, all  $m_l$ -states may be occupied with equal probability in a solid. Therefore the orbital moments may reduce in the solid. A second reason for the suppression of the orbital moments is the symmetry reduction of the ligand-field potential induced by the presence of neighboring atoms. The total potential acting on the electrons in the crystal has thus a lower symmetry than in an atom. Then the orbital angular momentum  $L$  is not an appropriate symmetry operator to calculate the related orbital moments (azimuth quantum numbers  $l$  are not good quantum numbers). The eigenfunctions must be labeled according to the irreducible representations of the symmetry group of the crystal, which in general have low dimensions. Thus, in these irreducible representations the related orbital moments are strongly reduced or even totally quenched. Such intrinsic differences between atomic and bulk behaviors are characteristic for systems developing itinerant-electron magnetism. Consequently, investigations of orbital magnetism on the way from the atom to the solid are prime important. As it was discussed, current density functional theory can provide a practical way to achieved properly the individual orbital and spin moments in the considered solid, what is subject of this context.

### 3.1 Definition of spin and orbital moments in DFT

The spin density is well defined in relativistic spin-DFT. Using (Eq.2.37), one can define the total spin moment in a collinear system which is simply read as

an integral over spin density  $\mathbf{S}$ :

$$\mathbf{M}_s = \int_V 2 \mathbf{S}(\mathbf{r}) d^3r = \int (n^\uparrow(\mathbf{r}) - n^\downarrow(\mathbf{r})) d^3r, \quad (3.2)$$

where  $n^\uparrow$  ( $n^\downarrow$ ) stands for spin up (down) density. However this quantity is comparable with those values obtain in experiments. The  $\mathbf{M}_s$  value depends of course on the quality of the XC potential (LSDA) that is used for an actual calculation. The spin magnetization density  $\mathbf{S}(\mathbf{r})$ , is clearly a consequence of the imbalance of electrons with spin-up or spin-down and therefore, the quantity defined in equation above is called spin moment.

From relativistic DFT, first term in KSD equation (Eq.2.46) contains spin-orbit coupling implicitly, which provides a mechanism that leads to orbital magnetism. The electron, traveling on a classical trajectory around the nucleus, experiences the magnetic field originates from the screened nucleus. This field couples to the magnetic (spin) moment of electron and thus, leads to a preferential orientation of orbital motion. In analogy with (Eq.3.2), the total orbital moment can be defined as an integral over orbital density  $\mathbf{L}(\mathbf{r})$ ,

$$\mathbf{M}_l = \int_V d^3r \mathbf{L}(\mathbf{r}), \quad (3.3)$$

where  $\mathbf{L}$  is introduced in (Eq.2.38) and the integration extends over the total volume of the sample. The provided  $\mathbf{L}$  vanishes on the boundary of the range of integration  $V$  and contains a large gauge freedom.

It has to be pointed out that the calculated orbital moments in the framework of LSDA are typically too small compared with experiment [21, 42, 43, 44, 45, 46]. Besides many limitations of the LSDA caused by the homogeneous electron gas picture for exchange and correlation energies, the failure may imply an even more functional problem in this approximation. Based on LSDA in the spin-DFT, the total energy  $E_{\text{LSDA}}[n(\mathbf{r}), \mathbf{m}_s(\mathbf{r})]$  is the explicit functional of the charge  $n(\mathbf{r})$  and the spin magnetization  $\mathbf{m}_s(\mathbf{r})$  densities. Even if an exact SDFT was able to include all magnetic orbital effects implicitly, there is no guarantee that the orbital-related quantities can be reproduced explicitly on the level of fictitious single-particle Kohn-Sham-Dirac equations. The explicit formulation for orbital magnetism gave rise to the concept of orbital polarizations (OP) in band structure calculations. The purpose of this chapter is to clarify the fundamental feature, origins OP in the problem of orbital magnetism.

## 3.2 Semi-empirical orbital polarization correction

In order to improve the small orbital moments calculated in the LSDA, an *ad hoc* orbital polarization correction was suggested by M.S.S. Brooks [19] in

1985. An extended version was proposed by O. Eriksson *et al.* [20, 21]. In this context it is called as OPB scheme. They put forward an idea to connect the OPB entirely with Hund's second rule. The concept of OPB, empirically is taken from the theory of open shell atoms within the Russell-Saunders coupling, where it is responsible for Hund's second rule. It is proposed an ansatz for OPB functional, which is based on two assumptions: (i) OPB is proportional to  $\mathbf{M}_l^2$ ; (ii) it is derived by Racah parameter  $I^{\text{Racah}}$  [54, 55]. The expectation value  $\mathbf{M}_l$  and the atomic  $I^{\text{Racah}}$  values can calculate self consistently from the KS orbitals including the effects of the OPB functional. The OPB correction has attracted considerable attention in the computational electronic structure community because of its simplicity and relatively encouraging results obtained along this line for several classes of metallic compounds (see for instance [21, 47, 48, 49, 50, 51, 52, 53], and upcoming chapters).

The energy functional OPB can be added to the total LSDA exchange-correlation energy functional and is given by,

$$E^{\text{OPB}} = -\frac{1}{2} \sum_{\sigma} I_{\sigma}^{\text{Racah}} \mathbf{M}_{l\sigma}^2, \quad (3.4)$$

where  $\mathbf{M}_{l\sigma}$  is the orbital moment of the spin- $\sigma$   $d(f)$ -subshell. We use spin dependent orbital moment  $\mathbf{M}_{l\sigma}$  instead of  $\mathbf{M}_l$ . One should note that for  $\mathbf{M}_{l\sigma}$  only one spin channel will be considered at a time due to Hund's first rule. The Racah parameters for  $3d$  and  $4f$  electrons are called  $B$  and  $E^3$ , respectively. The Racah parameters can be expressed in terms of integrals over the single particle wave-functions and are recalculated for each iteration step. They gain following expressions:

$$I^{\text{Racah}}(3d) = B_{\sigma} = (9F_{\sigma}^2 - 5F_{\sigma}^4)/441, \quad (3.5)$$

$$I^{\text{Racah}}(4f) = E_{\sigma}^3 = \left( \frac{5}{225} F_{\sigma}^2 + \frac{6}{1089} F_{\sigma}^4 - \frac{91}{7361.64} F_{\sigma}^6 \right), \quad (3.6)$$

where  $F_{\sigma}^k$  are called Slater integrals and given by:

$$F_{\sigma}^k = \int dr_i r_i^2 \int dr_j r_j^2 \Phi_{\sigma}^2(r_i) \frac{r_{<}^k}{r_{>^{k+1}}} \Phi_{\sigma}^2(r_j), \quad (3.7)$$

where  $r_{<} = \min(r_i, r_j)$  and  $r_{>} = \max(r_i, r_j)$  and  $\Phi_{\sigma}$  are radial part of  $3d$  or  $4f$  atomic wave functions [32, 56, 57].

Applying this energy functional to solids one can find that it leads to energy shifts for the single particle states with different magnetic quantum numbers  $m_l$ , according to:

$$v_{m_l}^{\text{OPB},\sigma} = \delta E^{\text{OPB}} / \delta n_{m_l}^{\sigma} = -I^{\text{Racah}} M_{l\sigma} m_l, \quad (3.8)$$

where  $n_{m_l}^{\sigma}$  are the occupation numbers for the  $m_l$  states with the spin characters  $\sigma$ .

It has to be mentioned that there are some discrepancies for the OPB approach. For instance, if one apply the OPB correction to actinide compounds, the evaluated orbital moments are overestimated compared with experiment [58]. A second argument follows from the fact that the OPB is a semi-empirical correction and there is no direct improvement for this scheme based on the basis of DFT. For this latter problem, an effective justification of OP corrections in the framework of relativistic density functional theory will be given in the next section.

### 3.3 Orbital polarization energies in KSD theory

In the previous section, a semi-empirical OP correction was discussed where an empirical OP correction was added to the total energy functional. However, it was also mentioned that so far, density functional theory has been lacking a deeper theoretical basis of orbital polarization. In this section, a systematic derivation of orbital polarization corrections from four-current density functional theory is presented. The formulation is an extension to the early work of H. Eschrig *et al.* [23] and the evaluated correction is called OPE.

In the previous chapter, the KSD equation was introduced in its complete form. The last integral gained in the KSD equation (Eq.2.46) contributes to the orbital polarization corrections:

$$\mu_B \frac{\beta}{n_k} \int d^3 r' \left( \mathbf{H}(\mathbf{r}') + \mathbf{H}^C(\mathbf{r}') \right) \cdot \frac{\delta \mathbf{L}(\mathbf{r}')}{\delta \bar{\psi}_k(\mathbf{r})}. \quad (3.9)$$

The first part (external field) is the diamagnetic term, and the second is the correlation term. In the following we skip the diamagnetic term. The spin polarization dependence of the correlation energy  $\varepsilon^C$  in LSDA was suggested by U. von Barth and L. Hedin [35] with an interpolation between the paramagnetic ( $\xi = 0$ ) and the saturated ferromagnetic ( $\xi = 1$ ) cases. The resulted expression can be approximated via (Eq.2.50):

$$\varepsilon^C(n, \xi) = \varepsilon^C(n, 0) + [\varepsilon^C(n, 1) - \varepsilon^C(n, 0)] f(\xi). \quad (3.10)$$

Within 2 % accuracy in a relevant range of spin polarization degree ( $-0.4 \leq \xi \leq 0.4$ ), the von Barth-Hedin interpolation function can be approximated according to:

$$f(\xi) \approx 0.855 \xi^2. \quad (3.11)$$

In the framework of LSDA, the correlation energy functional has the following form:

$$E^C = \int d^3 r \, n \, \varepsilon^C(n, \xi). \quad (3.12)$$

According to (Eq.2.42), the spin correlation field in SDFT and in collinear LSDA can be evaluated as:

$$\mathbf{H}_z^{C,S}(\mathbf{r}) = \frac{\delta E^C}{\delta \mathbf{m}_S} = \frac{\delta E^C}{\delta(n\xi)} \frac{\mathbf{m}_S}{|\mathbf{m}_S|} = \frac{\partial \varepsilon^C(n, \xi)}{\partial \xi} \frac{\mathbf{m}_S}{|\mathbf{m}_S|} = F(n(\mathbf{r})) 2\mathbf{S}_z(\mathbf{r}), \quad (3.13)$$

where  $\mathbf{m}_S = 2\mathbf{S}_z(\mathbf{r})$  and  $\mathbf{S}_z(\mathbf{r})$  is the spin density, in the  $z$ -direction. The function  $F(n)$  in the basis of the LSDA is given by:

$$F(n) = 2 \frac{\varepsilon^C(n, 1) - \varepsilon^C(n, 0)}{n}. \quad (3.14)$$

In the spirit of CDFT, where  $\mathbf{m} = \mathbf{m}_S + \mathbf{m}_L = -\mu_B(\mathbf{L} + 2\mathbf{S})$ , we can split  $\mathbf{H}^C(\mathbf{r})$  into its orbital and spin components, namely  $\mathbf{H}^C(\mathbf{r}) = \mathbf{H}^{C,L}(\mathbf{r}) + \mathbf{H}^{C,S}(\mathbf{r})$ . Therefore in analogy with (Eq.3.13), the orbital correlation field may be read as:

$$\mathbf{H}_z^{C,L}(\mathbf{r}) = F(n(\mathbf{r}))\mathbf{L}_z(\mathbf{r}), \quad (3.15)$$

and one can get the orbital correlation term,

$$\mu_B \frac{\beta}{n_k} \int d^3r' \left( \mathbf{H}^{C,S}(\mathbf{r}') + \mathbf{H}^{C,L}(\mathbf{r}') \right) \cdot \frac{\delta \mathbf{L}(\mathbf{r}')}{\delta \bar{\psi}_k(\mathbf{r})}. \quad (3.16)$$

Although the derivations up to here were fully relativistic, at the end we are mainly interested in leading contributions of zeroth order in  $1/c$ . All the following expressions related to OP are understood in this non-relativistic limit. The KSD equation includes automatically the kinematic spin-orbit coupling. In this limit, the directions in spin and orbital spaces are decoupled, and hence no vector coupling between spin and orbital quantities should appear in the non-relativistic KS equation. Hence, for the full non-local and non-collinear theory we demand  $\int d^3r \mathbf{H}^{C,S}(\mathbf{r}) \cdot \mathbf{L}(\mathbf{r}) = 0$  in leading order in powers of  $1/c$ . In view of (Eq.3.13) and (Eq.3.15) this implies,

$$(\mathbf{S}|\mathbf{L}) = \int d^3r F(n(\mathbf{r})) \mathbf{S}(\mathbf{r}) \cdot \mathbf{L}(\mathbf{r}) = 0, \quad (3.17)$$

which also means  $\int d^3r \mathbf{S}(\mathbf{r}) \cdot \mathbf{H}^{C,L}(\mathbf{r}) = 0$ . The LSDA expressions of (Eq.3.13) and (Eq.3.15) do not obey the last relation. They also do not yield  $\mathbf{H}^C$  as a curl according to (Eq.2.42). We correct  $\mathbf{H}^{C,L}$  according to:

$$\mathbf{H}^{C,L} = \mathbf{H}_{LDA}^{C,L} - \mathbf{H}_{LDA}^{C,S} \frac{(\mathbf{S}_{LDA}|\mathbf{L}_{LDA})}{(\mathbf{S}_{LDA}|\mathbf{S}_{LDA})}. \quad (3.18)$$

We call it LDA here because it implies both  $\mathbf{S}$  and  $\mathbf{L}$ . This yields the final orbital correlation term

$$\frac{\mu_0 e \beta}{2n_k} \int d^3r' \mathbf{H}^{C,L}(\mathbf{r}') \cdot \frac{\delta \mathbf{L}(\mathbf{r}')}{\delta \bar{\psi}_k(\mathbf{r})}, \quad (3.19)$$

which is independent from the direction of  $\mathbf{S}$ .

### 3.3.1 The orbital density $\mathbf{L}(\mathbf{r})$

Now, we introduce an explicit expression for the orbital density  $\mathbf{L}(\mathbf{r})$  as a function of the particle density. The orbital current  $\mathbf{I}(\mathbf{r}) = (1/2)\nabla \times \mathbf{L}(\mathbf{r})$  can be read as:

$$\mathbf{I}(\mathbf{r}) = \sum_k n_k \left( -\text{Re} (\bar{\psi}_k(\mathbf{r}) i \nabla \psi_k(\mathbf{r})) + \mathbf{A}(\mathbf{r}) \bar{\psi}_k(\mathbf{r}) \psi_k(\mathbf{r}) \right), \quad (3.20)$$

where  $\mathbf{A}$  includes both the external  $\mathbf{A}^{ext}$  and the correlation  $\mathbf{A}^C$  magnetic vector potentials. We apply the collinear approximation,  $\mathbf{H} = \mathbf{e}_z H$ ,  $\mathbf{L} = \mathbf{e}_z L$ , and symmetric gauge,  $\mathbf{A}(\rho, \phi, z) = \mathbf{e}_\phi A(\rho, z)$ . Thus,

$$\rho A(\rho, z) = \mu_0 \int_0^\rho d\rho' \rho' H(\rho', z). \quad (3.21)$$

Taking local basis functions  $\varphi_{m_l} \sim e^{im_l \phi}$  with vanishing small component, the  $\phi$ -averaged current is

$$\frac{e\phi}{\rho} \sum_k n_k \left( \sum_{m_l} m_l |\varphi_{m_l}(\mathbf{r})|^2 \langle \psi_k | \varphi_{m_l} \rangle \langle \varphi_{m_l} | \psi_k \rangle + \rho A(\mathbf{r}) \bar{\psi}_k(\mathbf{r}) \psi_k(\mathbf{r}) \right) = -\frac{e\phi}{2} \frac{\partial L}{\partial \rho}, \quad (3.22)$$

where the  $\phi$ -averaging removes the off-diagonal terms  $\sim e^{i(m'_l - m_l)\phi}$ . Integration over  $\rho$  yields

$$L(\mathbf{r}') = 2 \sum_k n_k \int_{\rho'}^\infty d\rho'' \left( \sum_{m_l} \frac{m_l}{\rho''} |\varphi_{m_l}(\mathbf{r}'') \langle \varphi_{m_l} | \psi_k \rangle|^2 + A(\mathbf{r}'') \bar{\psi}_k(\mathbf{r}'') \psi_k(\mathbf{r}'') \right). \quad (3.23)$$

This expression should be useful for unfilled inner shells in a solid while for outer valence electron states the orbital currents from neighboring atoms to a far extent cancel each others like in Peierls' argument on diamagnetism of the homogeneous electron gas [59].

### 3.3.2 Orbital magnetism in an intra-shell with Hartree-Fock interaction

Additional to the correlation energy, orbital magnetism also can be understood as a contribution of asphericity for the charge density for an open valence shell. It has to be pointed out that an atom with full spherical symmetry dose not arise any orbital moment. For instance the orbital moment of  $s$  electrons are vanished. In a quantum regime, as it was discussed in Chapter 2, one of the interactions which can be involved for the many electron systems is the Hartree-Fock interaction. The Hartree-Fock interaction is subject to form an

orbital polarization in an unfilled shell of an atom. In the Dirac notations the Hartree-Fock energy in a spin- $\sigma$  subshell can be given by,

$$W_l^{\text{HF}} = \frac{1}{2} \sum_{m_l m'_l}^{\text{occ.}} \left[ \langle m_l m'_l | \frac{1}{r_{ij}} | m_l m'_l \rangle - \langle m_l m'_l | \frac{1}{r_{ij}} | m'_l m_l \rangle \right], \quad (3.24)$$

where like in (Eq.2.30) the first term is the Hartree energy and the second term is the exchange energy. The  $|m_l m'_l\rangle$  denote two Kohn-Sham electron states with magnetic quantum numbers  $m_l$  and  $m'_l$ , respectively. We can expand the  $1/r_{ij}$  in terms of complex spherical harmonics functions (see Appendix B):

$$\frac{1}{r_{ij}} = \frac{1}{|\mathbf{r}_i - \mathbf{r}_j|} = \sum_{k=0}^{\infty} \frac{r_{<}^k}{r_{>}^{k+1}} \frac{4\pi}{2k+1} \sum_{m_l=-k}^k Y_{km_l}(\mathbf{r}_i) Y_{km_l}^*(\mathbf{r}_j). \quad (3.25)$$

Substitution of above equation in to (Eq.3.24), yields the Hartree-Fock energy in a more explicit form, namely:

$$\begin{aligned} W_l^{\text{HF}} = & \frac{1}{2} \sum_{m_l m'_l}^{\text{occ.}} \left( F^0 (1 - \delta_{m_l m'_l}) + \right. \\ & + \sum_{k=1}^l F^{2k} \frac{4\pi}{2k+1} \left[ (Y_{lm_l} | Y_{2k,0} | Y_{lm_l}) (Y_{lm'_l} | Y_{2k,0} | Y_{lm'_l}) - \right. \\ & \left. \left. (-1)^{m_l - m'_l} (Y_{lm_l} | Y_{2k, m_l - m'_l} | Y_{lm'_l}) (Y_{lm'_l} | Y_{2k, m'_l - m_l} | Y_{lm_l}) \right] \right), \end{aligned} \quad (3.26)$$

where  $(Y_{l_1 m_1} | Y_{l_2 m_2} | Y_{l_3 m_3})$  are the Gaunt coefficients [60]<sup>1</sup> and  $F^k$  are Slater integrals which were already defined in (Eq.3.7). The  $(m, m')$  spherical averages for  $d$  and  $f$  shells with  $N_v$  electrons in the spin sub-shell yield [57, 62]:

$$\begin{aligned} W_0^d = & \frac{N_v(N_v-1)}{2} (F^0 - \frac{1}{14} F^2 - \frac{1}{14} F^4) = \\ = & \frac{N_v(N_v-1)}{2} (F^0 - \sum_{k=1}^l \bar{a}_k^l F^{2k}), \end{aligned} \quad (3.27)$$

$$\begin{aligned} W_0^f = & \frac{N_v(N_v-1)}{2} (F^0 - \frac{2}{45} F^2 - \frac{1}{33} F^4 - \frac{50}{1287} F^6) = \\ = & \frac{N_v(N_v-1)}{2} (F^0 - \sum_{k=1}^l \bar{a}_k^l F^{2k}). \end{aligned} \quad (3.28)$$

---

<sup>1</sup>The Gaunt coefficients are given in terms of  $3j$ -symbols by,  $(Y_{l_1 m_1} | Y_{l_2 m_2} | Y_{l_3 m_3}) = (-1)^m \left( \frac{(2l_1+1)(2l_2+1)(2l_3+1)}{4\pi} \right)^{\frac{1}{2}} \begin{pmatrix} l_1 & l_2 & l_3 \\ -m_1 & m_2 & m_3 \end{pmatrix} \begin{pmatrix} l_1 & l_2 & l_3 \\ 0 & 0 & 0 \end{pmatrix}$ , and for the properties of  $3j$ -symbols see Ref. [61].



After extracting the  $W_0^l$  expression from the Hartree-Fock energy  $W_l^{\text{HF}}$ , one can obtain the Hartree-Fock orbital polarization energy with remaining term for a given spin sub-shell with  $N_v$  electrons:

$$\begin{aligned} \Delta E_{\text{OP}}^{\text{HF}} &= W_l^{\text{HF}} - W_0^l = \\ &= \sum_{k=1}^l F^{2k} \left( \frac{N_v(N_v-1)}{2} \bar{a}_k^l + \sum_{m_l m_l'}^{\text{occ.}} \frac{2\pi}{2k+1} \left[ (Y_{lm_l} | Y_{2k,0} | Y_{lm_l}) (Y_{lm_l'} | Y_{2k,0} | Y_{lm_l'}) - \right. \right. \\ &\quad \left. \left. (-1)^{m_l-m_l'} (Y_{lm_l} | Y_{2k,m_l-m_l'} | Y_{lm_l'}) (Y_{lm_l'} | Y_{2k,m_l'-m_l} | Y_{lm_l}) \right] \right). \end{aligned} \quad (3.29)$$

In most implementations of the KSD equation for different electronic systems, a spherical averaged Hartree-Fock potential is used. However when one considers the orbital magnetism of the system, the contribution of the Hartree-Fock orbital polarization has to be taken into account.

### 3.4 Complete KSD equation

A careful treatment of the functional derivative in (Eq.3.19) with  $L(\mathbf{r})$  from (Eq.3.23) [see Appendix A] results in a number of additional correlation terms for the KSD equation:

$$\begin{aligned} &\left[ -ic\boldsymbol{\alpha} \cdot \nabla + \beta c^2 + V(\mathbf{r}) + V^{\text{H}}(\mathbf{r}) + V^{\text{XC}}(\mathbf{r}) + C^V(\mathbf{r}) + \right. \\ &\quad \left. + \left( \mu_B (\mathbf{H}(\mathbf{r}) + \mathbf{H}^{\text{XC}}(\mathbf{r})) + \mathbf{C}^{\Sigma}(\mathbf{r}) \right) \cdot \beta \boldsymbol{\Sigma}_z \right] \psi_k(\mathbf{r}) + \\ &\quad + \beta \sum_{m_l} C_{m_l}^{\text{C,L}} \langle \varphi_{m_l} | \psi_k \rangle \varphi_{m_l}(\mathbf{r}) = \psi_k(\mathbf{r}) \epsilon_k, \end{aligned} \quad (3.30)$$

where  $C^V$  is a scalar potential correction and  $\mathbf{C}^{\Sigma}$  is a correction to the XC field, while the  $C_{m_l}^{\text{C,L}}$  provide a non-local potential sensitive to OP. After using definition  $\tilde{n} = \sum_k n_k \bar{\psi}_k \psi_k$ , they are given with following expressions:

$$\begin{aligned} C^V(\mathbf{r}) &= 2\mu_B \left\{ \frac{\beta}{\mu_0} A^{\text{C,L}}(\mathbf{r}) A^{\text{C}}(\mathbf{r}) + \int d^3 r'' A^{\text{C,L}}(\mathbf{r}'') \tilde{n}(\mathbf{r}'') \times \right. \\ &\quad \left. \times \int_0^{\rho'} d\rho' \frac{\rho'}{\rho''} \left( \frac{\delta H^{\text{C}}(\rho', z'')}{\delta n(\mathbf{r})} - \frac{\zeta(\mathbf{r})}{n(\mathbf{r})} \frac{\delta H^{\text{C}}(\rho', z'')}{\delta \zeta(\mathbf{r})} \right) \right\}, \end{aligned} \quad (3.31)$$

$$C^{\Sigma}(\mathbf{r}) = 2\mu_B \int d^3 r'' A^{\text{C,L}}(\mathbf{r}'') \tilde{n}(\mathbf{r}'') \int_0^{\rho'} d\rho' \frac{\rho'}{\rho''} \frac{1}{n(\mathbf{r})} \frac{\delta H^{\text{C}}(\rho', z'')}{\delta \zeta(\mathbf{r})}, \quad (3.32)$$

$$C_{m_l}^{\text{C,L}} = e \int d^3 r'' A^{\text{C,L}}(\mathbf{r}'') \frac{m_l}{\rho''} |\varphi_{m_l}(\mathbf{r}'')|^2 + O((H^{\text{C}})^2). \quad (3.33)$$

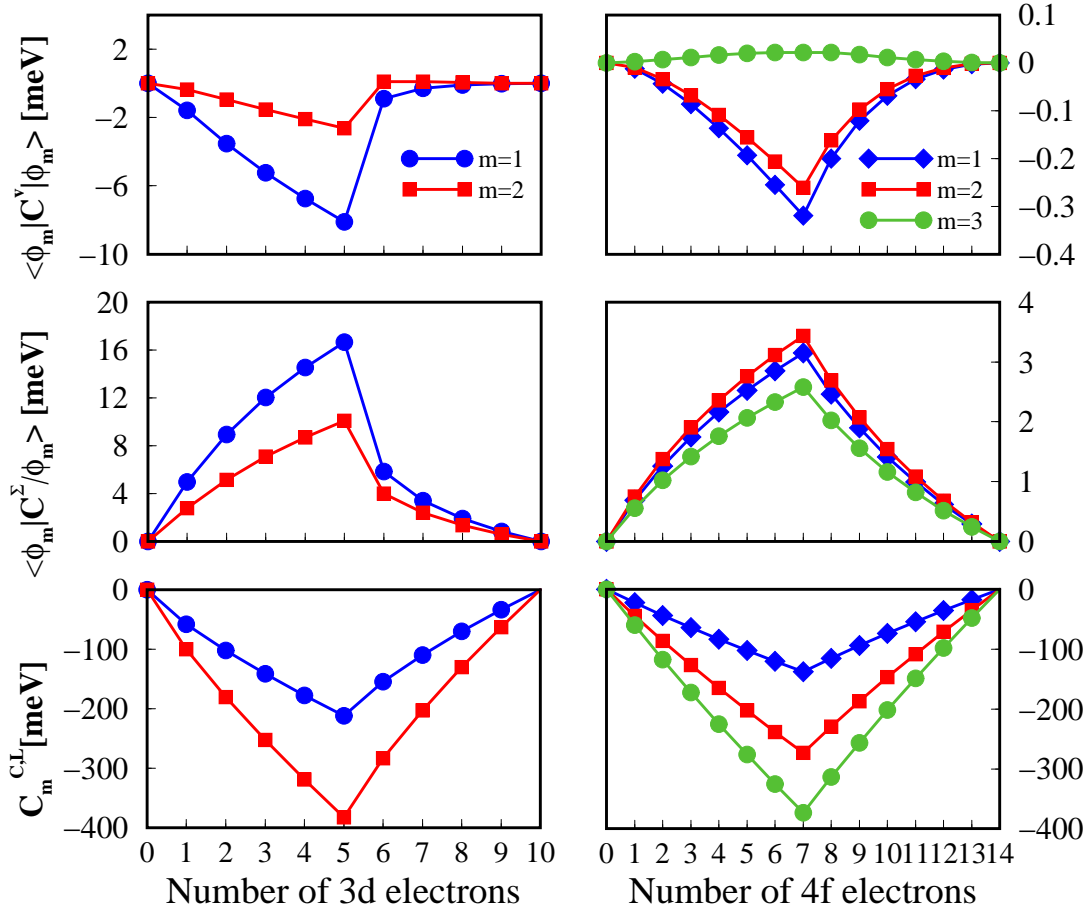


Figure 3.1: The expectation values of  $\langle C^V \rangle$ ,  $\langle C^\Sigma \rangle$  and  $C_{m_l}^{C,L}$  coefficients for 3d (left panel) and 4f (right panel) ions.

In a full-potential treatment of LSDA, which is standard nowadays,  $V^H + V^{XC}$  also have some dependence on OP which has to be compared with the HF results. Since in both cases the orbital occupation numbers have to be 0 or 1 (apart from degeneracies), the OP energies are to be referred to the configuration average of total energies for all possible configurations of all electrons of an atom with given  $z$ -component of spin. The difference between the OP energy contributions of HF plus correlation part and of full-potential LSDA,

$$E^{\text{OPE}} = \Delta E_{\text{OP}}^{\text{HF}} + \Delta E^{C,L} - \Delta E_{\text{OP}}^{\text{LSDA}}, \quad (3.34)$$

should be provided by an effective OP potential correction in the KSD equation.

### 3.4.1 Numerical results

For 2+ ions of the 3d elements and 3+ ions of the 4f elements, the matrix elements  $\langle nlm_l | C^V | nlm_l \rangle$  and  $\langle nlm_l | C^\Sigma | nlm_l \rangle$  as well as the coefficients  $C_{m_l}^{C,L}$  have been calculated for KS orbitals. We find  $\langle C^V \rangle < \langle C^\Sigma \rangle \ll C_{m_l}^{C,L}$ . In the 3d case,  $\langle C^\Sigma \rangle$  is more than one order of magnitude while in the 4f case two orders of magnitude smaller than  $C_{m_l}^{C,L}$  (see Figure 3.1). Also, the second term of  $C_{m_l}^{C,L}$  (Eq.3.33) is in the second order to  $H^C$ , which is comparable with the expectation values of  $C^V$  and  $C^\Sigma$  and therefore can be neglected.

In view of the still approximative character of the whole approach, one can hence neglect all correction terms except for the leading term of  $C_{m_l}^{C,L}$ . This is due to the smallness of  $H^C$  and  $A^C$ . All corrections except the leading term of  $C_{m_l}^{C,L}$  are of second and higher orders in the correlation field,  $H^C$ . Thus we arrive at the following result for the orbital polarization corrected KSD equation:

$$\begin{aligned} & \left[ -ic\boldsymbol{\alpha} \cdot \nabla + \beta c^2 + V_{\text{LSDA}}(\mathbf{r}) + \mu_B H_{\text{LSDA}}(\mathbf{r}) \beta \Sigma_z \right] \psi_k(\mathbf{r}) + \\ & + \beta \sum_{m_l} v_{m_l}^{\text{OPE}} \langle \varphi_{m_l} | \psi_k \rangle \varphi_{m_l}(\mathbf{r}) = \psi_k(\mathbf{r}) \epsilon_k, \end{aligned} \quad (3.35)$$

$$V_{\text{LSDA}} = V + V^H + V_{\text{LSDA}}^{\text{XC}}, \quad H_{\text{LSDA}} = H + H_{\text{LSDA}}^{\text{XC}}.$$

The  $v_{m_l}^{\text{OPE}}$  includes Hartree-Fock, LSDA and correlation correction via (Eq.3.34). The leading correlation contribution to  $v_{m_l}^{\text{OPE}}$  is

$$C_{m_l}^{C,L} = e \int d^3r A^{C,L}(\mathbf{r}) \frac{m_l}{\rho} |\varphi_{m_l}(\mathbf{r})|^2, \quad (3.36)$$

where  $A^{C,L}$  has to be taken from (Eq.3.21) with  $H^{C,L}$  from (Eq.3.15) to (Eq.3.18) and the first term of (Eq.3.23) for  $L$ . The orbital correlation energy to the total OP energy to leading order is now,

$$\Delta E^{C,L} = -\frac{\mu_B}{2} \int d^3r H^{C,L}(\mathbf{r}) L(\mathbf{r}). \quad (3.37)$$

Corrections of order  $1/c$  should in most cases even be small compared with the spin-orbit contribution following from the kinetic energy operator in (Eq.3.35). The results for the OPE energy (Eq.3.34) and its separate components for free ions of 3d and 4f elements are shown in Figure 3.2. It compares qualitatively with the results of J. Melsen *et al.* [63], who used the OPB correction. Our OP energies for lanthanide series indicated in Figure 3.2, are also in semi-qualitative agreement with M. Higuchi *et al.* calculations [64], who used the OPB correction.

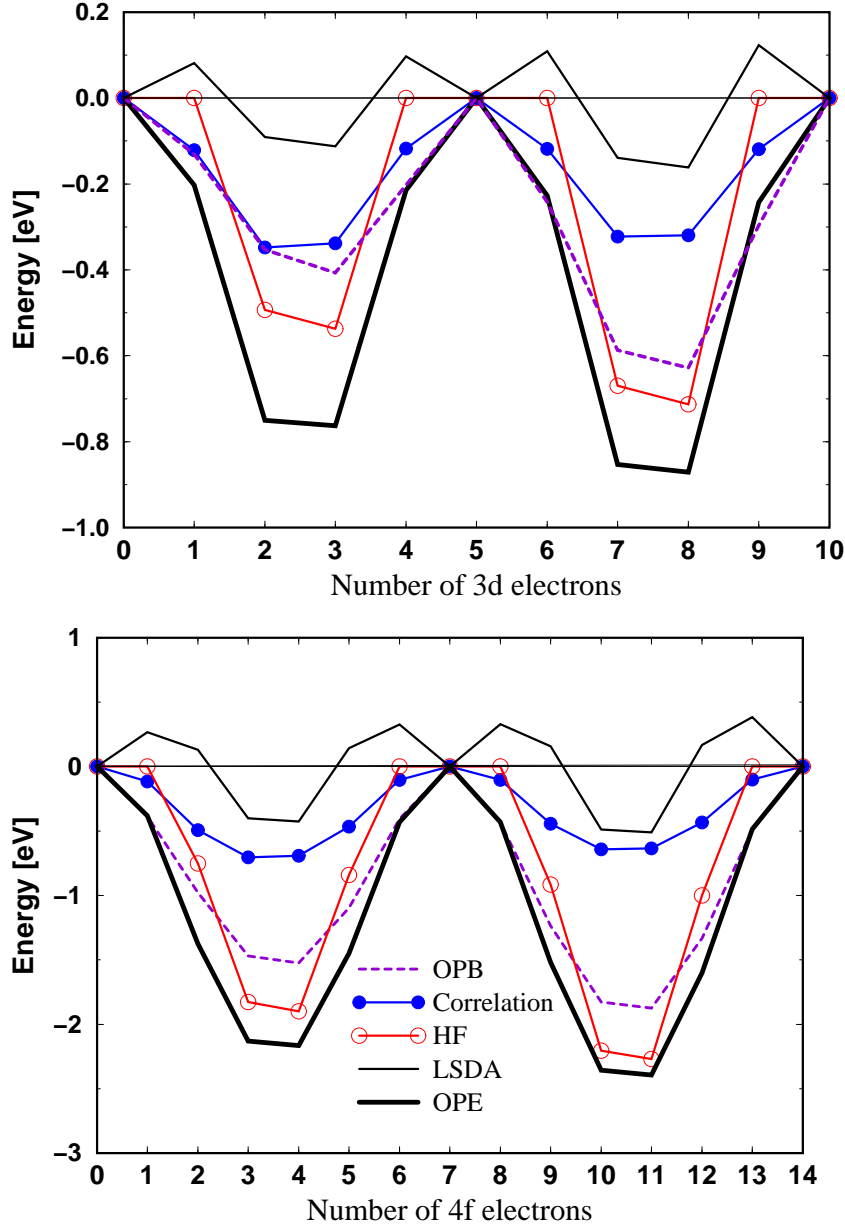


Figure 3.2: Orbital polarization corrections to the total energy of 2+ ions of 3d elements (upper panel) and 3+ ions of 4f elements (lower panel): the contributions to  $E^{\text{OPE}}$  (black thick lines) according to (Eq.3.37) are denoted by black thin lines ( $\Delta E_{\text{OP}}^{\text{LSDA}}$ ), blue thin lines with bullets ( $\Delta E_{\text{OP}}^{\text{C,L}}$ ) and red thin lines with open circles ( $\Delta E_{\text{OP}}^{\text{HF}}$ ). The  $E^{\text{OPB}}$  values are shown with violet dashed lines.

The OP is generally expected to be dependent on the spin subshell filling and on the subshell moment, where essential parts are second order in the orbital moment. We represent the OPE functional with:

$$E^{\text{OPE}} = -\frac{1}{2} \sum_{\sigma} I(N_{\sigma}) M_{L\sigma}^2, \quad M_{l\sigma} = \sum_{k,m} n_k \langle \psi_k | \phi_{m_l\sigma} \rangle m_l \langle \phi_{m_l\sigma} | \psi_k \rangle, \quad (3.38)$$

where the  $I(N_{\sigma})$ , and  $N_{\sigma}$  are given by:

$$I(N_{\sigma}) = \frac{1}{2} \Upsilon_l N_{\sigma} ((2l+1) - N_{\sigma}), \quad N_{\sigma} = \sum_k n_k |\langle \psi_k | \phi_{m_l\sigma} \rangle|^2, \quad (3.39)$$

and  $\sigma = \uparrow, \downarrow$  denote the spin directions. The coefficients  $\Upsilon_l$  slightly linearly increase within a shell from left to right;

$$\Upsilon_{3d} = (48 \cdots 64) \text{ meV}, \quad \Upsilon_{4f} = (19 \cdots 22) \text{ meV}. \quad (3.40)$$

The final coefficient of the potential correction in the KSD equation becomes;<sup>2</sup>

$$v_{m_l}^{\text{OPE}} = -I(N_{\sigma}) M_{l\sigma} m_l - \frac{1}{2} I'(N_{\sigma}) M_{l\sigma}^2. \quad (3.41)$$

Note that, for 1,  $2l$ ,  $2l+2$ , and  $4l+1$  electrons per shell the total energy must be  $m$ -independent and hence the orbital polarization energy  $E^{\text{OP}}$  must be vanished. This is provided by Hartree-Fock, but not by LSDA and also not by correlation correction and OPB correction (see Figure 3.2).

### 3.5 Conclusion

In summary, a systematic derivation of orbital polarization corrections from the four-current density functional theory has been achieved (OPE). The related orbital polarization energies of 3d and 4f free ions are compared with the results obtained by empirical orbital polarization corrections (OPB). Both methods are equally simple to implement. Of course the OPE is apt to future improvements of the correlation energy functional. In the next chapter, the complete KSD equation together with its OP corrections will be consider as a subject to orbital magnetism in solid.

---

<sup>2</sup>Note that  $I'(N_{\sigma}) = \frac{dI(N_{\sigma})}{dN_{\sigma}}$



## Chapter 4

# The Kohn-Sham-Dirac equation in solids

The aim of this chapter is to present practical expressions of the two different orbital polarization schemes discussed in the previous chapter as additional terms to the KSD equation. For this purpose, a short introduction into the relativistic full potential local orbital method (FPLO) for electronic structure calculations is given. It is based on the CDFT within the framework of KSD equation. At the beginning we neglect the OP corrections and solve the KSD equation. Afterward, we apply the orbital polarization corrections to KSD equation and then as examples, we will calculate orbital moments of bcc Fe, hcp Co, and fcc Ni.

The main aspect of the FPLO is that the extended states are expressed as a linear combination of local orbitals which are solutions to an atomic like Schrödinger equation with spherically averaged potentials. The orbitals are classified: states from different sites which do not overlap are treated as core states and all other states having overlap are valence states. The calculation of the valence states is modified by introducing an additional confining potential. It serves to compress the ranging tail of the orbitals and finally increases the accuracy, efficiency and performance of the scheme for calculating the electronic structure. Details can be found in Ref. [65, 66, 67].

Since, the Dirac operator couples the spin and spatial degrees of freedom, a separation into spin up and down states is no longer possible and the dimension of the eigenvalue problem is doubled in comparison to the non-relativistic theory. In addition, due to the four-component nature of the KSD equation a larger number of real space integrations is required. These last two points make the approximate variants of KSD equation so attractive for solid state calculations.

On the lowest level, scalar-relativistic schemes allow for a very effective approximative treatment of relativistic effects. One should keep in mind that the label 'scalar' refers to a class of approaches [68, 69] rather than a unique

method. Their common feature is that they neglect the spin-orbit interaction by averaging it out, the various approaches differing in this averaging procedure. As a consequence, the solutions of the scalar-relativistic equations are spin eigenstates with non-relativistic symmetry. Recall that for an adequate description of the electronic structure of heavy elements and the certain aspects of magnetism, like the magneto crystalline anisotropy energy or a number of magneto optical effects, the spin-orbit interaction has to be included in the Hamiltonian. In the following we discuss the practical implementation of the relativistic FPLO-method.

The KSD equation for crystals when at the first step OP corrections are neglected, may be cast into:

$$\left[ -ic\boldsymbol{\alpha} \cdot \boldsymbol{\nabla} + \beta c^2 + V^{cr} + \beta \boldsymbol{\Sigma} \cdot \mathbf{B}^{cr} \right] \Psi_k(\mathbf{r}) = \Psi_k(\mathbf{r}) \varepsilon_k, \quad (4.1)$$

where  $\Psi_k$  is KSD state and  $V^{cr}$  is the effective crystal potential including the Hartree potential  $V^H$ , the external potential  $V^{ext}$  of the nuclei and the exchange and correlation potential  $V^{xc}$ . The  $\mathbf{B}^{cr}$  is the effective magnetic potential due to the applied field  $\mathbf{B}$  and the exchange-correlation field  $\mathbf{B}^{xc}$ . In a collinear approximation with the XC-field  $\mu_B H^{XC} = B^{cr} \hat{z}$  aligned along the (arbitrary)  $\hat{z}$ -axis. This equation neglects all orbital diamagnetic effects. Knowing the functional  $V^{xc}$  and  $B^{xc}$ , in the framework of LSDA, the KSD equation has to be solved self-consistently to find out the ground state energy and the ground state (spin) density.

In a local orbital method it is advantageous to use a strictly local language for all relevant quantities, so that computationally expensive transformations between different numerical representations are avoided during the self consistency cycle. In the FPLO method,  $V^{cr}(\mathbf{r})$ ,  $B^{cr}(\mathbf{r})$ , the density  $n(\mathbf{r})$  and the magnetization density  $\mathbf{m}(\mathbf{r}) = m(\mathbf{r})\hat{z}$  are represented as lattice sums:

$$f(\mathbf{r}) = \sum_{\mathbf{R}, \mathbf{s}} f_{\mathbf{s}}^{lm}(|\mathbf{r} - \mathbf{R} - \mathbf{s}|) y_L(\mathbf{r} - \mathbf{R} - \mathbf{s}), \quad (4.2)$$

where  $f$  denote for all four scalar functions mentioned above and  $f_{\mathbf{s}}^{lm}$  are radial functions centred at atomic sites  $\mathbf{s}$  in the elementary cell defined by the Bravais lattice vectors  $\mathbf{R}$ . The  $y_L$  are real spherical harmonics (see Appendix B) with a multi index  $L = lm$ .

Hence, no shape restrictions are made for the potentials and densities, a necessary condition for reliable calculations on open structures, usually referred to as full potential. Of course the  $L$ -sum has to be restricted. In the current implementation of FPLO, a cut-off momentum up to  $l_{max} = 12$  is used.

As starting point for the self consistency cycle we use a density  $n(\mathbf{r})$  and magnetization density  $m(\mathbf{r})$  represented as lattice sum (Eq.4.2). These initial densities may be either obtained from an atomic or a scalar-relativistic band calculation, the latter choice reducing the number of iterations required for self



consistency. From the density  $n(\mathbf{r})$  and the magnetization density  $m(\mathbf{r})$ , the crystal potential is given by

$$V^{\text{cr}}(\mathbf{r}) = \int \frac{n(\mathbf{r}')}{|\mathbf{r} - \mathbf{r}'|} d^3r' - \sum_{\mathbf{R}\mathbf{s}} \frac{Z_{\mathbf{s}}}{|\mathbf{r} - \mathbf{R} - \mathbf{s}|} + \frac{1}{2} (V_{\uparrow}^{\text{XC}}[n(\mathbf{r}), m(\mathbf{r})] + V_{\downarrow}^{\text{XC}}[n(\mathbf{r}), m(\mathbf{r})]), \quad (4.3)$$

where  $Z_{\mathbf{s}}$  are positive charges located at sites  $\mathbf{s}$  and  $\uparrow, \downarrow$  denote spin directions. The crystal XC-field can be read as

$$B^{\text{cr}}(\mathbf{r}) = \frac{1}{2} (V_{\uparrow}^{\text{XC}}[n(\mathbf{r}), m(\mathbf{r})] - V_{\downarrow}^{\text{XC}}[n(\mathbf{r}), m(\mathbf{r})]). \quad (4.4)$$

The eigenvectors of the lattice periodic Hamiltonian of the KSD equation are Bloch states  $|\mathbf{k}n\rangle$  with crystal momentum  $\mathbf{k}$  and band index  $n$ . They are expressed by the ansatz

$$|\mathbf{k}n\rangle = \frac{1}{\sqrt{N_{\text{uc}}}} \sum_{\mathbf{R}\mathbf{s}\nu} C_{\mathbf{s}\nu,n}^{\mathbf{k}} |\mathbf{R}\mathbf{s}\nu\rangle e^{i\mathbf{k}(\mathbf{R}+\mathbf{s})}, \quad (4.5)$$

as a Bloch sum of localized atom-like four-spinor orbitals  $|\mathbf{R}\mathbf{s}\nu\rangle$  centred at the atomic positions  $\mathbf{R} + \mathbf{s}$  and  $C_{\mathbf{s}\nu,n}^{\mathbf{k}}$  are coefficient matrices. The label  $\nu = (\xi, \kappa, \mu)$  contains a complete set of atomic quantum numbers in relativistic notation and  $N_{\text{uc}}$  count the unit cells in the Born-von Karman torus. The chosen ansatz includes only electron-like spinors. This ensures (i) a minimum size of the matrix, namely twice the size of the non-relativistic problem and (ii) a restriction of the solutions to the electron sector of the Hilbert space. Inserting the ansatz (Eq.4.5) into KSD equation (Eq.4.1), we obtain a matrix equation,  $HC - SCE = 0$ , which has to be diagonalized to find out the related eigenstates and eigenvectors.

In a minimum basis scheme, the proper choice of the local basis states  $|\mathbf{R}\mathbf{s}\nu\rangle$  is crucial for accurate and efficient calculations, since the numerical effort for solving the eigenvalue problem scales with the third power of the number of basis states. A trick proposed by H. Eschrig *et al.* [70] is to obtain the atom-like four-spinor orbitals  $|\mathbf{R}\mathbf{s}\nu\rangle$ , where the local basis states are chosen as solutions of a single particle Dirac equation which is given by:

$$\hat{H}_{\mathbf{s}\nu}^{\text{at}} |\mathbf{R}\mathbf{s}\nu\rangle = [-ic\boldsymbol{\alpha} \cdot \boldsymbol{\nabla} + \beta c^2 + V_{\mathbf{s}\nu}^{\text{at}} + \beta \Sigma_z B_{\mathbf{s}}^{\text{at}}] |\mathbf{R}\mathbf{s}\nu\rangle = |\mathbf{R}\mathbf{s}\nu\rangle \varepsilon_{\mathbf{R}\mathbf{s}\nu}. \quad (4.6)$$

This equation includes a spherical and orbital dependent atomic potential,

$$\begin{aligned} V_{\mathbf{s}\nu}^{\text{at}}(r) &= V_{\mathbf{s}}^{\text{ac}}(r) + V_{\mathbf{s}\nu}^{\text{conf}}(r) \\ &= \frac{1}{4\pi} \int_{|\mathbf{r}-\mathbf{s}|=r} d\Omega V^{\text{cr}}(\mathbf{r} - \mathbf{s}) + \delta_{\nu v} \frac{1+\beta}{2} \left( \frac{r}{r_{0,\mathbf{s}}} \right)^{\eta}. \end{aligned} \quad (4.7)$$

It is defined as the sum of the spherical averaged crystal potential  $V_{\mathbf{s}}^{ac}$  and an additional confining potential term  $V_{\mathbf{s}\nu}^{conf}$ , which is only applied to valence states (denoted by the symbolic writing  $\delta_{\nu v}$ ). The atomic XC-field  $B_{\mathbf{s}}^{at}$  is the spherical averaged of the crystal XC-field  $B_{\mathbf{s}}^{xc} = B_{\mathbf{s}}^{cr}$ ,

$$B_{\mathbf{s}}^{at}(r) = \frac{1}{4\pi} \int_{|\mathbf{r}-\mathbf{s}|=r} d\Omega B^{cr}(\mathbf{r} - \mathbf{s}). \quad (4.8)$$

The confining potentials  $V_{\mathbf{s}\nu}^{conf}(r)$  compress the local valence orbitals and shift their energies, so that they come close to the valence band centers, thus provide the optimized basis for the construction of extended states. They contain orbital dependent variational parameters  $x_{0,\mathbf{s}}$  defined as:

$$r_{0,\mathbf{s}} = \left( \frac{x_{0,\mathbf{s}} r_{NN}}{2} \right)^{\frac{3}{2}}, \quad (4.9)$$

where  $r_{NN}$  is the nearest neighbor distance of the nuclei in the crystal. The parameters  $x_{0,\mathbf{s}}$  are independent from the lattice spacing and together with  $\eta$  are used to adjust the local basis states such that the total energy is minimized. The exponents  $\eta$  also depend on the power of positive charges  $Z_{\mathbf{s}}$  located at the sites  $\mathbf{s}$  and as a matter of experience the values of  $\eta$  are at the range of  $4 \leq \eta \leq 6$ . Of course, they have to be optimized for every states in an element.

## 4.1 Orbital moment and occupation number in FPLO

The orbital moment  $M_l$  is the total  $\hat{L}_z$  expectation value of the  $l$ -shell. Although we cannot say anything about the multiplet wave function from a single particle theory, we can state that  $M_l = \sum_{\nu} m_{\nu}$  for maximum  $M_l$ , where  $m_{\nu} = \langle \hat{l}_{\nu z} \rangle$  is the expectation value of the  $\nu$ -th single particle  $z$ -component of  $\hat{l}_{\nu}$ . The  $M_l$  is not really a well defined number and must be approximated by physical arguments. The orbital moment expectation value of the Kohn-Sham-Dirac single determinant wave function is

$$M_l = \sum_{kn} N_{kn} \langle kn | \hat{l}_z | kn \rangle, \quad (4.10)$$

where  $N_{kn}$  is occupation number of the Bloch state,<sup>1</sup> and now the orbital moment becomes  $k$ -dependent. However the polar vector operator  $\hat{l}_z$  opens the problem of coordinate origin and of course the angular momentum of an extended state is a dubious concept. We formally proceed by expanding the

---

<sup>1</sup>Number of electrons in the unit cell can be evaluated as  $N_e = \frac{1}{N_{uc}} \sum_{kn} N_{kn}$ .

KS states into local basis. The band index  $n$  may be classifiable with respect to spin, which is not indicated since spin is an approximate quantum number in full relativistic calculations. Expansion of orbital moment  $M_l$  defined in (Eq.4.10) with the Bloch states (Eq.4.5) yields orbital moment per unit cell as:

$$M_l = \sum_{kn} \frac{N_{kn}}{N_{uc}^2} \sum_{\mathbf{R}\mathbf{s}\nu} \sum_{\mathbf{R}'\mathbf{s}'\nu'} \left\langle \mathbf{R}\mathbf{s}\nu | \hat{l}_z | \mathbf{R}'\mathbf{s}'\nu' \right\rangle C_{\mathbf{s}\nu,n}^{\mathbf{k}\dagger} C_{\mathbf{s}'\nu',n}^{\mathbf{k}} e^{i\mathbf{k}(\mathbf{R}' - \mathbf{R} + \mathbf{s}' - \mathbf{s})}. \quad (4.11)$$

We restrict these sums onto (the diagonal) onsite terms only and because we focus to calculate the total orbital moment of a specific unit cell with its individual components, therefore an approximate expression for  $M_l$  can be read as:

$$M_l \approx \sum_{kn} \frac{N_{kn}}{N_{uc}} \sum_{\mathbf{s}\nu} \left\langle \mathbf{s}\nu | \hat{l}_z | \mathbf{s}\nu \right\rangle C_{\mathbf{s}\nu,n}^{\mathbf{k}\dagger} C_{\mathbf{s}\nu,n}^{\mathbf{k}}. \quad (4.12)$$

The orbital moment now is sum over all sites with the net occupation weighted sum of the single orbital moments.

#### 4.1.1 Projection arguments

The orbital moment may be derived by projection techniques. In non-orthogonal basis one can define a quasi orthogonal projector onto states  $|i\rangle$  by introducing the contragredient basis  $|i\rangle = \sum_j |j\rangle (S^{-1})_{ji}$  with  $\langle k|i\rangle = \delta_{ki}$  and overlap matrix elements are defined with  $S_{ij} = \langle i|j\rangle$ . The projector onto  $|i\rangle$  then reads,

$$P_i^o = |i\rangle\langle i| = \sum_j |i\rangle (S^{-1})_{ij} \langle j|, \quad (4.13)$$

with  $P_i^o|k\rangle = |i\rangle\delta_{ik}$ . One may think of

$$P_i^h = |i\rangle\langle i|, \quad (4.14)$$

with  $P_i^o|k\rangle = |i\rangle S_{ik}$ , to be a proper projector in this context. The index  $o$  and  $h$  denote the orthogonal and non-orthogonal (hybrid) projections, respectively. To use a common notion, we define a general projector as

$$P_i^g = \sum_j |i\rangle P_{ij} \langle j|, \quad P_{ij}^o = (S^{-1})_{ij}, \quad P_{ij}^h = \delta_{ij}. \quad (4.15)$$

Using these techniques we arrive at the formulation that the orbital moment in an unit cell may be defined as a suitable projection of the expression (Eq.4.10),

$$M_l = \sum_{\mathbf{s}\nu} \sum_{kn} N_{kn} \langle kn | P_{\mathbf{s}\nu}^{g\dagger} | \hat{l}_z | P_{\mathbf{s}\nu}^g | kn \rangle. \quad (4.16)$$

Using  $P_i^g$ , the Bloch states  $|kn\rangle$  will be projected to localized atom-like four-spinor orbitals, namely

$$P_{\mathbf{s}\nu}^g |kn\rangle = \frac{1}{\sqrt{N_{uc}}} |\mathbf{s}\nu\rangle e^{i\mathbf{k}\mathbf{s}} \left[ P^{\mathbf{k}} S^{\mathbf{k}} C^{\mathbf{k}} \right]_{\mathbf{s}\nu,n}, \quad (4.17)$$

where matrices  $P^{\mathbf{k}}$  and  $S^{\mathbf{k}}$  are defined in general with:

$$G_{\mathbf{s}\zeta, \mathbf{s}'\eta}^{\mathbf{k}} = \sum_{\mathbf{R}'} G_{\mathbf{s}\zeta, \mathbf{R}'\mathbf{s}'\eta} e^{i\mathbf{k}(\mathbf{R}' + \mathbf{s}' - \mathbf{s})}. \quad (4.18)$$

The following expression can be read for local orbital moment in a given spin- $\sigma$  shell at site  $\mathbf{s}$ , namely:

$$M_{\mathbf{s}\sigma} = \sum_{\nu} \sum_{kn} \frac{N_{kn}}{N_{uc}} \left| \left( P^{\mathbf{k}} S^{\mathbf{k}} C^{\mathbf{k}} \right)_{n, \mathbf{s}\nu} \right|^2 p_{\nu\sigma} \langle \mathbf{s}\nu | \hat{l}_z | \mathbf{s}\nu \rangle p_{\nu\sigma}, \quad (4.19)$$

where the  $\nu$ -sum would be the sum over all quantum numbers, which fully specify the spin- $\sigma$  shell. In relativistic case the spin-projector  $p_{\nu\sigma}$  selects the  $\nu$ -states of the shell, which have a certain spin character. In this way, we may use the spin concept approximately.<sup>2</sup> The orthogonal projector (Eq.4.13) gives the similar expression to (Eq.4.12),

$$M_{\mathbf{s}\sigma}^o = \sum_{\nu} \left( \sum_{kn} \frac{N_{kn}}{N_{uc}} \left| C_{\mathbf{s}\nu,n}^{\mathbf{k}} \right|^2 \right) p_{\nu\sigma} \langle \mathbf{s}\nu | \hat{l}_z | \mathbf{s}\nu \rangle p_{\nu\sigma}, \quad (4.20)$$

and with the non-orthogonal projector (Eq.4.14) we get,

$$M_{\mathbf{s}\sigma}^h = \sum_{\nu} \left( \sum_{kn} \frac{N_{kn}}{N_{uc}} \left| \left( S^{\mathbf{k}} C^{\mathbf{k}} \right)_{\mathbf{s}\nu,n} \right|^2 \right) p_{\nu\sigma} \langle \mathbf{s}\nu | \hat{l}_z | \mathbf{s}\nu \rangle p_{\nu\sigma}. \quad (4.21)$$

Now we provide functional derivative of  $M_{\mathbf{s}\sigma}$  (Eq.4.19) with respect to the KS states  $\langle kn|$  and we get the expression:

$$\frac{1}{N_{kn}} \frac{\delta M_{\mathbf{s}\sigma}}{\delta \langle kn|} = \frac{1}{N_{uc}} \sum_{\nu} \left( |kn\rangle P^{\mathbf{k}} \right)_{\mathbf{s}\nu} p_{\nu\sigma} \langle \mathbf{s}\nu | \hat{l}_z | \mathbf{s}\nu \rangle p_{\nu\sigma} \left[ P^{\mathbf{k}} S^{\mathbf{k}} C^{\mathbf{k}} \right]_{\mathbf{s}\nu,n}. \quad (4.22)$$

Finally, we introduce a projector for the occupation number. The number of electrons in a given spin- $\sigma$  shell at site  $\mathbf{s}$  reads as:

$$N_{\mathbf{s}\sigma} = \sum_{\mathbf{s}\nu} \sum_{kn} N_{kn} \langle kn | P_{\mathbf{s}\nu}^{g\dagger} | \frac{1 + \sigma \hat{\Sigma}_z}{2} | P_{\mathbf{s}\nu}^g | kn \rangle, \quad (4.23)$$

---

<sup>2</sup>Recall that there is no spin quantum number in a full relativistic world. However in all important cases the spin character should be pronounced.

where the operator  $\frac{1+\sigma\hat{\Sigma}_z}{2}$  is a projector onto the spin direction for collinear relativistic calculations. In analogy with (Eq.4.19), the following expression can be read for local occupation number in a given spin- $\sigma$  shell at site  $\mathbf{s}$ ,

$$N_{\mathbf{s}\sigma} = \sum_{\nu} \sum_{kn} \frac{N_{kn}}{N_{uc}} \left| \left( P^{\mathbf{k}} S^{\mathbf{k}} C^{\mathbf{k}} \right)_{n, \mathbf{s}\nu} \right|^2 p_{\nu\sigma} \langle \mathbf{s}\nu | \frac{1+\sigma\hat{\Sigma}_z}{2} | \mathbf{s}\nu \rangle p_{\nu\sigma}, \quad (4.24)$$

Now we provide functional derivative of  $N_{\mathbf{s}\sigma}$  (Eq.4.24) with respect to the KS states  $\langle kn |$  and we get the expression:

$$\frac{1}{N_{kn}} \frac{\delta N_{\mathbf{s}\sigma}}{\delta \langle kn |} = \frac{1}{N_{uc}} \sum_{\nu} \left( |kn\rangle P^{\mathbf{k}} \right)_{\mathbf{s}\nu} p_{\nu\sigma} \langle \mathbf{s}\nu | \frac{1+\sigma\hat{\Sigma}_z}{2} | \mathbf{s}\nu \rangle p_{\nu\sigma} \left[ P^{\mathbf{k}} S^{\mathbf{k}} C^{\mathbf{k}} \right]_{\mathbf{s}\nu, n}. \quad (4.25)$$

## 4.2 The OPB functional

The orbital polarization energy functional in OPB approach, which has to be added to the XC-energy functional in a rather practical form is given by:

$$E^{\text{OPB}} = -\frac{1}{2} N_{uc} \sum_{\sigma \mathbf{s} \in \{tl\}} I_{\mathbf{s}\sigma}^{\text{Racah}} M_{\mathbf{s}\sigma}^2, \quad (4.26)$$

where  $t$  denote the Wyckoff positions of the sites  $\mathbf{s}$  and  $l$  is the angular momentum of the  $l$ -shell to be corrected and  $\sigma$  denote spin channels of the  $l$ -shell. The OPB-Hamiltonian is obtained as the functional derivative of the functional (Eq.4.26) with respect to the KS states:

$$H^{\text{OPB}} |kn\rangle = \frac{1}{N_{kn}} \frac{\delta}{\delta \langle kn |} E^{\text{OPB}} = -N_{uc} \sum_{\sigma \mathbf{s} \in \{tl\}} I_{\mathbf{s}\sigma}^{\text{Racah}} \frac{1}{N_{kn}} \frac{\delta M_{\mathbf{s}\sigma}}{\delta \langle kn |} \quad (4.27)$$

and the matrix elements of the above Hamiltonian are:

$$H_{*,*}^{\text{OPB}} = - \sum_{\sigma \mathbf{s} \in \{tl\}} I_{\mathbf{s}\sigma}^{\text{Racah}} M_{\mathbf{s}\sigma} \sum_{\nu} \left( S^{\mathbf{k}} P^{\mathbf{k}} \right)_{*, \mathbf{s}\nu} p_{\nu\sigma} \langle \mathbf{s}\nu | \hat{l}_z | \mathbf{s}\nu \rangle p_{\nu\sigma} \left[ P^{\mathbf{k}} S^{\mathbf{k}} \right]_{\mathbf{s}\nu, *}, \quad (4.28)$$

where  $*$  denote the arbitrary matrix indices. Therefore we get the Hamiltonian matrix elements in orthogonal projection,

$$H_{*,*}^{o, \text{OPB}} = - \sum_{\sigma \mathbf{s} \in \{tl\}} I_{\mathbf{s}\sigma}^{\text{Racah}} M_{\mathbf{s}\sigma} \sum_{\nu} \delta_{*, \mathbf{s}\nu} p_{\nu\sigma} \langle \mathbf{s}\nu | \hat{l}_z | \mathbf{s}\nu \rangle p_{\mu\sigma} \delta_{\mathbf{s}\nu, *}, \quad (4.29)$$

where  $\delta_{ij}$  is zero, unless the matrix elements belong to the block, which belongs to a corrected orbital. With the non-orthogonal projection, we get

$$H_{*,*}^{\text{h, OPB}} = - \sum_{\sigma \mathbf{s} \in \{tl\}} I_{\mathbf{s}\sigma}^{\text{Racah}} M_{\mathbf{s}\sigma} \sum_{\nu} S_{*, \mathbf{s}\nu}^{\mathbf{k}} p_{\nu\sigma} \langle \mathbf{s}\nu | \hat{l}_z | \mathbf{s}\nu \rangle p_{\nu\sigma} S_{\mathbf{s}\nu, *}^{\mathbf{k}}. \quad (4.30)$$

### 4.3 The OPE functional

In the previous chapter we also introduced the OPE correction as a new approach for orbital polarization in the framework of CDFT. Now, the introduced OPE functional in more effective way, can be expressed as a function of occupation numbers,

$$E^{\text{OPE}} = -\frac{1}{2}N_{\text{uc}} \sum_{\sigma \mathbf{s} \in \{tl\}} I_{\mathbf{s}\sigma}(N_{\mathbf{s}\sigma}) M_{\mathbf{s}\sigma}^2. \quad (4.31)$$

The OPE-Hamiltonian is obtained as the functional derivative of the functional (Eq.4.31) with respect to the KS states:

$$\begin{aligned} H^{\text{OPE}}|kn\rangle &= \frac{1}{N_{kn}} \frac{\delta}{\delta \langle kn|} E^{\text{OPE}} = \\ &-N_{\text{uc}} \sum_{\sigma \mathbf{s} \in \{tl\}} \left[ \frac{1}{2} I'_{\mathbf{s}\sigma}(N_{\mathbf{s}\sigma}) M_{\mathbf{s}\sigma}^2 \frac{1}{N_{kn}} \frac{\delta N_{\mathbf{s}\sigma}}{\delta \langle kn|} + I_{\mathbf{s}\sigma}(N_{\mathbf{s}\sigma}) M_{\mathbf{s}\sigma} \frac{1}{N_{kn}} \frac{\delta M_{\mathbf{s}\sigma}}{\delta \langle kn|} \right]. \end{aligned} \quad (4.32)$$

Substitution of the related equations (Eq.4.22 and Eq.4.25), in to the above equation and using orthogonal projection, the matrix elements of OPE-Hamiltonian can be read,

$$\begin{aligned} H_{*,*}^{o,\text{OPE}} &= - \sum_{\sigma \mathbf{s} \in \{tl\}} \sum_{\nu} \left[ \delta_{*,\mathbf{s}\nu} \left( \frac{1}{2} I'_{\mathbf{s}\sigma}(N_{\mathbf{s}\sigma}) M_{\mathbf{s}\sigma}^2 p_{\nu\sigma} \langle \mathbf{s}\nu | \frac{1 + \sigma \hat{\Sigma}_z}{2} | \mathbf{s}\nu \rangle p_{\nu\sigma} + \right. \right. \\ &\quad \left. \left. + I_{\mathbf{s}\sigma}(N_{\mathbf{s}\sigma}) M_{\mathbf{s}\sigma} p_{\nu\sigma} \langle \mathbf{s}\nu | \hat{l}_z | \mathbf{s}\nu \rangle p_{\nu\sigma} \right) \delta_{\mathbf{s}\nu,*} \right], \end{aligned} \quad (4.33)$$

and with non-orthogonal projection we get:

$$\begin{aligned} H_{*,*}^{h,\text{OPE}} &= - \sum_{\sigma \mathbf{s} \in \{tl\}} \sum_{\nu} \left[ S_{*,\mathbf{s}\nu}^{\mathbf{k}} \left( \frac{1}{2} I'_{\mathbf{s}\sigma}(N_{\mathbf{s}\sigma}) M_{\mathbf{s}\sigma}^2 p_{\nu\sigma} \langle \mathbf{s}\nu | \frac{1 + \sigma \hat{\Sigma}_z}{2} | \mathbf{s}\nu \rangle p_{\nu\sigma} + \right. \right. \\ &\quad \left. \left. + I_{\mathbf{s}\sigma}(N_{\mathbf{s}\sigma}) M_{\mathbf{s}\sigma} p_{\nu\sigma} \langle \mathbf{s}\nu | \hat{l}_z | \mathbf{s}\nu \rangle p_{\nu\sigma} \right) S_{\mathbf{s}\nu,*}^{\mathbf{k}} \right]. \end{aligned} \quad (4.34)$$

The discussed OP Hamiltonians have to be added to the Hamiltonian of the XC-LSDA energy functional. In this sense, eventually we can calculate most accurate values for the individual orbital moments of the considered system. In the next section we will show that how those OP corrections can work for three elements.

## 4.4 Orbital magnetism in bcc Fe, hcp Co and fcc Ni

In this section we study the relativistic effects on orbital magnetism of three light elemental metals, Fe, Co, and Ni, using introduced functionals in FPLO scheme. In most electronic systems LSDA in the framework of scalar relativistic calculations can give accurate structural properties [65] and clarified spin magnetism of the system. However, sometimes the existing orbital moments have to be taken into account via spin-orbit interaction, which needs full-relativistic treatment. Additionally, in the present section we show even in the full relativistic regime, LSDA with spin-orbit coupling, cannot predict proper orbital moments compared with experiments. It is pointed out to add orbital polarization corrections to our functionals.

We focus on the magnetic properties of the bcc Fe, hcp Co, and fcc Ni. The spin magnetism of these 3d elements has been studied extensively over the last decades [7, 18, 71]. The bcc Fe, hcp Co and fcc Ni are regarded as trial materials for probing theories of metallic magnetism. The magnetism in these elements is caused by the 3d electrons, which on the one hand, are relatively itinerant, but the 3d orbitals also have a tendency towards localization. The latter may provide the orbital moments in these systems.

### 4.4.1 Computational details

For our calculations the bcc Fe, hcp Co, and fcc Ni analyzed in space groups,  $Im\bar{3}m$  (No.229),  $P6_3/mmc$  (No.194), and  $Fm\bar{3}m$  (No.225) in International Tables, respectively. The following basis sets were adopted:  $3s3p$ ;  $3d4s4p$  states of Fe, Co, and Ni were treated as valence states. The site-centred potentials and densities in FPLO code were expanded in spherical harmonic contributions up to  $l_{max} = 12$ . The convergence of the total energies ( $10^{-6}$  Hartree) and magnetic moments ( $10^{-4}\mu_B$ ) with respect to the k-space integrations ( $20 \times 20 \times 20$  k-points) was checked separately for each of the considered elements. The spatial extension of the basis orbitals, controlled by a confining potential  $(\frac{r}{r_0})^4$ , was optimized to minimize the total energies of the three elements.

### 4.4.2 Results and discussion

To explain the spin moments in Fe, Co and Ni, it is important to point out that the majority spin bands are mostly filled in all these systems. Therefore, when we go from Fe to Co and then to Ni, which have the effect of adding more valence electrons, the minority spin band will be more populated due to extra electrons and the spin moment drops accordingly (see Figure 4.1).

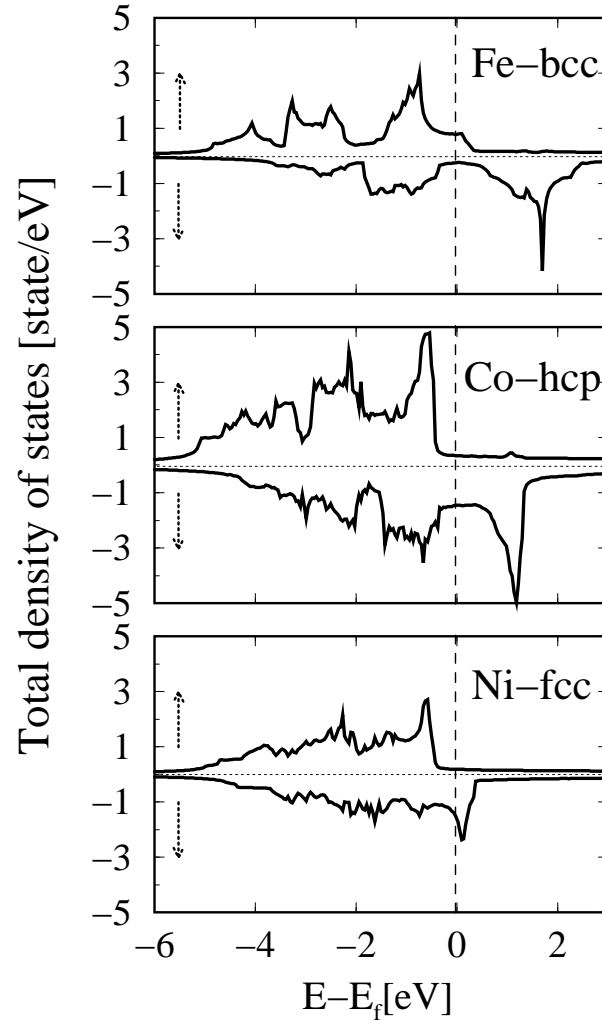


Figure 4.1: Total spin density of states for bcc Fe, hcp Co, and fcc Ni, evaluated with full relativistic FPLO scheme. Indices  $\uparrow$  and  $\downarrow$  denote for majority and minority density of states, respectively.



Table 4.1: Spin ( $M_s$ ) and orbital ( $M_l$ ) moments of bcc Fe, hcp Co and fcc Ni. The indices a and b show the results based on orthogonal and non-orthogonal projections to OP corrections. Experimental values are presented by Stearns [72].

| Scheme                 | $M_s^{\text{Fe}}$ | $M_l^{\text{Fe}}$ | $M_s^{\text{Co}}$ | $M_l^{\text{Co}}$ | $M_s^{\text{Ni}}$ | $M_l^{\text{Ni}}$ |
|------------------------|-------------------|-------------------|-------------------|-------------------|-------------------|-------------------|
| non-relativistic       | 2.21              | 0                 | 1.58              | 0                 | 0.60              | 0                 |
| scalar-relativistic    | 2.19              | 0                 | 1.60              | 0                 | 0.63              | 0                 |
| full-relativistic (SO) | 2.18              | 0.05              | 1.60              | 0.08              | 0.63              | 0.05              |
| LSDA+OPB(a)            | 2.18              | 0.09              | 1.60              | 0.14              | 0.63              | 0.06              |
| (b)                    |                   | 0.08              |                   | 0.12              |                   | 0.05              |
| LSDA+OPE(a)            | 2.18              | 0.12              | 1.60              | 0.19              | 0.63              | 0.06              |
| (b)                    |                   | 0.13              |                   | 0.14              |                   | 0.05              |
| Experiment [72]        | 2.13              | 0.08              | 1.52              | 0.14              | 0.57              | 0.05              |

The calculated spin and orbital moments are listed in Table.4.1. Here we list the spin and orbital moments obtained from different schemes. The orbital moments are strongly depend on the schemes what were applied, whereas the spin moments are not so much sensitive. The two first rows in Table 4.1 show that the orbital moments are vanished in a non-relativistic regime and even when we average out spin-orbit coupling (scalar relativistic calculations).

The orbital moments are small quantities in 3d ferromagnets, ranging from 0.05 to 0.20  $\mu_B$ , as essentially quenched by the bonding (the ligand field). However, the orbital moments in 3d systems are expected to result from the spin-orbit interaction. Therefore, one may intuitively expect an orbital moment that correlates with the spin moment. However, experiments show that this is not the case, since the orbital moment of Co is much larger than in Fe and Ni. In Table 4.1, the third line includes results of the full relativistic calculations in presence of the spin-orbit coupling.

Using OP corrections for Fe and Co can give orbital moments in good agreement with experiment. While LSDA obtains the orbital moment of Ni in a good coincidence with experiment, the orbital moments of Ni based on both OP schemes in their orthogonal projections are over-estimated. However when we compare the orbital moments of Fe and Co obtained in the OPB correction with the OPE results in the form of orthogonal projection, then the latter

gives rise the orbital moments larger than the experimental values. On the other side, the hybridized version of OPE predicts the orbital moment of Co very close to experiment and the same situation takes place when orthogonal version of OPB has been used.

It has to be mentioned, that comparing the orbital moments of Fe, Co, and Ni determine with OPB in FPLO approach, with the OPB values implemented in the Korringa-Kohn-Rostoker (KKR) method [73], the linear-muffin-tin-orbital (LMTO) method [74], and in the spin- and orbital-polarized relativistic multiple-scattering theory (SOPR-MST) method [75], shows a qualitative agreement.

## 4.5 Conclusion

In summary, we have implemented both orbital polarization corrections into band structure FPLO method. The results have shown that the inclusion of relativistic effects (such as spin-orbit coupling) in Kohn-Sham equation is important to get reasonable structural properties compared with experiment. However, we also show that for some systems orbital polarization corrections have to be involved in the relativistic formalism, when we want to determine properly the orbital magnetic moments of the individual atoms in the considered system.

## Chapter 5

# Orbital magnetism in full-Heusler alloys ( $\text{Co}_2\text{YZ}$ )

The aim of the present chapter is to study the coexistence of spin and orbital magnetism in full-Heusler alloys using two discussed orbital polarization corrections in the pervious chapters.

Intense experimental [76, 77, 78, 79] and theoretical [80, 81, 82, 83] efforts have been devoted to Heusler alloys [84] recently. An intriguing property, disclosed for  $\text{Co}_2\text{YZ}$  Heusler compounds by J. Kübler *et al.* [85], is so-called half-metallic ferromagnetism [86], where one spin band is metallic and the other is semiconducting. Much of the recent interest is just due to this feature [87], a 100% spin-polarization at Fermi level that promises potential application in spin-electronic devices. It is, however, frequently overlooked that half-metallicity is bound to well-ordered bulk compounds in most cases [88] and considerable experimental difficulties often prevent the preparation of well-ordered thin films [89] as a precondition for the desired application.

Apart from the mentioned application-driven interest, the magnetism of ideally ordered bulk Heusler compounds still poses a challenge to the theoretical understanding of electronic structure. If orbital magnetism is neglected, any half-metallic ground state is invariant with zero Pauli susceptibility in an external field smaller than a critical field [10]. It is also obvious that the spin magnetic moment per unit cell in such a state must be integer. A number of other, system-specific theoretical [85, 90, 91, 92, 93] and experimental studies [94, 95] of spin-only magnetism leading to half-metallicity of the full-Heusler alloys have been published. On the other hand, less attention has been paid in the past to the orbital degrees of freedom in these compounds. It is clear that the concept of half-metallicity neglects spin-orbit coupling. For instance, neither complete spin-polarization at the Fermi level nor integer magnetic moments can be expected if spin-orbit coupling is taken into account [96, 97]. It is thus interesting to study the magnitude of the related deviations from the idealized case.

Commonly, ligand fields largely quench the orbital magnetic moment in cubic systems containing 3d transition metals. H.J. Elmers *et al* [98] have shown in their x-ray magnetic circular dichroism (XMCD) studies, however, that the orbital moment in the cubic  $\text{Co}_2\text{FeAl}$  full-Heusler compound is quite sizeable,  $M_l \approx 0.5\mu_B/\text{f.u.}$ , and even somewhat larger values were reported for this compound in a more recent study by the same group [100]. With the same method, K. Miyamoto *et al.* and S. Wurmehl *et al.* also found noticeable orbital moments in  $\text{Co}_2\text{MnGe}$  [101] and in  $\text{Co}_2\text{FeSi}$ , [102] respectively.

I. Galanakis [104] considered the orbital magnetic moments of different Heusler compounds in a theoretical approach using the local (spin) density approximation [L(S)DA]. He employed a fully relativistic KKR multiple-scattering Green's function method and found very small orbital magnetic moments on each constituent. Compared with the mentioned experimental results, the orbital moments found by I. Galanakis are smaller by factors of 2-4. This problem was also observed for the alloy system  $\text{Co}_2\text{Cr}_{1-x}\text{Fe}_x\text{Al}$  by S. Wurmehl *et al.*, who found [100] only a slight improvement by using orbital polarization (OP) corrections, and for  $\text{Co}_2\text{FeSi}$  by the same group. In the latter case, neither OP corrections nor relativistic LDA+ $U$  calculations could close the gap between measured and calculated orbital moments, though both approximations improved the mismatch in comparison with LSDA [102].

With the intention to resolve this discrepancy, we focus the present investigation on  $\text{Co}_2\text{YZ}$  full-Heusler compounds with  $\text{Y} = \text{Mn}$  or  $\text{Fe}$ ;  $\text{Z} = \text{Al}$ ,  $\text{Ga}$ ,  $\text{Si}$ , or  $\text{Ge}$ . All combinations of these elements are considered. Some of them, such as  $\text{Co}_2\text{MnSi}$  and  $\text{Co}_2\text{MnGe}$ , were found to be half-metallic in earlier electronic structure calculations [91]. We study the magnetic and electronic properties of these eight compounds with a particular emphasis on the influence of spin-orbit coupling and orbital magnetism. The under-estimation of orbital moments in the LSDA approach reported by I. Galanakis and S. Wurmehl is confirmed. We demonstrate, however, that explicit consideration of orbital polarization effects brings theoretical and experimental data systematically in better coincidence. Finally, we suggest an alternative explanation for the recently [102] measured magnetic moment of  $\text{Co}_2\text{FeSi}$  that can resolve the apparent discrepancy between the two experimental facts of integer total moment and large orbital moment.

This chapter is organized based on very recently work by M. Sargolzaei *et al.* [105] which contains details about the crystal structure, the numerics and the results and discussion including calculated spin moments, orbital moments, a qualitative model for the orbital moments, volume dependent properties of  $\text{Co}_2\text{FeSi}$ , and remarks about half-metallicity.

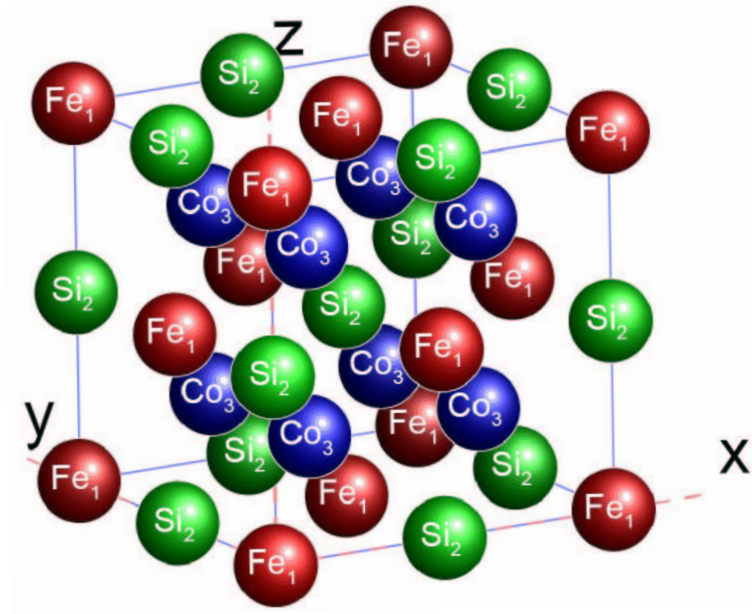


Figure 5.1: Crystal structure of full-Heusler alloy,  $\text{Co}_2\text{FeSi}$ .

## 5.1 Crystal structure and computational details

The considered full-Heusler alloys  $\text{Co}_2\text{YZ}$  adopt the ordered  $\text{L2}_1$ -type structure (space group  $\text{Fm}\bar{3}\text{m}$ ), which may be understood as the result of four interpenetrating face-centered-cubic (fcc) lattices. The Y and Z atoms occupy two fcc sublattices with origin at  $(0\ 0\ 0)$  and  $(1/2\ 1/2\ 1/2)$ , respectively. The Co atoms are located in sublattices with origins at  $(1/4\ 1/4\ 1/4)$  and  $(3/4\ 3/4\ 3/4)$ . For instance, the crystal structure of  $\text{Co}_2\text{FeSi}$  is shown in Figure 5.1.

We have carried out density functional calculations [3, 4] using the relativistic version [67] of the full-potential local-orbital (FPLO) minimum-basis band-structure method [66]. In this scheme the four-component Kohn-Sham-Dirac (KSD) equation, which implicitly contains spin-orbit coupling up to all orders, is solved self consistently. For the present calculations, the following states were included in the valence basis: the  $3s3p;3d4s4p$  states of Co, Mn, Fe, Ga, and Ge and the  $2s2p;3s3p;3d$  states of Al and Si. The inclusion of Ga, Ge, and transition metals  $3s$  and  $3p$  semicore states together with  $2s$  and  $2p$  semicore states of Al and Si into the valence basis was used to account for their non-negligible overlap with neighboring core states. The Al and Si  $3d$  polarization states were used to improve the completeness of the basis set. All radial basis states are provided numerically on a grid and adjusted to the potential in each iteration step. The site-centered potentials and densities were expanded

in spherical harmonic contributions up to  $l_{max} = 12$ . The convergence of the total energies ( $10^{-6}$  Hartree) with respect to the k-space integrations was checked separately for each of the considered Heusler alloys. We found that  $30 \times 30 \times 30 = 27,000$  k-points in the full Brillouin zone were sufficient in all cases. The related stability of charge and magnetic population numbers was better than  $10^{-4}$ . The Spatial extension of the basis orbitals, controlled by a confining potential  $(\frac{r}{r_0})^4$ , was optimized to minimize the total energy.

The Perdew-Wang parametrization [39] of the exchange-correlation (XC) potential in the LSDA was used. In the local spin density approximation for bcc Fe and hcp Co, magnetic spin moments are obtained within typically 5% deviation from experiment. On the other hand, the orbital moments of Fe and Co are found a factor of 2 smaller compared with experimental values in this approach. For a better description of orbital magnetism in the d shell of Fe and Co atoms, two different orbital polarization (OPB and OPE) corrections to LSDA suggested in chapter 3, have been taken into account. Here, the final values of spin and orbital moments are obtained from corresponding projections on the atomic basis states [65, 67].

## 5.2 Results and discussion

We optimized the equilibrium lattice parameters using LSDA total energy calculations. The calculated lattice constants,  $a$ , are 2-3 % smaller than the experimental (mostly, room-temperature) values, [106] Table 5.1. Such deviations are common in the LSDA. We also checked that the OP corrections do not significantly change the evaluated lattice constants. If not indicated otherwise, the LSDA lattice constants are used in the further calculations in order to be model consistent. The LSDA and LSDA+OP spin and orbital moments for each single constituent are summarized in Table 5.2.

### 5.2.1 Calculated spin moments

OP corrections turned out to influence the spin moments only marginally. Thus, we discuss only LSDA spin moments (Table 5.2). As expected, the Mn and Fe atoms as Y components carry the largest spin moments ( $2.65\mu_B$ - $3.09\mu_B$ ) in the considered compounds. The sp atoms are weakly spin-polarized and couple anti-ferromagnetically with Mn, Fe and Co. One should note that the Mn and Co spin moments in the case of  $\text{Co}_2\text{MnZ}$  increase when we substitute Si for Al or Ge for Ga. This is in accordance with the Slater-Pauling behavior [107] discussed by I. Galanakis *et al.* [93]. The total spin magnetic moments of  $\text{Co}_2\text{MnAl}$ ,  $\text{Co}_2\text{MnSi}$ , and  $\text{Co}_2\text{MnGe}$  are very close to an integer value ( $4\mu_B$ ,  $5\mu_B$ , and  $5\mu_B$ , respectively). In particular,  $\text{Co}_2\text{MnSi}$  and  $\text{Co}_2\text{MnGe}$  are found to be half-metals in the calculations, if spin-orbit coupling is ne-

Table 5.1: The experimental lattice constants (Villars *et al.*[106] ) are compared with the calculated LSDA lattice constants. The values are in atomic units.

| Co <sub>2</sub> YZ   | $a^{\text{LSDA}}$ | $a^{\text{exp}}$ |
|----------------------|-------------------|------------------|
| Co <sub>2</sub> MnAl | 10.56             | 10.88            |
| Co <sub>2</sub> MnSi | 10.44             | 10.69            |
| Co <sub>2</sub> MnGa | 10.56             | 10.91            |
| Co <sub>2</sub> MnGe | 10.62             | 10.86            |
| Co <sub>2</sub> FeAl | 10.54             | 10.83            |
| Co <sub>2</sub> FeSi | 10.40             | 10.67            |
| Co <sub>2</sub> FeGa | 10.56             | 10.84            |
| Co <sub>2</sub> FeGe | 10.60             | 10.85            |

glected. The tiny deviation from integer Bohr magneton number is due to spin-orbit coupling that slightly reduces the spin moment. The compound Co<sub>2</sub>MnAl is very close to half-metallicity (see Figure 5.2, and Table 5.5) without spin-orbit coupling, while the isoelectronic Co<sub>2</sub>MnGa is not a half-metal in our approach. The probable reason for this dissimilarity is the larger size of the Ga atom compared with the Al atom that leads to a stronger hybridization with the transition metal valence states and a related broadening of the bands, see Figure 5.2. The gap in the minority spin density of states is more narrow than the related gap of Co<sub>2</sub>MnAl and the broadened minority states cross the Fermi level. A different situation is found for the case of Co<sub>2</sub>MnSi and Co<sub>2</sub>MnGe. Here, the Fermi level is situated close to the unoccupied minority states since the number of valence electrons is by one larger than in the Co<sub>2</sub>MnAl and Co<sub>2</sub>MnGa compounds. Thus, the gap narrowing by replacing Si with Ge does not destroy the half-metallicity.

The Co<sub>2</sub>FeZ compounds are normal ferromagnetic metals with both majority and minority bands crossing the Fermi level, see Figure 5.2. The Fe and Co spin moments are less affected by changing the alloying element Z in these compounds and the total spin moment stays close to 5  $\mu_B$  per formula unit. This behavior violates the Slater-Pauling behavior, as it was already discussed by I. Galanakis *et al.* for the two cases of Co<sub>2</sub>FeAl and Co<sub>2</sub>FeSi [93]. The particular case of Co<sub>2</sub>FeSi is discussed in more detail in Section 5.2.4.

Table 5.2: Spin ( $M_s$ ) and orbital ( $M_l$ ) moments for constituents of the  $\text{Co}_2\text{YZ}$  full-Heusler alloys together with total spin and total orbital moments and their sum, calculated at the LSDA lattice constant. The first line for each compound gives the LSDA results and related model results (see text) in parentheses. Lines with the indices OPB and OPE show results of calculations with orbital polarization corrections suggested by O. Eriksson *et al.* [20, 21] and by H. Eschrig *et al.* [23] added to the LSDA-XC energy functional, respectively. The influence of OP corrections on the spin moments is marginal and left out in the Table.

| $\text{Co}_2\text{YZ}$   | $M_s^{\text{Co}}$ | $M_l^{\text{Co}}$ | $M_s^{\text{Y}}$ | $M_l^{\text{Y}}$ | $M_s^{\text{Z}}$ | $M_s^{\text{total}}$ | $M_l^{\text{total}}$ | $M^{\text{total}}$ |
|--------------------------|-------------------|-------------------|------------------|------------------|------------------|----------------------|----------------------|--------------------|
| $\text{Co}_2\text{MnAl}$ | 0.740             | 0.014 (0.068)     | 2.650            | 0.010            | -0.133           | 3.997                | 0.038                | 4.035              |
| OPB                      |                   | 0.023             |                  | 0.008            |                  |                      | 0.054                | 4.051              |
| OPE                      |                   | 0.027             |                  | 0.007            |                  |                      | 0.061                | 4.058              |
| $\text{Co}_2\text{MnSi}$ | 1.022             | 0.029 (0.077)     | 3.028            | 0.010            | -0.078           | 4.994                | 0.069                | 5.063              |
| OPB                      |                   | 0.040             |                  | 0.013            |                  |                      | 0.095                | 5.089              |
| OPE                      |                   | 0.045             |                  | 0.015            |                  |                      | 0.107                | 5.101              |
| $\text{Co}_2\text{MnGa}$ | 0.715             | 0.011 (0.067)     | 2.698            | 0.014            | -0.089           | 4.039                | 0.036                | 4.075              |
| OPB                      |                   | 0.020             |                  | 0.013            |                  |                      | 0.053                | 4.092              |
| OPE                      |                   | 0.024             |                  | 0.017            |                  |                      | 0.065                | 4.104              |
| $\text{Co}_2\text{MnGe}$ | 0.978             | 0.031 (0.065)     | 3.089            | 0.015            | -0.050           | 4.995                | 0.078                | 5.073              |
| OPB                      |                   | 0.044             |                  | 0.020            |                  |                      | 0.109                | 5.104              |
| OPE                      |                   | 0.049             |                  | 0.023            |                  |                      | 0.122                | 5.117              |
| $\text{Co}_2\text{FeAl}$ | 1.116             | 0.050 (0.058)     | 2.704            | 0.040 (0.051)    | -0.098           | 4.838                | 0.140                | 4.978              |
| OPB                      |                   | 0.058             |                  | 0.072            |                  |                      | 0.189                | 5.027              |
| OPE                      |                   | 0.067             |                  | 0.082            |                  |                      | 0.217                | 5.055              |
| $\text{Co}_2\text{FeSi}$ | 1.198             | 0.038 (0.065)     | 2.671            | 0.072 (0.031)    | -0.034           | 5.033                | 0.149                | 5.182              |
| OPB                      |                   | 0.053             |                  | 0.127            |                  |                      | 0.235                | 5.268              |
| OPE                      |                   | 0.060             |                  | 0.159            |                  |                      | 0.281                | 5.314              |
| $\text{Co}_2\text{FeGa}$ | 1.114             | 0.040 (0.056)     | 2.738            | 0.054 (0.061)    | -0.061           | 4.905                | 0.134                | 5.039              |
| OPB                      |                   | 0.060             |                  | 0.077            |                  |                      | 0.197                | 5.102              |
| OPE                      |                   | 0.071             |                  | 0.090            |                  |                      | 0.232                | 5.137              |
| $\text{Co}_2\text{FeGe}$ | 1.257             | 0.045 (0.067)     | 2.752            | 0.080 (0.038)    | 0.006            | 5.272                | 0.170                | 5.442              |
| OPB                      |                   | 0.063             |                  | 0.140            |                  |                      | 0.267                | 5.539              |
| OPE                      |                   | 0.074             |                  | 0.184            |                  |                      | 0.333                | 5.605              |



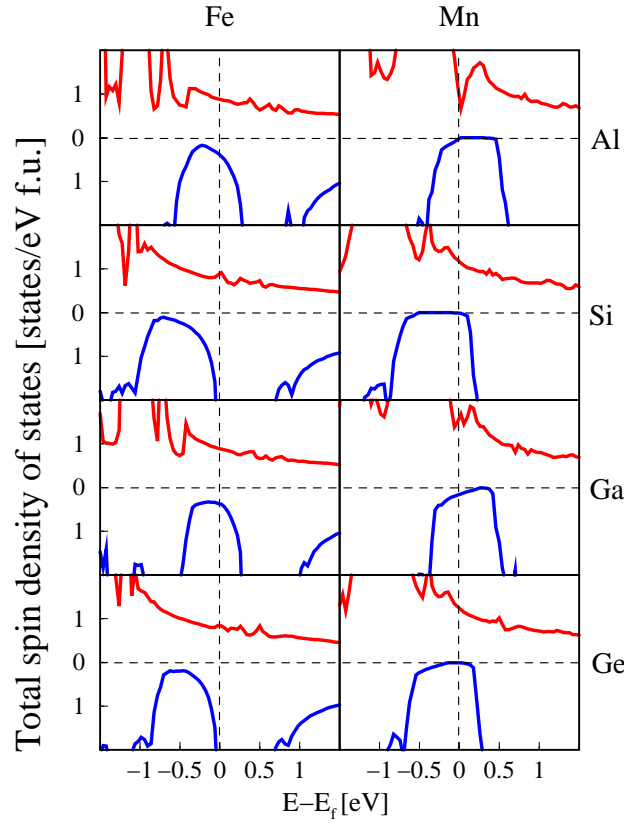


Figure 5.2: Total densities of states of all considered compounds close to the Fermi level, obtained by fully relativistic LSDA calculations. Majority (minority) spin channels with dashed red (solid blue) lines are shown in the upper (lower) parts of the individual panels.

### 5.2.2 Orbital moments

Total and site-resolved orbital moments calculated in different approximations are given in Table 5.2. Relativistic LSDA produces orbital moments induced from spin polarization via spin-orbit coupling. Our LSDA calculated orbital moments are in a very good agreement (within a deviation of  $0.005 \mu_B$  or less) with the orbital moments evaluated for four of the considered compounds by I. Galanakis [104].

The orbital moments are in all cases small compared with the spin moments as it is usual in cubic 3d transition metals. In particular, the Mn orbital moments are tiny since the Mn 3d shell is close to half-filling. Comparing the orbital moments of Fe and Co in  $\text{Co}_2\text{FeZ}$  with those of Mn and Co in  $\text{Co}_2\text{MnZ}$  reveals that the former are considerably larger.

To our knowledge, there are only three XMCD experiments to determine orbital moments for the considered compounds. Since the ratio  $M_l/M_s$  is more closely related to the original experimental data than the individual moments, we compare experimental and theoretical results of this ratio in Table 5.3. It should be pointed out that the analysis of the XMCD experiments give forth the ratio  $M_l/(M_s - 7\langle T_z \rangle)$ . The magnetic dipole term  $\langle T_z \rangle$  comes about by the anisotropy of the atomic spin density due to spin-orbit coupling or ligand field effects [108, 109, 110]. However, for 3d transition metal atoms in a cubic environment, the  $7\langle T_z \rangle$  is typically by a factor of about  $10^{-3}$  smaller than the spin magnetic moment  $M_s$ , [100, 111] and therefore can be neglected in the considered cubic compounds.

From their XMCD studies, K. Miyamoto *et al.* obtained a ratio of about 0.07 for Co and of about 0.01 for Mn in  $\text{Co}_2\text{MnGe}$  [101]. The Co value is more than two times larger than that obtained by our LSDA calculation, 0.03. The same LSDA value has been found by I. Galanakis *et al.* [104], and an even smaller value of about 0.02 has been obtained by S. Picozzi *et al.* [91] by means of generalized gradient approximation FLAPW calculations. However, when we compare the orbital magnetic moments calculated with the two variants of OP corrections ( $0.044\mu_B/\text{Co}$  and  $0.049\mu_B/\text{Co}$ , Table 5.2) which account for the direct non-relativistic interaction of the orbital moments with the inner field, they are in a much better agreement with experiment. This enhancement to about 0.05 is slightly dependent on the lattice constant, Table 5.3. Also, the LSDA+OP ratios for Mn are almost equal to the experimental value of 0.01, whereas the related LSDA results are smaller (0.005 in our calculation, 0.007 in Ref. [104] and 0.003 in Ref. [91]).

A further XMCD study was recently carried out on quaternary alloys by H.J. Elmers *et al.*, including the case of  $\text{Co}_2\text{FeAl}$  [98, 99]. They found that the ratios of  $M_l/M_s$  for Co and Fe are  $0.14 \pm 0.02$  and  $0.06 \pm 0.02$ , respectively. These ratios are found to be 0.045 for Co and 0.015 for Fe in our LSDA calculations. Even the application of OP corrections results in values that are

Table 5.3: Comparison of available experimental (XMCD) and calculated ratios  $M_l/M_s$ . Calculated data obtained by LSDA and LSDA+OPE [23] are given for both LSDA and experimental lattice constants.

| Element<br>in compound     | Exp                      | LSDA<br>at $a^{\text{LSDA}}$ | LSDA+OPE<br>at $a^{\text{LSDA}}$ | LSDA<br>at $a^{\text{exp}}$ | LSDA+OPE<br>at $a^{\text{exp}}$ |
|----------------------------|--------------------------|------------------------------|----------------------------------|-----------------------------|---------------------------------|
| Co in Co <sub>2</sub> MnGe | 0.07 [101]               | 0.032                        | 0.050                            | 0.034                       | 0.056                           |
| Mn in Co <sub>2</sub> MnGe | 0.01 [101]               | 0.005                        | 0.007                            | 0.006                       | 0.008                           |
| Co in Co <sub>2</sub> FeAl | $0.14 \pm 0.02$ [98, 99] | 0.045                        | 0.060                            | 0.041                       | 0.072                           |
| Fe in Co <sub>2</sub> FeAl | $0.06 \pm 0.02$ [98, 99] | 0.015                        | 0.030                            | 0.020                       | 0.033                           |
| Co in Co <sub>2</sub> FeSi | 0.1 [102]                | 0.032                        | 0.050                            | 0.037                       | 0.064                           |
| Fe in Co <sub>2</sub> FeSi | 0.05 [102]               | 0.027                        | 0.060                            | 0.026                       | 0.050                           |

roughly two times smaller than the experimental values.

Most recently, an XMCD experiment was reported by S. Wurmehl *et al.* for Co<sub>2</sub>FeSi [102]. Their  $M_l/M_s$  ratios, extrapolated to 0 K, are 0.1 for Co and 0.05 for Fe, respectively. Our corresponding LSDA ratios amount to 0.032 for Co and 0.027 for Fe. Using the two variants of OP corrections reveals a very good agreement with the experimental value for Fe, but both of them give two times smaller values than the experiment for Co (about 0.05...0.06 for both elements). It should be noted, that our result is closer to the experimental result for Fe than the LDA+ $U$  result given in Ref. [102] (0.05 for Co and 0.02 for Fe, respectively).

Summarizing this section, orbital polarization corrections reduce the difference between calculated and measured ratios  $M_l/M_s$  in comparison to plain LSDA for all six considered cases. In the mean, LSDA yields about 40% of the measured ratio, while LSDA+OPE yields about 70%, with moderate sensitivity to the choice of the lattice parameter.

### 5.2.3 Ligand field model for the orbital moments

In order to better understand the origin of the relatively small but yet different orbital moments of Co, Mn and Fe in the distinct Heusler alloys compiled in Table 5.2, we performed a simple model calculation for the LSDA orbital moment of the 3d shell, based on the model described in Ref. [112]. The value of the orbital moment is determined by an interplay between the ligand field and the spin-orbit coupling. The ligand field splitting tends to quench the orbital moment while spin-orbit interaction partially restores it. Since the

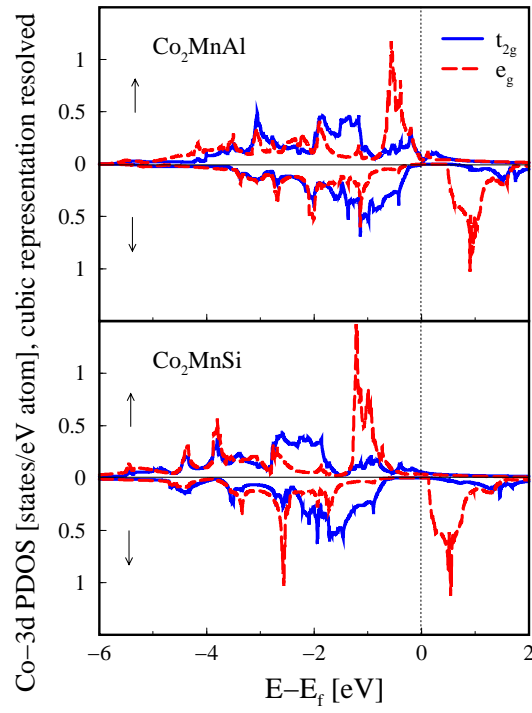


Figure 5.3: Co 3d partial DOS for  $\text{Co}_2\text{MnAl}$  (upper panel) and  $\text{Co}_2\text{MnSi}$  (lower panel). The three-fold degenerate  $t_{2g}$  (two-fold degenerate  $e_g$ ) states are shown with dashed red (solid blue) lines in majority ( $\uparrow$ ) and minority ( $\downarrow$ ) spin sub-shell.

systems at hand are cubic, the ligand field splits the five-fold degenerate 3d spin sub-shell in three-fold degenerate  $t_{2g}$  states ( $|yz\rangle, |zx\rangle, |xy\rangle$ ) and two-fold degenerate  $e_g$  states ( $|x^2 - y^2\rangle, |3z^2 - r^2\rangle$ ) in the standard notation of real d-orbitals. Each of the real spherical harmonics has zero orbital moment. Figure 5.3 shows this situation for two examples,  $\text{Co}_2\text{MnAl}$  and  $\text{Co}_2\text{MnSi}$ , in the absence of spin-orbit coupling. Assuming the quantization axes for spin and orbital moments to be the same (z-direction) and the majority spin projection to be positive, the Hamiltonian matrix of the sum of spin-orbit and ligand field interactions in the subspace of the  $t_{2g}$  and  $e_g$  functions for minority spin reads:

$$\begin{array}{l} |yz\rangle : \\ |zx\rangle : \\ |xy\rangle : \\ |x^2 - y^2\rangle : \\ |3z^2 - r^2\rangle : \end{array} : \begin{pmatrix} 0 & -i\xi/2 & 0 & 0 & 0 \\ +i\xi/2 & 0 & 0 & 0 & 0 \\ 0 & 0 & 0 & -i\xi & 0 \\ 0 & 0 & +i\xi & \Delta & 0 \\ 0 & 0 & 0 & 0 & \Delta \end{pmatrix}, \quad (5.1)$$

where  $\Delta$  is the ligand field splitting between the  $e_g$  and  $t_{2g}$  levels and  $\xi \sum_i \hat{l}_{z,i} \hat{s}_{z,i}$  is the spin-orbit coupling operator with the positive spin-orbit coupling constant  $\xi$ . Under the condition  $\xi \ll \Delta$ , which is usually fulfilled in 3d transition metals, the new minority  $t_{2g}$ -like eigenstates have energies  $-\xi/2$ ,  $-\xi^2/\Delta$ , and  $\xi/2$  and the  $e_g$ -like eigenstates have energies  $\Delta$ , and  $\Delta + \xi^2/\Delta$ . The orbital moment is calculated by the following approximate expression:

$$M_l = - \sum_{\sigma=\uparrow,\downarrow} \sum_{i=1}^5 \langle l_z \rangle_i \times \text{sgn}(\sigma) \int_{-\infty}^{\epsilon_F} \text{PDOS}(i, \sigma) dE, \quad (5.2)$$

where  $\langle l_z \rangle_i = 1, 4\xi/\Delta, -1$  are the orbital moment projections of the minority  $t_{2g}$ -like new eigenstates and  $\langle l_z \rangle_i = 0, -4\xi/\Delta$  are the orbital moment projections of the minority  $e_g$ -like new eigenstates. PDOS is the partial density of states for the  $t_{2g}$ -like and  $e_g$ -like new eigenstates.

Using a calculated spin-orbit coupling constant  $\xi$  of 0.054 (0.045) eV for Co (Fe) [113] and typical ligand field splitting  $\Delta$  of 1 eV, we obtained the numbers given in parentheses in Table 5.2. These orbital magnetic moments are in qualitative agreement with the orbital moments obtained by the full calculation, though the individual numbers differ by factors up to 6. While the model provides the principal mechanisms of spin-orbit coupling on the orbital moment, the reason for the deviations lies in the simplification of the model Hamiltonian, where the action of the ligand field is described by a single parameter. The densities of states presented in Figure 5.3 show, that this approximation is not well justified:  $t_{2g}$  and  $e_g$  states are not simply split but exhibit considerably different shapes of the DOS.

Another, yet more simplified, model was suggested some time ago by Eriksson *et al.* [114] and, in parallel, by Ebert *et al* [115]. In that model, spin-orbit

Table 5.4: Comparison of available experimental and calculated total magnetic moments per formula unit. Calculated data obtained by LSDA and LSDA+OPE are given for both LSDA and experimental lattice constants. The degree of order within the  $\text{L2}_1$  structure has not always been analyzed. All experimental data were obtained at low temperature.

| Compound                 | $M_{\text{exp}}^{\text{tot}}$                   | $M_{\text{LSDA}}^{\text{tot}}$<br>at $a^{\text{LSDA}}$ | $M_{\text{OPE}}^{\text{tot}}$<br>at $a^{\text{LSDA}}$ | $M_{\text{LSDA}}^{\text{tot}}$<br>at $a^{\text{exp}}$ | $M_{\text{OPE}}^{\text{tot}}$<br>at $a^{\text{exp}}$ |
|--------------------------|---|--|---|---|--|
| $\text{Co}_2\text{MnAl}$ | $4.01 \pm 0.05$ [118]                           | 4.035  | 4.058   | 4.066   | 4.095  |
| $\text{Co}_2\text{MnSi}$ | 4.90 [116], $5.07 \pm 0.05$ [118]               | 5.063  | 5.101   | 5.071   | 5.114  |
| $\text{Co}_2\text{MnGa}$ | $4.05 \pm 0.05$ [118]                           | 4.075  | 4.104   | 4.150   | 4.162  |
| $\text{Co}_2\text{MnGe}$ | 4.93 [116], $5.11 \pm 0.05$ [118, 119]          | 5.073  | 5.117   | 5.078   | 5.129  |
| $\text{Co}_2\text{FeAl}$ | 4.96 [116], 5.29 [99]                           | 4.978  | 5.055   | 5.083   | 5.193  |
| $\text{Co}_2\text{FeSi}$ | 5.18 [116], 5.7 [117],<br>$5.97 \pm 0.05$ [102] | 5.182  | 5.314   | 5.664   | 5.800  |
| $\text{Co}_2\text{FeGa}$ | 5.13 [116], 5.15 [95]                           | 5.039  | 5.137   | 5.149   | 5.270  |
| $\text{Co}_2\text{FeGe}$ | 5.54 [116]                                      | 5.442  | 5.605   | 5.700   | 5.857  |

coupling was assumed to shift the  $m_l$ -subbands rigidly. Such a shift yields negative orbital moment contributions in the majority spin subband and positive orbital moment contributions in the minority spin subband, in accordance with Hund's third rule. Applied to half-metals, a rigid shift would give zero orbital moment contribution for the spin channel which has a gap at the Fermi level. That means the rigid shift model would provide negative orbital moments for at least the two half-metallic compounds considered here, in contradiction with the full calculations and with experiment on  $\text{Co}_2\text{MnGe}$ .

As a consequence, the change of the orbital moment projection of the states due to spin-orbit coupling considered in the present model, (Eq.5.4), *is crucial for obtaining the correct sign* of the orbital moment. The values given in Table 5.2 are composed of relatively large (about  $0.3\mu_B$ ) and almost compensating contributions from the two spin channels. Thus, the quantitative result is sensitive to the discussed simplification of the model.

#### 5.2.4 Volume dependent properties of $\text{Co}_2\text{FeSi}$

The compound  $\text{Co}_2\text{FeSi}$  went into the focus of interest recently, when S. Wurmehl *et al.* measured a large total magnetic moment of about  $6\mu_B$  [102]. This value, which is higher than previously measured values of  $5.18\mu_B$  and

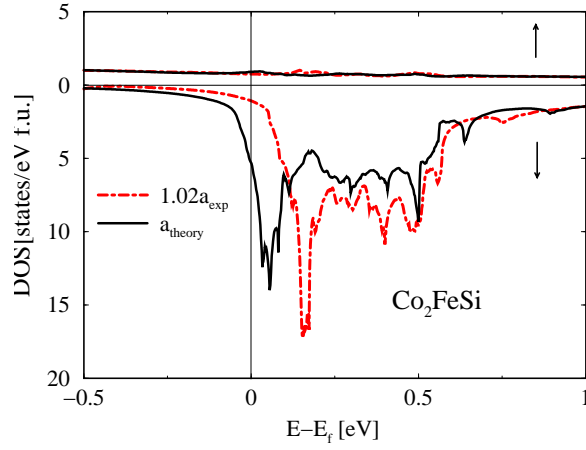


Figure 5.4: Density of states of  $\text{Co}_2\text{FeSi}$  close to the Fermi level, evaluated for two different lattice parameters. Theoretical lattice parameter: full black lines; 1.02-fold experimental lattice parameter: dashed red lines. Majority (minority) spin DOS are given in the upper (lower) part of the figure.

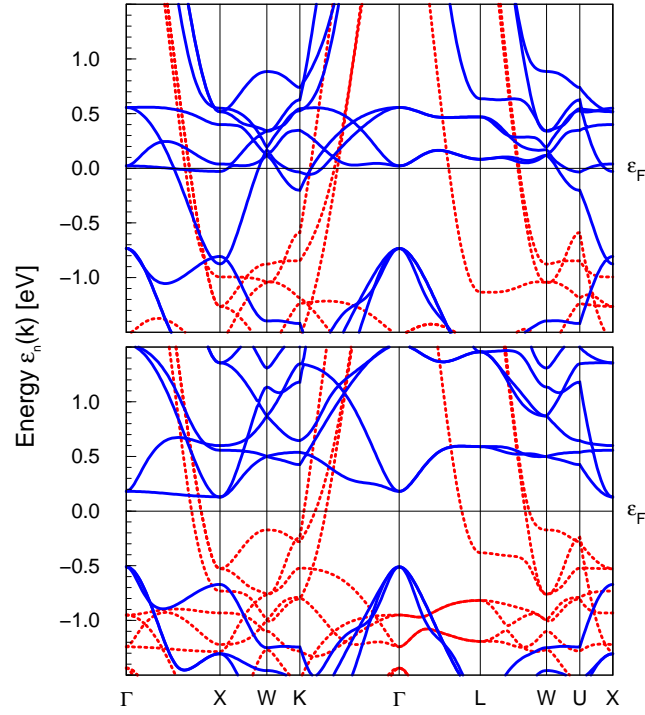


Figure 5.5: Band structure of  $\text{Co}_2\text{FeSi}$  (upper panel) and  $\text{Co}_2\text{MnSi}$  (lower panel) close to the Fermi level. The spin character is indicated by the red dashed lines (majority spin) and blue full lines (minority spin).

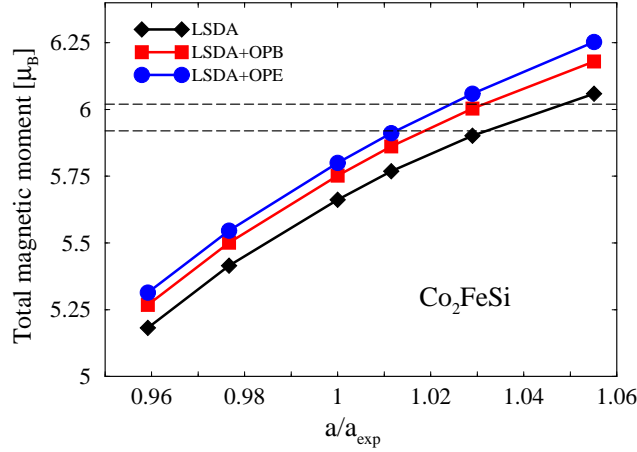


Figure 5.6: Volume dependence of the calculated total magnetic moment of  $\text{Co}_2\text{FeSi}$ . LSDA: black line with diamonds; LSDA+OPB: red line with squares; LSDA+OPE: blue line with bullets. The dashed lines show the range of experimental errors in Ref. [102] [ $(5.97 \pm 0.05)\mu_B$  at  $T=5$  K].

[116]  $5.7 \mu_B$  [117] indicates half-metallic behavior. Indeed, related LDA+ $U$  calculations yield a gap in the minority spin DOS at the Fermi level and a total moment of  $6 \mu_B$ . It was concluded that  $\text{Co}_2\text{FeSi}$  is a half-metal with important correlation effects [102, 103]. On the other hand, both LSDA and LSDA+OP calculations yield much smaller total moments, ( $\sim 5.2 \dots 5.3 \mu_B$ ) at theoretical lattice constant, see Table 5.2, and a large DOS in both spin channels, see Figure 5.2.

The question arises of why this compound shows strong correlation effects, while the other, chemically very similar compounds are well described by LSDA(+OP) theory. This fact is demonstrated in Table 5.4, where experimental total moments are compared with total moments calculated at both theoretical and experimental lattice constants. Concerning the Mn-containing compounds it can be stated that the agreement between experiment and theory is within two times the experimental error bounds (including the scatter of experimental results) for both choices of lattice parameters and for both LSDA and LSDA+OP approaches.

The situation is less satisfactory for the Fe-containing compounds. Here, on the one hand, significant scatter in the experimental data is found, pointing to sensitivity with respect to the preparation. For instance, the experimental scatter could be caused by different degrees of disorder in the samples, as observed for  $\text{Co}_2\text{FeAl}$  earlier [100]. Also, the calculated data confirm such a sensitivity; while the total moment of Mn-containing compounds is almost insensitive to lattice expansion, the Fe-containing compounds show considerably different moments at  $a^{\text{LSDA}}$  and  $a^{\text{exp}}$ , respectively. To be specific, LSDA+OPE data



will be compared with experiment, since this approach describes the  $M_l/M_s$  ratio reasonably well.

The calculated total moments of  $\text{Co}_2\text{FeAl}$ ,  $\text{Co}_2\text{FeGa}$ , and  $\text{Co}_2\text{FeGe}$  are close to (at  $a^{\text{LSDA}}$ ) or moderately larger than (at  $a^{\text{exp}}$ ) the measured ones. On the other hand, the calculated total moments of  $\text{Co}_2\text{FeSi}$  are within the scatter of the experimental moments. Most obvious is the large dependence of the total moment of  $\text{Co}_2\text{FeSi}$  on the lattice spacing: it changes by 10% between theoretical and experimental lattice constant.

The reason for this sensitivity is elucidated in Figure 5.4. At the theoretical lattice constant, the Fermi level is situated in a steep slope at the band edge of an almost empty minority spin  $3d$  band. The related band structure is shown in Figure 5.5 and compared with the band structure of  $\text{Co}_2\text{MnSi}$ . The dominating spin character of the states is indicated by red dashed lines (majority) and blue full lines (minority). Spin-orbit interaction mixes the spins, but this effect is small in the considered  $3d$  elements, see Section 5.2.5. At the Fermi level, almost pure majority spin bands are present in  $\text{Co}_2\text{MnSi}$ , whereas flat minority spin bands cross the Fermi level in  $\text{Co}_2\text{FeSi}$ . The latter give rise to the discussed steep band edge (Figure 5.4) and, thus, to the sensitivity of the magnetic moment of  $\text{Co}_2\text{FeSi}$  with respect to the lattice spacing. Similar flat bands are present in  $\text{Co}_2\text{MnSi}$  as well, but here they are unoccupied due to the larger exchange splitting of Mn in comparison with Fe.

If the volume of  $\text{Co}_2\text{FeSi}$  is increased, the flat minority spin band becomes more narrow and is further emptied. In turn, the exchange splitting increases, reinforcing the magneto-volume effect. At a lattice constant slightly larger than the experimental one, the band is empty (Figure 5.4, red dashed line). The resulting dependence of the total moment on the lattice parameter in all three employed approximations is shown in Figure 5.6. An expansion of slightly more than 1% beyond the experimental lattice parameter brings the calculated LSDA+OPE moment into the range defined by the experimental error bounds of the newest data [102]. At this spacing, the ratios  $M_l/M_s$ , calculated with LSDA+OPE, amount to 0.08 for Co and 0.045 for Fe, in very nice agreement with the experimental values of 0.1 and 0.05, respectively [102]. This model dependence of the magnetic moment on the lattice parameters could be experimentally checked under pressure to decide whether  $\text{Co}_2\text{FeSi}$  is a half-metal or not.

These results suggest an alternative explanation of the measured integer total moment of  $\text{Co}_2\text{FeSi}$ , contrasting the suggested correlation-induced half-metallicity. While the LDA+ $U$  approach yields a half-metallic state with an integer total moment and a total orbital moment of about  $0.2\mu_B$  at the experimental lattice constant, [102] the LSDA+OPE approach yields the experimental total moment at a 1.5...2% expanded lattice constant, and a total orbital moment of about  $0.35\mu_B$ . This is close to the experimental value of about  $0.45\mu_B$ , estimated from the measured moment ratios and the calculated site

Table 5.5: Spin polarization degree for half-ferromagnetic  $\text{Co}_2\text{YZ}$  full-Heusler alloys. SPD values at LSDA lattice constants without spin-orbit coupling (SO: no) and with spin-orbit coupling (SO: yes) are given in percent.

| Y  | SO  | Al | Si  | Ga | Ge  |
|----|-----|----|-----|----|-----|
| Mn | no  | 97 | 100 | 81 | 100 |
|    | yes | 95 | 97  | 81 | 99  |
| Fe | no  | 39 | -77 | 43 | -67 |
|    | yes | 38 | -72 | 41 | -65 |

spin moments given in Ref. [102]. The degree of spin polarization at the Fermi level (see Section 5.2.5) is very small in the suggested alternative approach, see Figure 5.4.

What remains open is the question why a lattice expansion is needed to simulate the experimental situation. It is clear from Figure 5.4, that the electronic structure of well-ordered  $\text{Co}_2\text{FeSi}$  at theoretical lattice spacing bears a tendency toward enhancement of the magnetic moment. A small site-disorder, that cannot be completely excluded on the basis of the existing data, [102] could provide such a moment enhancement, as it was found for the sister compound  $\text{Co}_2\text{FeAl}$  [100] which is much less susceptible to parameter changes than  $\text{Co}_2\text{FeSi}$ , see Table 5.4.

Summarizing this section, we propose that the measured moment of  $\text{Co}_2\text{FeSi}$  need not be caused by a correlated half-metallic state. It could, e.g., arise from a small but influential disorder of the sample. In the latter case, the spin polarization at Fermi level would be very small.

### 5.2.5 Half-metallicity

We have finally studied the effect of spin-orbit coupling and orbital polarization on the half-metallicity of the considered full-Heusler alloys. The spin polarization degree (SPD) of the density of states (DOS) is defined by

$$\text{SPD} = \frac{n^\uparrow(\varepsilon_F) - n^\downarrow(\varepsilon_F)}{n^\uparrow(\varepsilon_F) + n^\downarrow(\varepsilon_F)}, \quad (5.3)$$

where  $n^\sigma(\varepsilon_F)$  corresponds to majority ( $\uparrow$ ) and minority ( $\downarrow$ ) spin DOS at the Fermi level. In Table 5.5, we present the SPD values in percent, with and without spin-orbit coupling at LSDA lattice constants. Recall, in perfect half-metals, SPD amounts to 100%. According to our band structure calculations,

only  $\text{Co}_2\text{MnSi}$  and  $\text{Co}_2\text{MnGe}$  are fully spin polarized in the absence of spin-orbit coupling. However, spin-orbit coupling reduces SPD by 3% and 1%, respectively for those intermetallic compounds. Adding OP corrections to the LSDA-XC functional does not significantly change the spin polarization degree.

Moreover, the calculated SPD values for the considered compounds indicate that the Mn-based full-Heusler alloys seem to be more suitable candidates for half-metallicity, whereas SPD values for Fe-based full-Heusler alloys considerably deviate from 100%. For instance,  $\text{Co}_2\text{FeSi}$  has a relatively large negative SPD value at LSDA lattice constant. From Figure 3 and the discussion in previous section it is, however, obvious that lattice expansion considerably reduces the SPD value.

Recently, S.V. Karthik *et al.* [120] have shown in their point contact Andreev reflection (PCAR) experiments that  $\text{Co}_2\text{FeAl}$  is a normal ferromagnet with PCAR spin polarization value of 56%. This finding is in qualitative agreement with our result (SPD 38%) and KKR result (30%) obtained by Y. Miura *et al.* [80]. One should note that there is no one-to-one correspondence between PCAR data and SPD values obtained from the DOS [121]. Only in an ideal half-metal are both values equal to 100%. Note further that the measurement of spin polarization value at the Fermi level is a quantity very sensitive to the sample preparation. S. Picozzi *et al.* have shown that defects such as Mn and Co antisites destroy the half-metallicity for  $\text{Co}_2\text{MnSi}$  and  $\text{Co}_2\text{MnGe}$  [122].

Concerning  $\text{Co}_2\text{FeGa}$ , our calculated SPD (41%) falls in between two other calculated values (37%, LMTO-ASA calculation by R.Y. Umetsu *et al.* [123]; 58%, FLAPW result by M. Zhang *et al.* [95]). All these results qualitatively match the related PCAR data (58%) [95].

The fully ordered  $\text{Co}_2\text{MnSi}$  with  $\text{L2}_1$  structure is predicted to be a half-metal in our calculations which is in good agreement with LSDA results obtained by S. Ishida *et al.* [90] with the LMTO-ASA method and by H.C. Kandpal *et al.* [103] with the FLAPW approach. In contrast with these theoretical predictions, L. Ritchie *et al.* in their PCAR experiments have found that  $\text{Co}_2\text{MnSi}$  is a normal ferromagnet with PCAR spin polarization of 55% [94]. As they discussed the PCAR values are strongly dependent on surface segregation and disorder.

### 5.3 Conclusion

Density functional FPLO calculations were performed for  $\text{Co}_2\text{YZ}$  ( $\text{Y}=\text{Mn}, \text{Fe}$  and  $\text{Z}=\text{Al}, \text{Si}, \text{Ga}, \text{Ge}$ ) full-Heusler alloys. We have calculated the spin and orbital moments of individual components in each compound including spin-orbit coupling and two variants of orbital polarization corrections.

Calculated orbital moments are in a reasonable agreement with experiment if orbital polarization corrections are taken into account. A rigid-band model for the orbital moment yields the wrong sign in the case of half-metals. Considering changes of the character of ligand field states split by spin-orbit in-

teraction yields orbital moments with the correct sign and order of magnitude, but a single ligand field parameter does not provide quantitative agreement with the full calculations. A large value of about  $0.18\mu_B$  is predicted for the Fe orbital moment in Co<sub>2</sub>FeGe. Further experiments to check this prediction are desirable. An explanation is proposed for the recently measured total moment of Co<sub>2</sub>FeSi and its orbital contributions. This explanation relies on a combination of orbital polarization enhancement (mainly driven by exchange) and residual site-disorder. It predicts almost balanced spin-up and spin-down densities of states.

# Chapter 6

## Co impurities in Au host matrices

In the previous chapters, it has been shown that the orbital moment,  $M_l$ , in magnetic materials is determined by the interplay of several effects, such as Coulomb interaction, the spin-orbit interaction, hybridization, and the ligand fields. To study those effects, the independent determination of  $M_l$  and spin magnetic moments,  $M_s$ , was carried out.

Recall, in free atoms Hund's second rule predicts a maximum orbital moment. In contrast, the orbital moments in solids are more or less quenched as a result of electron delocalization and band formation. For instance, in chapter 5 it was shown that the individual orbital moments in the considered full-Heusler alloys are very small due to the action of the ligand fields. However, for exceptional cases orbital moments can be large even in a solid. An example for the latter situation will be presented in this chapter.

Among of the magnetic elements, Co has attracted special attention in the field of orbital magnetism. In depending on the chemical and structure environment, Co exhibits considerable differences in the size of its orbital moment. For instance, Co films sandwiched between Au layers [124] and single cobalt atoms deposited onto platinum [125] show almost unquenched orbital moments ( $1.1 \mu_B$ ). Co nanoclusters on Au ( $0.16$ - $0.21 \mu_B$ ) [126], one dimensional Co monoatomic chains ( $0.68 \mu_B$ ) [127], ultrathin Co films on Ge ( $0.14$ - $0.22 \mu_B$ ) [128], Co on Ni ( $0.13 \mu_B$ ), Co on Pd ( $0.29 \mu_B$ ) and Co on Pt ( $0.21 \mu_B$ ) [129], show different orbital moments per Co atom.

The investigation of magnetic impurities in non-magnetic metals is an old problem with particular subtleties [130, 131]. In particular, direct investigation of the orbital moments is one of the main interests in the field of magnetism. Recently, W.D. Brewer *et al.* [132], managed to perform a direct observation of the orbital magnetism in cubic solids (Cu and Au) by means of X-ray magnetic circular dichroism (XMCD). In this XMCD study on transition metal impurities in gold, a large enhancement of the orbital moment for Co, com-

pared with other 3d metals, has been observed. This is an astonishing result since a cubic environment is generally believed to suppress orbital magnetism [133]. So, it seems that either the ligand field of gold is weak or its spin-orbit coupling strong enough to produce a large orbital moment of Co. Recall that gold at its bulk phase does not show any sign of ordered magnetism. It appears that cobalt and gold are an interesting combination of metals which can be expected to show large orbital magnetism.

On the other hand, it is well known that Co-Au systems are characterized by a large positive heat of formation (+11 kJ/mol) [134]. This means that Co and gold cannot be formed as a regular compound in equilibrium, and Co impurities in a gold host matrix can be prepared only via a non-equilibrium procedure. In analogy with the metastable compound  $\text{Ag}_3\text{Co}$  [135], one can assume a high concentration (25%) of Co in Au, and suppose that they can form in a hypothetically metastable compound  $\text{Au}_3\text{Co}$  with  $\text{L}_{12}$  structure similar as  $\text{Cu}_3\text{Au}$  ordered compound [136]. For the  $\text{Au}_3\text{Co}$  compound, it has been shown that the orbital moment of Co is almost quenched due to strong hybridization [137]. Eventually, the magnetic behavior of low concentration of Co impurity in gold presents a conundrum. The aim of this chapter is to study the unusual magnitude of the orbital moment of single Co impurity in bulk Au with cubic symmetry.

## 6.1 Computational details

As a model to study the electronic structure and magnetic properties, an fcc-like supercell with a single Co atom surrounded by 31 Au atoms was used. This corresponds to a Co concentration of approximately 3% in the bulk gold. In the XMCD study [132], Co concentrations of 1.5% were investigated. For practical reasons 3% impurity concentration was taken into account in our study. In this model, each Co atom is surrounded by 5 shells of gold atoms in the supercell (see Figure 6.1).

Density functional calculations based on LMTO-ASA formalism for pairs of 3d impurities in Au have recently been done by S. Frota-Pessôa [138] to investigate the inter-atomic exchange coupling between two adjacent impurities. It has been found that for Co pairs that a ferromagnetic configuration is favored. In our study, we only focussed on the single-atom impurities which are dominating in the considered concentration range.

In the calculations, the average volume per atom was fixed to  $114 a_{\text{Bohr}}^3/\text{atom}$  corresponding to the experimental volume of bulk fcc-Au. However, since the atomic volume of Co is considerably smaller than that of Au, lattice relaxations in the vicinity of Co atom can be expected, resulting in a reduced Co-Au distance. This effect is accounted for in the present calculations by allowing a relaxation of the nearest neighbor Au shell surrounding the Co impurity. The

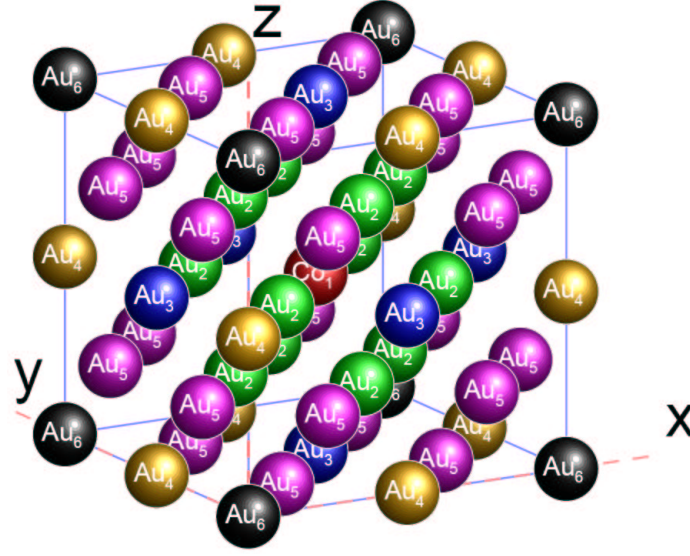


Figure 6.1: Supercell of gold atoms including a Co impurity. Red sphere shows the Co atom at the position of  $(\frac{1}{2}, \frac{1}{2}, \frac{1}{2})$  and the green spheres show the first nearest neighbor of gold atoms to Co atom in a cubic symmetry.

Au-Co distance has been optimized by means of total energy calculations with the relativistic version of the full potential local orbital minimum basis band structure scheme (FPLO) [66, 67]. The spin-orbit coupling and OP corrections in the framework of FPLO have been taken into account to evaluate the spin and orbital magnetic moments. In these calculations, the following basis sets were adopted: the  $5s5p$ ;  $5d6s6p$  states of Au were treated as valence states, while for Co, we used the  $3s3p$ ;  $3d4s4p$  states. The inclusion of  $3s3p$  semicore states for Co and  $5s5p$  semicore states for Au was used to account for non-negligible core-core overlap. For the site-centered potentials and densities we used expansions in spherical harmonics up to  $l_{max} = 12$ . The spatial extension of the basis orbitals, controlled by a confining potential  $(\frac{r}{r_0})^6$ , was optimized to minimize the total energy. The number of k points in the irreducible part of the Brillouin zone was  $6 \times 6 \times 6 = 216$ . The Perdew and Wang parameterization [39] of the exchange-correlation potential in the framework of local spin density approximation (LSDA) was used. To calculate the orbital moment of Co in the d shell, we also used the OPB and OPE corrections. Here, the final values of spin and orbital moments are obtained from corresponding projections on the atomic basis states of Co [67]. The quantization axis has been chosen in the direction of (001).

## 6.2 Results and discussion

### 6.2.1 Geometry optimization

The geometry optimization is carried out by calculation of the total energy as a function of Au displacement around Co impurity (see Figure 6.2). It reveals that the nearest neighbor Au shell around each Co impurity moves inwards by about 2%. The unrelaxed distance of Au-Co is 5.44 Bohr radii and the relaxed distance is 5.37 Bohr radii. Such relaxations also can be evaluated from scalar relativistic calculations [139]. Comparing full relativistic geometry optimization with scalar relativistic results show that the spin-orbit coupling and OP corrections have only a minor influence on the internal lattice parameters of the whole matrix (see Figure 6.2). We also considered shrinkage of the sphere included by first nearest neighbors of gold atoms when the impurity is removed and replaced by a vacancy. It is found out that the relaxation of such a sphere is 4.5%, the gold atoms moving inwards to the center of sphere. However, we did not find any magnetic solution for the considered vacancy. Our vacancy calculations guarantee that the magnetic properties of Co impurities in gold are dominated by the Co atoms.

Figure 6.3 shows the scalar relativistic total energy of pure gold ( $\text{Au}_{32}$ ) and gold with Co impurity ( $\text{Au}_{31}\text{Co}$ ) including first layer relaxation around the Co atom. It shows that the calculated lattice constant of  $\text{Au}_{31}\text{Co}$  is smaller than the lattice constant of  $\text{Au}_{32}$  (the difference is about 0.4%). It has been shown [67], that the difference of lattice constants of fcc Au calculated with scalar and full-relativistic schemes is very small. This fact was also found for internal relaxations and lattice relaxations of the considered system.

### 6.2.2 Electronic structure and magnetic properties

The formation of a magnetic state is shown in Figure 6.4. The density of states (DOS) of the relaxed supercell structure and also the related Co projected DOS obviously show that the magnetic behavior of the whole matrix is dominated by the Co 3d electrons. The spin-up Co-projected DOS is situated at the upper edge of the Au-5d band, showing some broadening by 3d-5d hybridization. On the contrary, the spin-down Co-projected DOS is pinned to the Fermi level and shows only very weak hybridization effects. The exchange splitting between majority and minority spins is about 1.5 eV and Co-3d bands are much narrower than those of hcp Co (see Figure 4.1). Such a narrow band is favorable for the occurrence of showing orbital magnetism. It can be expected that the lattice relaxation reduces spin and orbital magnetic moments of Co in comparison with the unrelaxed case.

In Table 6.1, the spin and orbital magnetic moments of Co for unrelaxed and relaxed structure in the presence of both OP corrections are given. The



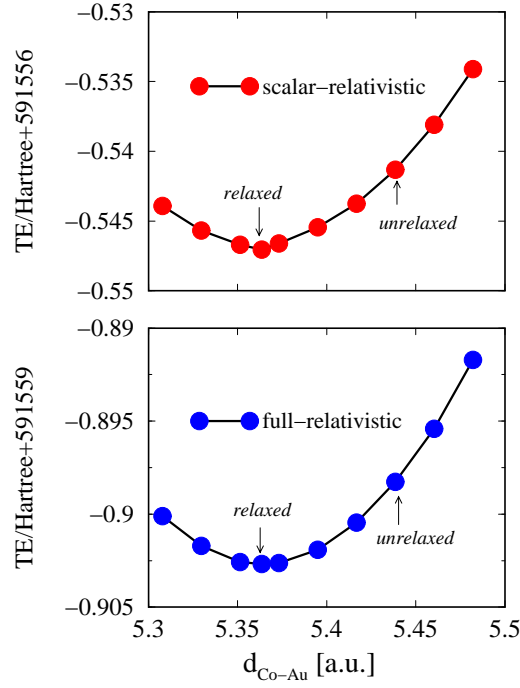


Figure 6.2: Geometry optimization I: calculated total energy (TE) in dependence of the nearest neighbor Co-Au distance in the scalar-relativistic (upper panel) and full-relativistic including spin-orbit coupling and OPB correction (lower panel) approaches.

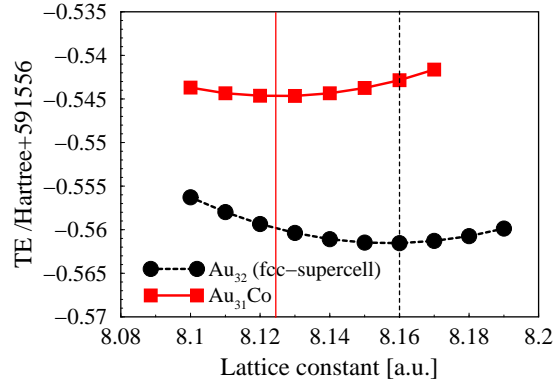


Figure 6.3: Geometry optimization II: calculated total energy of  $\text{Au}_{32}$  (black circle points) and  $\text{Au}_{31}\text{Co}$  (red square points) as a function of supercell lattice constant in the scalar-relativistic scheme. The total energy of  $\text{Au}_{32}$  is shifted to be compared with the total energy of  $\text{Au}_{31}\text{Co}$ . Dashed and solid vertical lines show the optimized lattice constants of  $\text{Au}_{32}$  and  $\text{Au}_{31}\text{Co}$ , respectively.

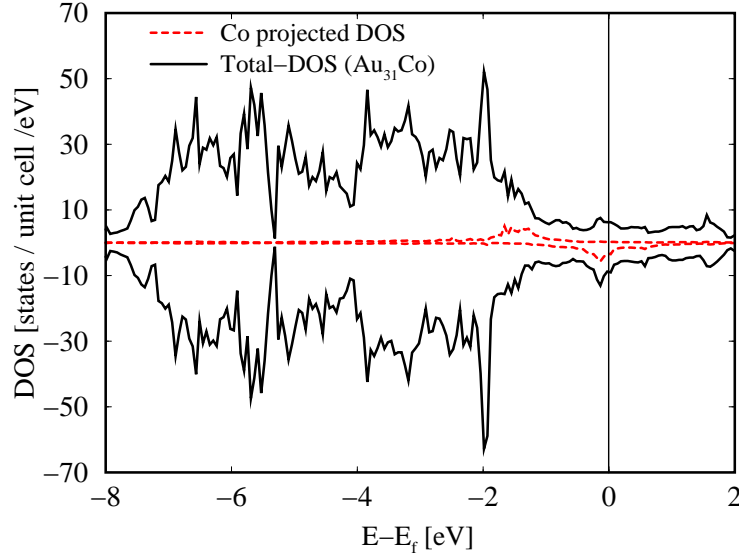


Figure 6.4: Calculated densities of states for supercell structure and Co atom. The solid line show the spin resolved DOS for the whole matrix and dashed lines show the Co projected DOS. The vertical line shows the Fermi level.

values in parentheses were calculated with hybridized OP correction functional to be compared with those values out of parentheses calculated with orthogonal functionals. The calculated ratios  $M_l/M_s$  are compared with the XMCD experimental ratio. In the LMTO method [140] the spin and orbital moments have also been calculated for one Co atom surrounded by a large fcc cluster of 9000 Au atoms but lattice relaxation as an important effect for reduction of the orbital moment has been neglected. Our present calculations reveal that lattice relaxation around the impurity change the spin magnetic moment of Co by about (+0.5...-2.5%). The OP corrections slightly enhance the spin magnetic moment of the Co impurity up to 10%. In Figure 6.5, the spin and orbital magnetic moments of Co in dependence of the distance between Co impurity and first layer of gold atoms are shown. Obviously, the lattice relaxation considerably reduces the orbital magnetic moment of the Co impurity. While in the LSDA an orbital moment of  $0.20 \mu_B$  is found for the unrelaxed structure (to be compared with the LSDA value  $0.23 \mu_B$  of the LMTO method [140]), the moderate relaxation of 2% yields a large orbital moment reduction by about 25%. This effect has been found in presence of both OP corrections as well (see Table 6.1). Calculations employing the OPE correction yield about 30% higher orbital moments than those using the OPB correction. In both approaches the ratio between orbital and spin moment is larger than the experimental value. Such an overestimation of orbital magnetism is frequently but not always found in the LSDA+OP approach (see Chapter 5).

Table 6.1: Calculated spin ( $M_s$ ) and orbital ( $M_l$ ) moments of Co impurities in Au and their ratios ( $M_l/M_s$ ). Values obtained with the LSDA and both version of orbital polarization corrections (OPB, OPE) are shown for relaxed and unrelaxed structures. All values are calculated at the lattice constant of  $\text{Au}_{31}\text{Co}$  ( $a = 8.125$  Bohr radii) The values of OPB and OPE indicated in parentheses have been calculated with hybridized OP functionals and values without parentheses have been calculated with orthogonal OP functionals.

|                             | $M_s$       | $M_l$       | $M_l/M_s$       |
|-----------------------------|-------------|-------------|-----------------|
| unrelaxed (LSDA)            | 1.74        | 0.20        | 0.11            |
| OPB                         | 1.84 (1.79) | 1.66 (1.37) | 0.90 (0.76)     |
| OPE                         | 1.91 (1.83) | 2.13 (1.80) | 1.12 (0.98)     |
| relaxed (LSDA)              | 1.72        | 0.15        | 0.09            |
| OPB                         | 1.78 (1.79) | 1.52 (1.21) | 0.85 (0.67)     |
| OPE                         | 1.86 (1.85) | 2.03 (1.69) | 1.09 (0.91)     |
| LMTO-unrelaxed (LSDA) [140] | 2.1         | 0.23        | 0.11            |
| OPB                         | 1.6         | 1.11        | 0.70            |
| Exp [132]                   | -           | -           | $0.35 \pm 0.05$ |

### 6.2.3 Model calculations

In order to better understand the evaluated orbital moments in the LSDA, the size of 3d orbital moments can be approximated to first order (spin-orbit coupling treated as a weak perturbation on the Co site) by the difference of the spin-split local densities of states at Fermi level [115].

In a simple tight binding model proposed by H. Ebert *et al.* [115], one can obtain a very simple expression for the orbital moment:

$$M_l \approx -\xi[n^\uparrow(\epsilon_F) - n^\downarrow(\epsilon_F)], \quad (6.1)$$

where  $n^\uparrow$  and  $n^\downarrow$  are the spin up and spin down local densities of states at the Fermi level for the considered atom and  $\xi$  is the spin-orbit coupling constant. It can be seen in Figure 6.4 that the majority band for Co is almost completely filled, while the minority bands are partially filled. The magnitude of the orbital moment of Co can be basically estimated from  $n^\downarrow(\epsilon_F)$  of the local density of states. This naturally explains the calculated orbital moments based on LSDA. Taking into account  $\xi = 0.054$  eV for Co (see Chapter 5) and the calculated spin up and down local densities of states for Co atom ( $n^\uparrow(\epsilon_F) =$

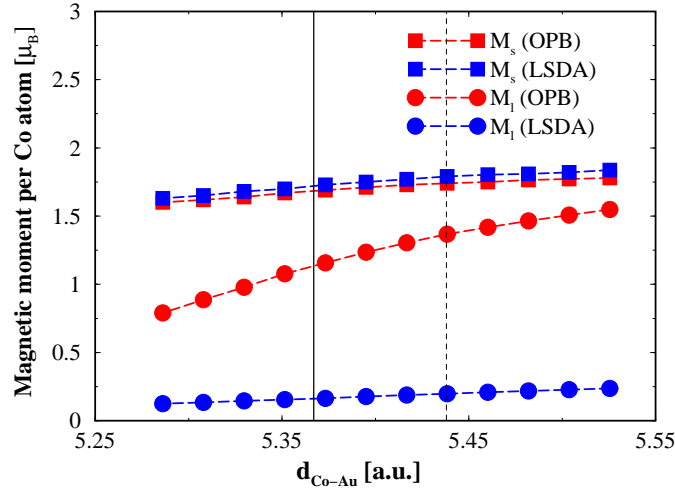


Figure 6.5: Spin and orbital magnetic moments of Co in dependence of the distance between Co and nearest neighbor Au atoms. The red (blue) filled squares show the spin magnetic moments of Co in presence of OPB (in absence of OPB). The thick vertical line denotes the optimized neighbor distance, the vertical dotted line shows the Au-Au distance in the unrelaxed structure. The red (blue) filled circles show the orbital magnetic moment of Co with (without) OPB correction.

0.5 states/eV,  $n^\downarrow(\epsilon_F) = 3.5$  states/eV), an orbital moment of  $0.15\mu_B$  can be expected, which is in a good agreement with the LSDA values in the DFT calculations (see Table 6.1).

#### 6.2.4 Importance of OP corrections

The model discussed in the previous section cannot explain the size of the orbital moment of a Co impurity obtained in the XMCD experiment.

As it is pronounced the LSDA scheme is clearly inferior to LSDA+OP approach. The calculated orbital moment of Co impurity in LSDA is underestimated by a factor of two compared with XMCD experiment. However the estimated orbital moment based on both OP corrections are overestimated by a factor of two compared with experiment. These big differences can be understood from two factors, band broadening and occupation. From H. Ebert *et al* theory [115], we found that most contribution to orbital moment dominated from the minority bands of Co impurity at the Fermi level, either than majority bands which they are strongly hybridized with Au-5d bands of the gold matrix. The Figure 6.6 (a,b) show the LSDA and LSDA+OPB  $m_l$ -resolved minority density of states close to the Fermi level for d bands of Co atom, respectively. It is obviously visible that the OP correction makes the bands more

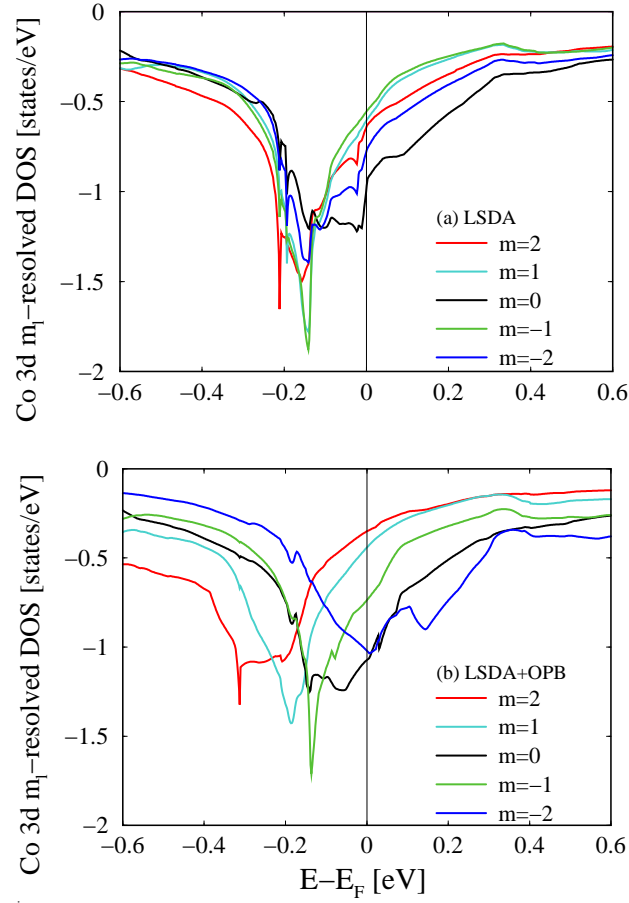


Figure 6.6: The  $m_l$ -resolved densities of states for 3d bands of a Co impurity in gold in the LSDA (upper panel) and in the LSDA+OPB (lower panel) approach.

Table 6.2: Occupation numbers  $n(m_l)$  for minority  $m_l$ -3d states of Co impurity in Au.

| $m_l$    | $m_l = -2$ | $m_l = -1$ | $m_l = 0$ | $m_l = 1$ | $m_l = 2$ |
|----------|------------|------------|-----------|-----------|-----------|
| LSDA     | 0.602      | 0.647      | 0.573     | 0.653     | 0.672     |
| LSDA+OPB | 0.402      | 0.568      | 0.574     | 0.707     | 0.786     |

splits. Such splitting comes into play from OPB potential  $-BL_\sigma m_l$  which acts over every  $m_l$  state to separate them more from each others at a given spin sub-shell. It means that bands with positive  $m_l$  characters will be more occupied and with negative  $m_l$  characters move more to unoccupied bands (see Figure 6.6).

Table 6.2 shows the occupation numbers of minority 3d-Co states in the LSDA and the LSDA+OPB approaches. It is visible now that OP correction enhances the occupation number differences in comparison with the LSDA values. This changing strongly affects on the magnitude of orbital moment. For a rough estimation of orbital moment as a function of occupation numbers, we use (Eq.4.10) in its  $k$ -independent form. As it is expected the Co impurity can be understood more or less as a free like character in the Au matrix. Therefore from this argument and using values in Table 6.2, the orbital moment of Co impurity in the LSDA approach was found to be  $0.15\mu_B$  and in LSDA+OPB approach is  $0.9\mu_B$ . Qualitatively, these values are in a very good agreement with the related values mentioned in Table 6.1.

The question arises whether the large ratio of  $M_l/M_s$  observed on Co in an Au matrix originates from the strong spin-orbit coupling of Au or from the weak Co-Au interaction. To answer, we can compare the orbital moment of Co in Au with Co in Ag. In our calculations, it is found out that the LSDA value of the orbital moment of Co in Ag is  $0.26\mu_B$  (LSDA value  $0.26\mu_B$  in the LMTO method [140]) and in presence of the OPB correction (hybridized version) is  $1.26\mu_B$  (to be compared with the related LMTO value  $1.40\mu_B$  [140]). Comparing similar values for orbital moment of Co in Au with Co in Ag, one can see the both LSDA and LSDA+OPB values in the Au matrix are smaller than those values in the case of Ag. Since Ag atoms are lighter than Au atoms and the spin-orbit coupling of heavy elements is stronger than that of the light elements, it can be concluded that the spin-orbit coupling on the gold atom cannot be a reason for the enhancement of the orbital moment of Co in Au. Finally, we argue that the weakness of Co-Au hybridization gives forth a reason for the large orbital moment of Co impurity. However, the relaxation of atoms adjacent to the impurity was taken into account to study the effect of host-impurity hybridization on orbital moments.

## 6.3 Conclusion

In this chapter, we presented results of density functional calculations on the electronic structure of Co impurities inside Au in the framework of local spin density approximation. The orbital and spin magnetic moment have been evaluated using the relativistic version of the full-potential local orbital minimum basis code, with and without inclusion of orbital polarization corrections. In agreement with experimental findings, the orbital moment is enhanced with respect to Co metal. On the other hand, lattice relaxation is found to reduce the orbital moment considerably, whereas the spin moment is less affected. From this finding we would also expect a rather strong pressure dependence of the orbital moment, which could be verified experimentally. Taking into account the bulk modulus of gold as  $B = 220/GPa$ , a pressure dependence of the Co orbital moment in gold,  $d\mu_l/dP \approx -0.03\mu_B/GPa$ , is predicted. The Co-3d states are only weakly hybridized and form narrow bands. In this respect the Co impurity maintains almost an atom-like character, which explains the large orbital moment observed in the experiment.





# Chapter 7

## Summary

Orbital magnetism in a solid is strongly influenced by the ligand field, originating from the structural environment and geometry of the solid. The orbital moments in a solid with cubic symmetry are expected to be quenched if spin-orbit coupling is neglected. However, spin-orbit coupling induces orbital moments, accordingly. The relativistic nature of the spin-orbit coupling requires orbital magnetism to be treated within QED, and the treatment of QED in solids is possible in the frame of current density functional theory.

The spin-orbit coupling is accounted for in many DFT calculations of magnetic systems within the LSDA. However, a strong deviation of the LSDA orbital moments from experiment is found in such approaches. To avoid such deviations, orbital polarization corrections would be desirable. In this Thesis, those corrections have been investigated in the framework of CDFT.

After a short review for CDFT in Chapter 2, in Chapter 3, an *ad hoc* OP correction term (OPB) suggested by Brooks and Eriksson is given. This correction in some cases gives quite reasonable corrections to orbital moments of magnetic materials. Another OP correction (OPE), which has been introduced recently, was derived from the CDFT in the non-relativistic limit. Unfortunately, the program can only incompletely be carried through, as there are reasonable but uncontrolled approximations to be made in two steps of the derivation. Nevertheless, the result is quite close to the *ad hoc* ansatz. The calculated OPE energies for 3d and 4f free ions are in qualitative agreement with OPB energies.

In Chapter 4, both corrections are implemented in the FPLO scheme to calculate orbital moments in solids. We found that both OPB and OPE corrections implemented in FPLO method, yield reasonably well the orbital magnetic moments of bcc Fe, hcp Co and fcc Ni compared with experiment.

In Chapter 5, the effect of spin-orbit coupling and orbital polarization corrections on the spin and orbital magnetism of full-Heusler alloys is investigated by means of local spin density calculations. It is demonstrated, that OP corrections are needed to explain the experimental orbital moments. Model

calculations employing one ligand field parameter yield the correct order of magnitude of the orbital moments, but do not account for its quantitative composition dependence. The spin-orbit coupling reduces the degree of spin polarization of the density of states at Fermi level by a few percent. We have shown that the orbital polarization corrections do not change significantly the spin polarization degree at the Fermi level. We also provide arguments that  $\text{Co}_2\text{FeSi}$  might not be a half-metal as suggested by recent experiments.

In Chapter 6, to understand recent XMCD data for Co impurities in gold, the electronic structure of Co impurities inside gold has been calculated in the framework of local spin density approximation. The orbital and spin magnetic moment have been evaluated. In agreement with experimental findings, the orbital moment is enhanced with respect to Co metal. On the other hand, internal relaxations are found to reduce the orbital moment considerably, whereas the spin moment is less affected. Both OPB and OPE yield a large orbital moment for Co impurities. However, those calculated orbital moments are almost by a factor of two larger than the experimental values. We also found that the orbital magnetic moment of Co may strongly depend on pressure.

# Appendix A

## Appendix: Functional derivatives

With cylindrical coordinate  $(\rho, z, \phi)$  and  $A = A^{C,S} + A^{C,L}$ , one finds for functional derivative of  $L(\mathbf{r})$ ,<sup>1</sup>

$$\begin{aligned} \frac{\delta L(\mathbf{r}')}{\delta \bar{\psi}_k(\mathbf{r})} &= \frac{n_k}{\pi} \int d^3 r'' \delta(z'' - z') \frac{\theta(\rho'' - \rho')}{\rho''} \times \\ &\times \left( \sum_m \frac{m}{\rho''} |\varphi_m(\mathbf{r}'')|^2 \langle \varphi_m | \psi_k \rangle \varphi_m(\mathbf{r}) + \sum_{k'} \frac{n_{k'}}{n_k} \bar{\psi}_{k'}(\mathbf{r}'') \psi_{k'}(\mathbf{r}'') \frac{\delta A^C(\mathbf{r}'')}{\delta \bar{\psi}_k(\mathbf{r})} \right) + \\ &+ \frac{n_k}{\pi} \delta(z - z') \frac{\theta(\rho - \rho')}{\rho} A^C(\mathbf{r}) \psi_k(\mathbf{r}). \end{aligned} \quad (\text{A.1})$$

The orbital correlation term becomes

$$\begin{aligned} \frac{\mu_0 e \beta}{2n_k} \int d^3 r' H^{C,L}(\mathbf{r}') \frac{\delta L(\mathbf{r}')}{\delta \bar{\psi}_k(\mathbf{r})} &= \mu_B \beta \left\{ \int d^3 r'' A^{C,L}(\mathbf{r}'') \times \right. \\ &\times \left( \sum_m \frac{m}{\rho''} |\varphi_m(\mathbf{r}'')|^2 \langle \varphi_m | \psi_k \rangle \varphi_m(\mathbf{r}) + \sum_{k'} \frac{n_{k'}}{n_k} \bar{\psi}_{k'}(\mathbf{r}'') \psi_{k'}(\mathbf{r}'') \frac{\delta A^C(\mathbf{r}'')}{\delta \bar{\psi}_k(\mathbf{r})} \right) + \\ &\left. + A^{C,L}(\mathbf{r}) A^C(\mathbf{r}) \psi_k(\mathbf{r}) \right\}. \end{aligned}$$

The functional derivative of  $A^C(\mathbf{r})$  is given by

$$\frac{\delta A^C(\mathbf{r}')}{\delta \bar{\psi}_k(\mathbf{r})} = \mu_0 \int_0^{\rho'} d\rho'' \frac{\rho''}{\rho'} \frac{\delta H^C(\rho'', z')}{\delta \bar{\psi}_k(\mathbf{r})}, \quad (\text{A.2})$$

---

<sup>1</sup>For integrations, we used the  $\int_{\rho'}^{\infty} d\rho'' \dots = \frac{1}{2\pi} \int d^3 r'' \delta(z'' - z') \frac{\theta(\rho'' - \rho')}{\rho''} \dots$

and, with

$$\zeta(\mathbf{r}) = \frac{1}{n(\mathbf{r})} \left( \sum_k n_k \bar{\psi}_k(\mathbf{r}) \beta \Sigma_z \psi_k(\mathbf{r}) + L_z(\mathbf{r}) \right), \quad \left. \frac{\delta \zeta_L(\mathbf{r}')}{\delta \bar{\psi}_k(\mathbf{r})} \right|_{n(\mathbf{r}')} = \frac{\delta L_z(\mathbf{r}')}{\delta \bar{\psi}_k(\mathbf{r})}, \quad (\text{A.3})$$

the functional derivative of  $H^C(\mathbf{r})$  presents with

$$\begin{aligned} \frac{\delta H^C(\mathbf{r}')}{\delta \bar{\psi}_k(\mathbf{r})} = & \beta n_k \left( \frac{\delta H^C(\mathbf{r}')}{\delta n(\mathbf{r})} - \frac{\zeta(\mathbf{r})}{n(\mathbf{r})} \frac{\delta H^C(\mathbf{r}')}{\delta \zeta(\mathbf{r})} + \frac{1}{n(\mathbf{r})} \frac{\delta H^C(\mathbf{r}')}{\delta \zeta(\mathbf{r})} \Sigma_z \right) \psi_k(\mathbf{r}) + \\ & + \beta n_k \int d^3 r'' \frac{1}{n(\mathbf{r}'')} \frac{\delta H^C(\mathbf{r}')}{\delta \zeta(\mathbf{r}'')} \frac{\delta L_z(\mathbf{r}'')}{\delta \bar{\psi}_k(\mathbf{r})}. \end{aligned}$$

## Appendix B

### Appendix: Complex and real spherical harmonics

Using Legendre polynomials,  $P_{|m|}^l(\cos\theta)$ , the complex spherical harmonics read as:

$$Y_L = (-1)^{(m+|m|)/2} P_{|m|}^l(\cos\theta) \sqrt{\frac{2l+1}{4\pi}} \sqrt{\frac{(l-|m|)!}{(l+|m|)!}} e^{im\phi}, \quad (\text{B.1})$$

and the real spherical harmonics are presented with:

$$y_L = P_{|m|}^l(\cos\theta) \sqrt{\frac{2l+1}{2\pi(1+\delta_{m0})}} \sqrt{\frac{(l-|m|)!}{(l+|m|)!}} \begin{cases} \cos(|m|\theta) & m \geq 0 \\ \sin(|m|\theta) & m < 0 \end{cases}. \quad (\text{B.2})$$

The complex and real spherical harmonics are related with following equation:

$$Y_L = a_m y_{lm} + b_m y_{lm}, \quad (\text{B.3})$$

with

|         | $a_m$                 | $b_m$                |
|---------|-----------------------|----------------------|
| $m < 0$ | $-\frac{i}{\sqrt{2}}$ | $\frac{1}{\sqrt{2}}$ |
| $m = 0$ | 1                     | 0                    |
| $m > 0$ | $\frac{1}{\sqrt{2}}$  | $\frac{i}{\sqrt{2}}$ |



# Bibliography

- [1] F.H. Hund, Postdoctoral University Teaching Qualification, Leipzig, (1925) and *Linienpektren und periodische system der elemente*, Springer, Berlin (1927).
- [2] H.N. Russell, Nature **115**, 735 (1925).
- [3] P. Hohenberg, and W. Kohn, Phys. Rev. **136**, B864 (1964).
- [4] W. Kohn, and L.J. Sham, Phys. Rev. **140**, A1133 (1965).
- [5] W. Kohn, Rev. Mod. Phys. **71** 1253 (1999).
- [6] M. Richter, *Density Functional Theory Applied to 4f and 5f Elements and Compounds*, in K.H.J. Buschow (Ed.), Handbook of Magnetic Materials, Vol.13, North-Holland, Amesterdam, pp 87-228 (2001).
- [7] P. Oppeneer, *Magneto-Optical Kerr Spectra*, in K.H.J. Buschow (Ed.), Handbook of Magnetic Materials, Vol.13, North-Holland, Amesterdam, pp 229-422 (2001).
- [8] A.K. Rajagopal, and J. Callaway, Phys. Rev. B **7**, 1912 (1973).
- [9] U. von Barth, and L. Hedin, J. Phys. C **5**, 1629 (1972).
- [10] H. Eschrig, and W.E. Pickett, Solid State Commun. **118**, 123 (2001).
- [11] G. Vignale, and M. Rasolt, Phys. Rev. Lett. **59**, 2360 (1987).
- [12] G. Vignale, and M. Rasolt, Phys. Rev. B **37**, 10685 (1988).
- [13] P. Skudlarski, and G. Vignale, Phys. Rev. B **48**, 8547 (1993).
- [14] B.M. Relovsky, and H. Ruder, Phys. Rev. A **53**, 4068 (1996).
- [15] G. Diener, J. Phys.: Condens. Matter. **3** 9417 (1991).
- [16] M. Richter, and H. Eschrig, Physica B **172**, 85 (1991).
- [17] B.I. Min, and Y-R. Jang, J. Phys.: Condens. Matter. **3**, 5131 (1991).

- [18] H. Ebert, M. Battochetti, and E.K.U. Gross, *Europhys. Lett.* **40**, 545 (1997)
- [19] M.S.S. Brooks, *Physica B* **130**, 6 (1985).
- [20] O. Eriksson, B. Johansson, and M.S.S. Brooks, *J. Phys. Cond. Mat.* **1**, 4005 (1989)
- [21] O. Eriksson, M.S.S. Brooks, and B. Johansson, *Phys. Rev. B* **41**, 7311 (1990)
- [22] L. Severin, M.S.S. Brooks and B. Johansson, *Phys. Rev. B* **71**, 3214 (1993).
- [23] H. Eschrig, M. Sargolzaei, K. Koepernik, and M. Richter, *Europhys. Lett.* **72**, 611 (2005).
- [24] I.V. Solov'yev, A.I. Liechtenstein, and K. Terakura, *Phys. Rev. Lett.* **80**, 5758 (1998).
- [25] B. Brandow, *Adv. Phys.* **26**, 651 (1977).
- [26] A. Mavromaras, L. Sandratskii, and J. Kübler, *Solid State Commun.* **106** 115 (1998).
- [27] H. Eschrig, *The Fundamentals of Density Functional Theory*, 2nd Edition, Edition am Gutenbergplatz, Leipzig, (2004).
- [28] A.K. Rajagopal, and J. Callawy, *Phys. Rev. B* **7**, 1912 (1973).
- [29] A.K. Rajagopal, *J. Phys. C* **11**, L943 (1978).
- [30] A.H. MacDonald and S.H. Vosko, *J. Phys. C: Solid State Phys.* **12**, 2977 (1979)
- [31] H. Eschrig, G. Seifert and P. Ziessche, *Solid State Commun.* **56**, 777 (1985).
- [32] J.C. Slater, *Quantum theory of atomic structure*, Mc Graw-Hill, New York (1960).
- [33] W. Pauli, *Z. Phys.* **31**, 765 (1925).
- [34] C. Froese-Fischer, *Hartree-Fock method for atoms*, Mc Graw-Hill, New York (1977).
- [35] U. von Barth, and L. Hedin, *J. Phys. C* **5**, 1629 (1972).
- [36] D.M. Ceperly, and B.J. Alder, *Phys. Rev. Lett.* **45**, 566 (1980).



- [37] S.H. Vosko, L. Wilk, and M. Nusair, *Canadian J. Phys.* **58**, 1200 (1980).
- [38] J.P. Perdew and A. Zunger, *Phys. Rev. B* **23**, 5048 (1983).
- [39] J.P. Perdew and Y. Wang, *Phys. Rev. B* **23**, 5048 (1992).
- [40] P.A.M. Dirac, *Proc. R. Soc. London A* **123**, 714 (1929).
- [41] P. Pyykkö, *Chem. Rev.* **88**, 565 (1988).
- [42] L.M. Sandratskii, and J. Kübler, *Phys. Rev. Lett.* **75**, 946 (1995).
- [43] J. Trygg, B. Johansson, O. Eriksson, and J.M. Wills, *Phys. Rev. Lett.* **75**, 2871 (1995).
- [44] M.R. Norman, *Phys. Rev. Lett.* **64**, 1162 (1990); **64**, 2466(E) (1990); *Phys. Rev. B* **44**, 1364 (1991).
- [45] I.V. Solov'ev, A.I. Liechtenstein, and V.A. Gubanov, *Sov. Phys. Solid States* **33**, 752 (1991).
- [46] S.V. Beiden, W.M. Temmerman, Z. Szotek, and G.A. Gehrig, *Phys. Rev. Lett.* **79**, 3970 (1997).
- [47] P. Söderlind, O. Eriksson, B. Johansson, R.C. Albers, and A.M. Boring, *Phys. Rev. B* **45**, 12911 (1992).
- [48] L. Nordström, M.S.S. Brooks, and B. Johansson, *J. Phys.: Condens. Matter.* **4** 3261 (1992).
- [49] C.O. Rodriguez, M.V. Ganduglia-Pirovano, E.L. Peltzer y Blanca, M. Petersen, and P. Novak, *Phys. Rev. B* **63**, 184413 (2001).
- [50] I. Opahle, M. Richter, M. D. Kuz'min, U. Nitzsche, K. Koepf, and L. Schramm, *J. Magn. Magn. Mat.* **290-291**, 374 (2005).
- [51] I. Opahle, S. Elgazzar, V. D. P. Servedio, Manuel Richter, and P. M. Oppeneer, *Europhys. Lett.* **74**, 124 (2006).
- [52] H. Ebert, A. Vernes, and J. Banhart, *Solid State Commun.*, **113**, 103 (2000).
- [53] M. Divis, L. Steinbeck, M. Richter, and P. Mohn, *J. Alloys and Compounds*, **321**, 10 (2001).
- [54] G. Racah, *Phys. Rev.* **61**, 186 (1942).
- [55] G. Racah, *Phys. Rev.* **62**, 438 (1942).

- [56] B.R. Judd, *Operator Techniques in Atomic Spectroscopy*. McGraw-Hill, New York, (1963).
- [57] R.D. Cowan, *The Theory of Atomic Structure and Spectra*, University of California Press Ltd. (1981).
- [58] A. Mavromaras, L. Sandratskii, and J. Kübler, *Solid State Commun.* **106**, 115 (1998).
- [59] R. Peierls, *Surprises in Theoretical Physics*, Princeton University Press, Princeton, (1979).
- [60] J.A. Gaunt, *Phil. Trans. R. Soc. A* **228**, 151 (1929).
- [61] D.A. Varshalovich, A.N. Moskalev, and V.K. Khersonskii, *Quantum Theory of Angular Momentum*, by World Scientific Publishing Co., (1988).
- [62] J.C. Slater, *Phys. Rev.* **165**, 655 (1968).
- [63] J. Melsen, J.M. Wills, B. Johansson, and O. Eriksson, *J. Alloys and Compounds*, **209**, 15 (1994).
- [64] M. Higuchi, and A. Hasegawa, *J. the Physical Society of Japan*, **67**, 2037 (1998).
- [65] H. Eschrig, M. Richter, and I. Opahle, *Relativistic Solid State Calculations*, in: *Relativistic Electronic Structure Theory-Part II: Applications*, edited by P. Schwerdtfeger, Elsevier, Amsterdam, pp.773-776 (2004).
- [66] K. Koepernik and H. Eschrig, *Phys. Rev. B* **59**, 1743 (1999) and <http://www.fplo.de>.
- [67] I. Opahle, PhD Thesis, Dresden University of Technology, 2001.
- [68] D.D. Koelling, and B.N. Harmon, *J. Phys. C* **10**, 3107 (1977).
- [69] J.C. Boettger, and S.B. Trickey, *J. Mol. Struct. (Theochem)*, **251-502**, 258 (2000).
- [70] H. Eschrig, and I. Bergert, *Phys. Stat. Sol. (b)* **90**, 621 (1978).
- [71] E.P. Wohlfarth, *Iron, Cobalt, Nickel*, in E.P. Wohlfarth (Ed.), *Handbook of Ferromagnetic Materials*, Vol 1, pp 1-70 (1980).

- [72] M.B. Stearns, in *Landolt-Börnstein Numerical Data and Functional Relationships in Science and Technology*, edited by H.P.J. Wijn (Springer-Verlag, Berlin, 1986), Group3, Vol. 19, Pt. a; D. Bonnenberg, K.A. Hempel, and H.P.J. Wijn, *ibid*.
- [73] T. Huhne, C. Zecha, H. Ebert, P.H. Dederichs, and R. Zeller, *Phys. Rev. B* **58**, 10236 (1998).
- [74] O. Eriksson, B. Johansson, R.C. Albers, A.M. Boring, and M.S.S. Brooks, *Phys. Rev. B* **42**, 2707 (1990).
- [75] G.Y. Guo, *Phys. Rev. B* **55**, 11619 (1997).
- [76] M.S. Lund, J.W. Dong, J. Lu, X.Y. Dong, C.J. Palmstrøm, and C. Leighton, *Appl. Phys. Lett.* **80**, 4798 (2002).
- [77] H.J. Elmers, G.H. Fecher, D. Valdaitsev, S.A. Nepijko, A. Gloskovskii, G. Jakob, G. Schönhense, S. Wurmehl, T. Block, C. Felser, P.C. Hsu, W.L. Tsai, and S. Cramm, *Phys. Rev. B* **67**, 104412 (2003).
- [78] C. Felser, B. Heitkamp, F. Kronast, D. Schmitz, S. Cramm, H.A. Dürr, H.J. Elmers, G.H. Fecher, S. Wurmehl, T. Block, D. Valdaitsev, S.A. Nepijko, A. Gloskovskii, G. Jakob, G. Schönhense, and W. Eberhardt, *J. Phys.: Condens. Matter* **15**, 7019 (2003).
- [79] X.Y. Dong, C. Adelman, J.O. Xie, C.J. Palmstrøm, X. Lou, J. Strand, P.A. Crowell, J.P. Barnes, and A.K. Petford-Long, *Appl. Phys. Lett.* **86**, 102107 (2005).
- [80] Y. Miura, K. Nagao, and M. Shirai, *Phys. Rev. B* **69**, 144413 (2004).
- [81] S.J. Hashemifar, P. Kratzer, and M. Scheffler, *Phys. Rev. Lett.* **94**, 096402 (2005).
- [82] A.T. Zayak, and P. Entel, *J. Magn. Magn. Mater.* **290-291**, 874 (2005).
- [83] Y. Kurtulus, R. Dronskowski, G.D. Samolyuk, and V.P. Antropov, *Phys. Rev. B* **71**, 014425 (2005).
- [84] F. Heusler, *Verh. Dtsch. Phys. Ges.* **5**, 219 (1903).
- [85] J. Kübler, A.R. Williams, and C.B. Sommers, *Phys. Rev. B* **28**, 1745 (1983).
- [86] R.A. de Groot, F.M. Mueller, P.G. van Engen, and K.H.J. Buschow, *Phys. Rev. Lett.* **50**, 2024 (1983).

- [87] J.M.D. Coey, M. Venkatesan, and M.A. Bari, *Half-Metallic Ferromagnets*, in: *Lecture Notes in Physics*, edited by C. Berthier, L.P. Levy, G. Martinez (Springer-Verlag, Heidelberg), Vol. 595, pp.377-396 (2002).
- [88] C.M. Fang, G.A. de Wijs, and R.A. de Groot, J. Appl. Phys. **91**, 8340 (2002).
- [89] J. Grabis, A. Bergmann, A. Nefedov, K. Westerholt, and H. Zabel, Phys. Rev. B **72**, 024437 (2005).
- [90] S. Ishida, S. Fujii, S. Kashiwagi, and S. Asano, J. Phys. Soc. Jpn. **64**, 2152 (1995).
- [91] S. Picozzi, A. Continenza, and A.J. Freeman, Phys. Rev. B **66**, 094421 (2002).
- [92] I. Galanakis, J. Phys.: Condens. Matter **16**, 3089 (2004).
- [93] I. Galanakis, P.H. Dederichs, and N. Papanikolaou, Phys. Rev. B **66**, 174429 (2002).
- [94] L. Ritchie, G. Xiao, Y. Ji, T.Y. Chen, C.L. Chien, M. Zhang, J. Chen, Z. Liu, G. Wu, and X.X. Zhang, Phys. Rev. B **68**, 104430 (2003).
- [95] M. Zhang, E. Brück, F. R de Boer, Z. Li, and G. Wu, J. Phys. D: Appl. Phys. **37**, 2049, (2004).
- [96] Ph. Mavropoulos, K. Sato, R. Zeller, P.H. Dederichs, V. Popescu, and H. Ebert, Phys. Rev. B **69**, 054424 (2004).
- [97] Ph. Mavropoulos, I. Galanakis, V. Popescu, and P.H. Dederichs, J. Phys.: Condens. Matter **16**, S5759 (2004).
- [98] H.J. Elmers, S. Wurmehl, G.H. Fecher, G. Jakob, C. Felser, and G. Schönhense, J. Magn. Magn. Mater. **272**, 758 (2004).
- [99] H.J. Elmers, S. Wurmehl, G.H. Fecher, G. Jakob, C. Felser, and G. Schönhense, Appl. Phys. A: Mater. Sci. Process. **79**, 557 (2004).
- [100] S. Wurmehl, G. H. Fecher, K. Kroth, F. Kronast, H. A. Dürr, Y. Takeda, Y. Saitoh, K. Kobayashi, H.J. Lin, G. Schönhense, and C. Felser, J. Phys. D: Appl. Phys. **39**, 803, (2006).
- [101] K. Miyamoto, A. Kimura, K. Iori, K. Sakamoto, T. Xie, T. Moko, S. Qiao, M. Taniguchi, and K. Tsuchiya, J. Phys.: Condens. Matter **16**, S5797 (2004).

- [102] S. Wurmehl, G.H. Fecher, H.C. Kandpal, V. Ksenofontov, C. Felser, H.J. Lin, and J. Morais, Phys. Rev. B **72**, 184434 (2005).
- [103] H.C. Kandpal, G.H. Fecher, C. Felser, and G. Schönhense, Phys. Rev. B **73**, 094422 (2006).
- [104] I. Galanakis, Phys. Rev. B **71**, 012413 (2005).
- [105] M. Sargolzaei, M. Richter, K. Koepernik, I. Opahle, H. Eschrig, and I. Chaplygin, Phys. Rev. B **74**, 224410 (2006).
- [106] P. Villars and L.D. Calvert, Pearson's *Handbook of Crystallographic Data for Intermetallic Phases* (2nd Edition), ASM International, (1991).
- [107] J. Kübler, *Theory of Itinerant Electron Magnetism*, Oxford Science Publications (2000).
- [108] T. Chen, Y.U. Idzerda, H.J. Lin, N.V. Smith, G. Meigs, E. Chaban, G.H. Ho, E. Pellegrin, and F. Sette, Phys. Rev. Lett. **75**, 152 (1995).
- [109] B.T. Thole, P. Carra, F. Sette, and G. van der Laan, Phys. Rev. Lett. **68**, 1943 (1992).
- [110] P. Carra, B.T. Thole, M. Altarelli, and X. Wang, Phys. Rev. Lett. **70**, 694 (1993).
- [111] A. Scherz, H. Wende, K. Baberschke, J. Minar, D. Benea, and H. Ebert, Phys. Rev. B **66**, 184401 (2002).
- [112] I. Tchapyguine, PhD Thesis, Dresden University of Technology (2002).
- [113] E. Francisco, and L. Pueyo, Phys. Rev. A **36**, 1978 (1987).
- [114] O. Eriksson, L. Nordström, A. Pohl, L. Severin, A.M. Boring, and B. Johansson, Phys. Rev. B **41**, 11807 (1990).
- [115] H. Ebert, R. Zeller, B. Drittler, and P.H. Dederichs, J. Appl. Phys. **67**, 4576 (1990).
- [116] K.H.J. Buschow, P.G. van Engen, and R. Jongebreur, J. Magn. Magn. Mater. **38**, 1 (1983).
- [117] V. Niculescu, J.I. Budnick, W.A. Hines, K. Raj, S. Pickart, and S. Skalski, Phys. Rev. B **19**, 452 (1979).
- [118] P.J. Webster, J. Phys. Chem. Solids **32**, 1221 (1971).

- [119] T. Ambrose, J.J. Krebs, and G.A. Prinz, *J. Appl. Phys.* **87**, 5463 (2000).
- [120] S.V. Karthik, A. Rajanikanth, Y.K. Takahashi, T. Okhubo, and K. Hono, *Appl. Phys. Lett.* **89**, 052505 (2006).
- [121] I.I. Mazin, *Phys. Rev. Lett.* **83**, 1427 (1999).
- [122] S. Picozzi, A. Continenza, and A.J. Freeman, *Phys. Rev. B* **69**, 094423 (2004).
- [123] R.Y. Umetsu, K. Kobayashi, A. Fujita, K. Oikawa, R. Kainuma, K. Ishida, N. Endo, K. Fukamichi, and A. Sakuma, *Phys. Rev. B* **72**, 214412 (2005).
- [124] J. Stöhr, *J. Magn. Magn. Mater.* **200**, 470 (1999).
- [125] P. Gambardella, S. Rusponi, M. Veronese, S.S. Dhesi, C. Grazioli, A. Dallmeyer, I. Cabria, R. Zeller, P.H. Dederichs, K. Kern, C. Carbone, and H. Brune, *Science* **300**, 1130 (2003).
- [126] T. Koide, H. Miyauchi, J. Okamoto, T. Shidara, A. Fujimori, H. Fukutani, K. Amemiya, H. Takeshita, S. Yuasa, T. Katayama, and Y. Suzuki, *Phys. Rev. Lett.* **87**, 257201 (2001).
- [127] P. Gambardella, A. Dallmeyer, K. Maiti, M.C. Malagoli, W. Eberhardt, K. Kern, and C. Carbone, *Nature* **416**, 301 (2002).
- [128] P. Ryan, R.P. Winarski, D.J. Keavney, J.W. Freeland, R.A. Rosenberg, S. Park, and C.M. Falco, *Phys. Rev. B* **69**, 054416 (2004).
- [129] D. Weller, Y. Wu, J. Stöhr, M.G. Samant, B.D. Hermsmeier, and C. Chappert, *Phys. Rev. B* **49**, 12888 (1994).
- [130] G. Grüner, and A. Zawadowski, *Rep. Prog. Phys.* **37**, 1497 (1974).
- [131] N. Papanikolaou, N. Stefanou, R. Zeller, and P.H. Dederichs, *Phys. Rev. B* **46**, 10858 (1992).
- [132] W.D. Brewer, A. Scherz, C. Sorg, H. Wende, K. Baberschke, P. Benck, and S. Frota-Pessôa, *Phys. Rev. Lett.* **93**, 077205 (2004).
- [133] I. Galanakis, P.M. Oppeneer, P. Ravindran, L. Nordström, P. James, M. Alouani, H. Dreysse, and O. Eriksson, *Phys. Rev. B* **63**, 172405 (2001).
- [134] F.R. doBoer, R. Boom, W.C.M. Mattens, A. Miedema, and A. Niessen, *Cohesion in Metals: Transition Metal Alloys*, North-Holland-Amsterdam (1989).

- 
- [135] J.B. Liu, Z.F. Li, J.X. Zhang, and B.X. Liu, Phys. Rev. B **64**, 054102 (2001).
  - [136] H.B. Guo, J.H. Li, and B.X. Liu, Phys. Rev. B **70**, 195434 (2004).
  - [137] M. Sargolzaei, I. Opahle, and M. Richter, Phys. Stat. Sol.(b) **243**, 286 (2006).
  - [138] S. Frota-Pessôa, J. Magn. Magn. Mater. **226-230**, 1021 (2001).
  - [139] M. Sargolzaei, I. Opahle, M. Richter, K. Koepernik, U. Nitzsche, and H. Eschrig, J. Magn. Magn. Mater. **290-291**, 364 (2005).
  - [140] S. Frota-Pessôa, Phys. Rev. B **69**, 104401 (2004).





# Acknowledgment

To my great teacher, Professor Dr. Helmut Eschrig, I would like to express my sincere gratitude for supervising my PhD program, for proposing an interesting research topic and providing me with guidance and constructive criticism both in research and in the presentation of scientific results. I got a deeper insight into physics by understanding and applying the fundamentals that he provides during his courses. He had always time to kindly answer my questions and clarify my strange ideas.

I would like to express my special thanks to my second adviser, PD Dr. Manuel Richter, who supported me with his vast knowledge in Density Functional Theory and Material Physics. I was getting increasingly fresh in my mind during lunch time with him at the IFW-restaurant.

I am also grateful to those people who contributed in some way to this work, especially Dr. Klaus Koepernik, and Dr. Ingo Opahle. Both of them taught me their deep physics background and their great and practical knowledge in computational physics.

As well, I would like to thank Professor Dr. Warren E. Pickett (Univ. California at Davis), Professor Dr. Roland Hayn (Univ. Marsille), Professor Dr. Klaus Baberschke (Freie Univ. Berlin), Professor Dr. Peter M. Oppeneer (Univ. Uppsala), Dr. Gerhard Fecher (Univ. Mainz), Dr. Sabine Wurmehl (Univ. Mainz), Dr. Stephan-Ludwig Drechsler (IFW-Dresden), Dr. Ferenc Tasnadi (IFW-Dresden), Dr. Michael Kuz'min (IFW-Dresden), Dr. Saad Elgazar (IFW-Dresden), Dr. Igor Chaplygin (TU-Dresden), Dr. Yury Dedkov (TU-Dresden), Dr. Jan Ruzs (Univ. Prague), Daniela Koudela (IFW-Dresden), and Wenxu Zhang (IFW-Dresden), who helped me to increase my knowledge by sharing their scientific background. Special thanks to IFW members with whom I attended many wonderful activities and received great help during these years, especially, our secretaries, Mrs. Grit Rotzer, Mrs. Ulrike Steere, and Mrs. Angela Heinrich. I would like to thank Mrs. Ulrike Nitzsche whose care about maintenance and performance of our computer system made the required calculations possible.

Financial support by Deutsche Forschungsgemeinschaft, SPP 1145, is gratefully acknowledged.

Finally, I would like to thank my family, first of all, my dear mother and

my dear father for help in life and giving me the basic motivations to become interested in science, simply by providing me with all possible means of doing science as a child. They did as much as parents can do for their children. I thank my dear sister and my dear brothers for their kind support during my undergraduate study in Iran and Ph.D years in Germany.

I wish to thank all my friends outside the scientific work who I met in Dresden and who turned these years into such pleasant time.

# Versicherung

Hiermit versichere ich, dass ich die vorliegende Arbeit ohne unzulässige Hilfe Dritter und ohne Benutzung anderer als der angegebenen Hilfsmittel angefertigt habe; die aus fremden Quellen direkt oder indirekt übernommenen Gedanken sind als solche kenntlich gemacht. Die Arbeit wurde bisher weder im Inland noch im Ausland in gleicher oder ähnlicher Form einer anderen Prüfungsbehörde vorgelegt.

Diese Dissertation wurde unter der Betreuung von Prof. Dr. H. Eschrig in dem Institut für Theoretische Festkörperphysik (ITF) am Leibniz-Institut für Festkörper- und Werkstoffforschung Dresden e.V. angefertigt.

Ich erkenne die Promotionsordnung an der Fakultät Mathematik und Naturwissenschaften der Technische Universität Dresden an.

Dresden, den 31. August 2006

Mahdi Sargolzaei



## **Abstract of Thesis:**

# **Orbital Polarization in Relativistic Density Functional Theory**

The description of the magnetic properties of interacting many-particle systems has been one of the most important goals of physics. The problem is to derive the magnetic properties of such systems from quantum mechanical principles. It is well understood that the magnetization in an atom described by quantum numbers, spin ( $S$ ), orbital ( $L$ ), and total angular momentum ( $J$ ) of its electrons. A set of guidelines, known as Hund's rules, discovered by Friedrich Hermann Hunds help us to determine the quantum numbers for the ground states of free atoms.

The question "to which extent are Hund's rules applicable on different systems such as molecules and solids?" is still on the agenda. The main problem is that of finding the ground state of the considered system. Density functional theory (DFT) methods apparently are the most widely spread self-consistent methods to investigate the ground state properties. This is due to their high computational efficiency and very good accuracy. In the framework of DFT, usually the total energy is decomposed into kinetic energy, Coulomb energy, and a term called the exchange-correlation energy. Taking into account the relativistic kinetic energy leads to direct and indirect relativistic effects on the electronic structure of a solid. The most pronounced direct effect (although not the biggest in magnitude) is the spin-orbit splitting of band states. A well-known indirect relativistic effect is the change of screening of valence electrons from the nuclear charge by inner-shell electrons. One can ask that how relativistic effects come into play in ordinary density functional theory. Of course ordinary density functional theory does not include those effect. Four-current density functional theory (CDFT), the quantum electrodynamic version of the Hohenberg-Kohn theory is a powerful tool to treat relativistic effects. Although it is principally designed for systems in strong magnetic fields, CDFT can also be applied in situations where currents are present without external magnetic fields. As already pointed out by Rajagopal and Callaway (1973), the most natural way to incorporate magnetism into DFT is the generalization to CDFT. These authors, however, treated its most simple approximation, the

spin density functional theory (SDFT), which keeps the spin current only and neglects completely correlation effects of orbital currents. By using the Kohn-Sham-Dirac (KSD) equation, spin-orbit coupling is introduced kinematically. The part of the orbital magnetism that is a consequence of Hund's second rule coupling is absent in this theory and there is not any more a one-to-one mapping of spin densities onto external fields. In solids, in particular in metals, the importance of Hund's second rule coupling (orbital polarization) and Hund's third rule (spin-orbit coupling) is usually interchanged in comparison to atoms. Thus, in applications of the relativistic CDFT to solids, the usual way has been to keep the spin-orbit coupling in the KSD equation (an extension to ordinary Kohn-Sham (KS) equation) and to neglect the orbital contribution to the total current density and approximate exchange-correlation energy functional with spin density only. This scheme includes a spontaneous exchange and correlation spin polarization. Orbital polarization, on the other hand, comes into play not as a correlation effect but also as an effect due to the interplay of spin polarization and spin-orbit coupling: In the presence of both couplings, time reversal symmetry is broken and a non-zero orbital current density may occur. Application of this scheme to 3d and 4f magnets yields orbital moments that are smaller than related experimental values by typically a factor of two.

Orbital magnetism in a solid is strongly influenced by the ligand field, originating from the structural environment and geometry of the solid. The orbital moments in a solid with cubic symmetry are expected to be quenched if spin-orbit coupling is neglected. However, spin-orbit coupling induces orbital moments, accordingly. The relativistic nature of the spin-orbit coupling requires orbital magnetism to be treated within QED, and the treatment of QED in solids is possible in the frame of current density functional theory.

The kinematic spin-orbit coupling is accounted for in many DFT calculations of magnetic systems within the LSDA. However, a strong deviation of the LSDA orbital moments from experiment is found in such approaches. To avoid such deviations, orbital polarization corrections would be desirable. In this Thesis, those corrections have been investigated in the framework of CDFT.

After a short review for CDFT in Chapter 2, in Chapter 3, an *ad hoc* OP correction term (OPB) suggested by Brooks and Eriksson is given. This correction in some cases gives quite reasonable corrections to orbital moments of magnetic materials. Another OP correction (OPE), which has been introduced recently, was derived from the CDFT in the non-relativistic limit. Unfortunately, the program can only incompletely be carried through, as there are reasonable but uncontrolled approximations to be made in two steps of the derivation. Nevertheless, the result is quite close to the *ad hoc* ansatz. The calculated OPE energies for 3d and 4f free ions are in qualitative agreement with OPB energies.

In Chapter 4, both corrections are implemented in the FPLO scheme to

calculate orbital moments in solids. We found that both OPB and OPE corrections implemented in FPLO method, yield reasonably well the orbital magnetic moments of bcc Fe, hcp Co and fcc Ni compared with experiment.

In Chapter 5, the effect of spin-orbit coupling and orbital polarization corrections on the spin and orbital magnetism of full-Heusler alloys is investigated by means of local spin density calculations. It is demonstrated, that OP corrections are needed to explain the experimental orbital moments. Model calculations employing one ligand field parameter yield the correct order of magnitude of the orbital moments, but do not account for its quantitative composition dependence. The spin-orbit coupling reduces the degree of spin polarization of the density of states at Fermi level by a few percent. We have shown that the orbital polarization corrections do not change significantly the spin polarization degree at the Fermi level. We also provide arguments that  $\text{Co}_2\text{FeSi}$  might not be a half-metal as suggested by recent experiments.

In Chapter 6, to understand recent XMCD data for Co impurities in gold, the electronic structure of Co impurities inside gold has been calculated in the framework of local spin density approximation. The orbital and spin magnetic moment have been evaluated. In agreement with experimental findings, the orbital moment is enhanced with respect to Co metal. On the other hand, internal relaxations are found to reduce the orbital moment considerably, whereas the spin moment is less affected. Both OPB and OPE yield a large orbital moment for Co impurities. However, those calculated orbital moments are almost by a factor of two larger than the experimental values. We also found that the orbital magnetic moment of Co may strongly depend on pressure.

Dresden, 31 August 2006

Mahdi Sargolzaei